Entropy-Based Image Registration Method Using the Curvelet Transform

by

Md. Mushfiqul Alam

M. Sc. Engg. (EE)

Department of Electrical and Electronic Engineering

BANGLADESH UNIVERSITY OF ENGINEEING AND TECHNOLOGY

July 2011

The thesis titled **Entropy-Based Image Registration Method Using the Curvelet Transform** submitted by **Md. Mushfiqul Alam** Roll No: **1009062053P** Session **2010-2011** has been accepted as satisfactory in partial fulfillment of the requirement for the degree of **Master of Science in Electrical and Electronic Engineering** on 30th July 2011.

BOARD OF EXAMINERS

1. _____
Dr. S. M. Mahbubur Rahman

Assistant Professor — Chairman (Supervisor)
Department of Electrical and Electronic Engineering
Bangladesh University of Engineering and Technology
Dhaka-1000, Bangladesh.

2. _____
Dr. Md. Saifur Rahman

Professor and Head — Member (Ex-officio)
Department of Electrical and Electronic Engineering
Bangladesh University of Engineering and Technology
Dhaka-1000, Bangladesh.

3. _____
Dr. Mohammed Imamul Hassan Bhuiyan

Associate Professor — Member
Department of Electrical and Electronic Engineering
Bangladesh University of Engineering and Technology
Dhaka-1000, Bangladesh.

4. _____
Dr. Md. Shafiul Alam

Associate Professor — Member (External)
Department of Applied Physics, Electronics and Communication Engineering
University of Dhaka
Dhaka-1000, Bangladesh.

CANDIDATE'S DECLARATION

It is hereby declared that this thesis or any part of it has not been submitted elsewhere for the award of any degree or diploma.

_____

Md. Mushfiqul Alam

Roll. 1009062053P

ACKNOWLEDGEMENTS

First, I thank God, the Almighty, for giving me the ability to finish my M.Sc. thesis. By the Merciful God's will it has become possible to complete the thesis work properly.

I am grateful to my supervisor Dr. S. M. Mahbubur Rahman for his continuous support for the thesis, from guidance in the early stages for conceptual foundation, through ongoing advice and encouragement to this day. I also want to thank him for spending many hours with me in discussion about my research.

I would like to acknowledge all the faculty members in the Department of Electrical and Electronic Engineering, Bangladesh University of Engineering and Technology. All the knowledge gathered from the classes in my B.Sc. and M.Sc. levels in this university helped me in this thesis.

I like to thank my parents for their unconditional support and interest, without whom I would be unable to complete my thesis. Special thanks to my wife, Talat Khan, whose patience, love, and unlimited support have made the successful completion of this thesis. At last, but not the least I like to thank my friends and colleagues who appreciated me for my work and motivated me a lot.

ABSTRACT

Integration of images from different sources is increasingly used in different visual signal processing applications. But before the integration it is of utmost importance that the images are geometrically aligned and this aligning process is very often referred to as ‘image registration’. There are two approaches of registering the reference and distorted images, viz., feature-based and intensity-based. The intensity-based methods give better accuracy comparing to the feature-based methods by considering entire pixels of the images, instead of considering just few selected geometric features as in the latter method. Traditionally, image registration is carried out in different transform domains to incorporate the facilities that these transforms provide. Discrete wavelet transform (DWT) has widely been used for image registration. But it has poor directional selectivity. The complex wavelet, ridgelet and shearlet transforms proved slight improvement in directional selectivity over the DWT. Recently, the curvelet transform proved its superiority in directional selectivity among all these wavelet-like transforms, being able to properly detect the commonly occurred curve and edge singularities in images. Hence, in this thesis, an image registration algorithm is developed that uses the curvelet coefficients of images.

Commonly-used probabilistic objective functions in the intensity-based registration algorithms include mutual information, joint entropy and cross-correlation of the transform coefficients of the distorted and reference images. None of these functions consider the conditional dependencies among the images which may exist as the images to be registered are usually captured from a same scene. In this thesis, a new conditional entropy-based objective function is developed using a suitable probabilistic modeling of the approximate level curvelet coefficients of images. The suitability of the probability distribution of the curvelet coefficients of images is validated with a standard statistical test of fit. For the purpose of alignment, a linear transformation, viz., affine transform is used. Extensive experimentations are carried out to test the performance of the proposed registration method as compared to other existing methods using commonly-used performance metrics.

Contents

List of Tables

List of Figures

List of Acronyms

CE	:	Conditional Entropy
CT	:	Computer Tomography
CWT	:	Complex Wavelet Transformation
DCT	:	Discrete Cosine Transformation
DFT	:	Discrete Fourier Transformation
DWT	:	Discrete Wavelet Transformation
MD	:	Mahalanobis Distance
MI	:	Mutual Information
ML	:	Maximum Likelihood
MRI	:	Magnetic Resonance Imaging
NCCC	:	Normalized Cross Correlation Coefficient
NRMSD	:	Normalized Root Mean Square Deviation
PDF	:	Probability Density Function
PRRMSE	:	Percent Root Mean Squared Error
RMSD	:	Root Mean Square Deviation
RV	:	Random Variable
SAR	:	Synthetic Aperture Radio Detection and Ranging
SPECT	:	Single Photon Emission Tomography

List of Symbols

A	:	Affine transform matrix
Θ	:	Angle of rotation of the curvelet basis in polar form
$\hbar$	:	Angle of rotation of the curvelet basis in Cartesian form
θ	:	Angle of rotation in affine transform
$\mathbb{S}$	:	Angular space
χ^2	:	Chi-square quantile
$\gamma(i,j)$	:	Coefficient of the curvelet transform of image
$\mathbb{C}$	:	Complex number space
ρ	:	Correlation coefficient
$\sum$	:	Covariance Matrix
$\boldsymbol{\Phi}_{n\hbar z}$	:	Curvelet basis in Cartesian form
$\boldsymbol{\Phi}_{\lambda\beta\Theta}$	:	Curvelet basis in polar form
I_{As}	:	Curvelet coefficients of the approximate level of the curvelet transform of the distorted image
$\hat{\theta}$	:	Desired angle of rotation found from the algorithm output
$\hat{c}_x$		Desired scaling parameter in x-direction found from the algorithm output
$\hat{c}_y$	:	Desired scaling parameter in y-direction found from the algorithm output
$\hat{s}_h$	:	Desired shear parameter in horizontal direction found from the algorithm output
$\hat{s}_v$	:	Desired shear parameter in vertical direction found from the algorithm output
$\hat{t}_x$	:	Desired translation parameter in x-direction found from the algorithm output
$\hat{t}_y$	:	Desired translation parameter in y-direction found from the algorithm output
$X \times Y$	:	Dimension of the reference and registered images
I_D	:	Distorted image by the affine transform applied over the sensed image
$H(\cdot)$	:	Entropy function

$H(\Gamma_r \mid \Gamma_s)$	:	Entropy of the random variable Γ_r given in the condition of random variable Γ_s
$H(\Gamma_s \mid \Gamma_r)$	:	Entropy of the random variable Γ_s given in the condition of random variable Γ_r
L_2	:	Euclidian space
(x', y')	:	Geometrically distorted location of the pixel index (x, y) by the affine transform
s_h	:	Horizontal shearing parameter in affine transform
$F(i, j)$	:	Index dependent objective function
$\Gamma_r(i, j)$		Index dependent random variable in the approximate curvelet coefficients of the reference image
$\Gamma_s(i, j)$	:	Index dependent random variable in the approximate curvelet coefficients of the sensed image
(x, y)	:	Index of pixel in image
(i, j)	:	Index on coefficient of approximate level of the curvelet transform of image
$H(\Gamma_r, \Gamma_s)$	:	Joint entropy among the random variable Γ_r and Γ_s
$p_{rs}(\gamma_r, \gamma_s)$	:	Joint probability density function of the random variables Γ_r and Γ_s
β	:	Location of curvelet basis in the 2D plane in polar form
z	:	Location of curvelet basis in the 2D plane in Cartesian form
$H(\Gamma)$	:	Marginal entropy
$E[\cdot]$	:	Mathematical Expectation
μ	:	Mean value
$\bar{I}_r$		Mean of the pixel values of the reference image
$\overline{\hat{I}_s}$	:	Mean of the pixel values of the sensed image
μ_r	:	Mean of random variable Γ_r
μ_s	:	Mean of random variable Γ_s
Z	:	Normalized random variable for bivariate case
z	:	Normalized random variable for univariate case
φ_n	:	Number of division for angle of rotation of the curvelet basis
N	:	Number of parameters taken for the registration algorithm
F	:	Objective function

$I(x, y)$	:	Pixel intensity of image at index (x, y)
$p(\cdot)$	:	Probability density function
$\mathbb{R}$	:	Real number space
I_g	:	Registered image
$\gamma_r(i, j)$	:	Sample value of the random variable $\Gamma_r(i, j)$ in $S(i, j)$
$\gamma_s(i, j)$	:	Sample value of the random variable $\Gamma_s(i, j)$ in $S(i, j)$
n	:	Scale parameter of curvelet basis in Cartesian form
λ	:	Scale parameter of curvelet basis in polar form
c_x	:	Scaling parameter in x-direction in affine transform
c_y	:	Scaling parameter in y-direction in affine transform
$D_x \times D_y$	:	Size of the approximate level of the curvelet transform of the image
$S(i, j)$	:	Square-shaped local window centered at (i, j) position in the approximate level of the curvelet transform of the images
σ_r	:	Standard deviation of random variable Γ_r
σ_s	:	Standard deviation of random variable Γ_s
M	:	Total number of coefficients in the local neighboring region in $S(i, j)$
t_x	:	Translation in x-direction in affine transform
t_y	:	Translation in y-direction in affine transform
s_v	:	Vertical shearing parameter in affine transform
α	:	Weight parameter of the proposed algorithm

CHAPTER 1: INTRODUCTION

1.1 Introduction

Living in today‟s technology dependent world, we cannot separate ourselves from the dominance of digital kingdom and digital images play the role of vanguard in this sovereign. Images are connected to our daily life like a spider web. Every single time we browse the internet, do the social networking, read the newspaper, watch any movie or use our mobile network we have to get in touch of digital images. Even when we are sick, we need to go through some medical imaging tests for diagnosis. Our advanced security measures also incorporate digital images through fingerprint detection, face recognition or Irish scan. Scientists dedicated for the research of our earth and the outer space very often have to analyze huge amount of terrestrial images for research purpose. Now, every single digital image we see has gone through some little or extensive processing and the techniques behind those processing are the study materials of digital image processing. Therefore, observing the widespread use of digital images in our day-to-day life we can certainly assume how important image processing is for humankind.

Recently, it is of general interest to integrate knowledge from different sources to increase the information content. Now, as images carry visual information, they play very crucial role as an information source. Very often it becomes necessary to fuse two or more number of images into a single image to provide a better visualization and the process is called „image fusion‟. But before fusing images, it is a challenge to align those images properly. Generally, the images which are needed to be fused are found in geometrically nonaligned condition. For example, in a satellite orbiting around the earth, there are a number of cameras or sensors which capture images of the same scene in different angles and in different modes. The images found from individual cameras vary in geometrical alignment due to the fact that the physical positions of the cameras vary from each other. Another example can be, two x-ray images of the same patient in prone and supine position will spatially mismatch from each other because dislocation happens in the patient‟s body when changing his or her position. Whether the misalignments happened due to the spatial difference in the positions of the image

capturing devices or due to the movement of the target objects, the misaligned images are needed to be geometrically aligned correctly before fusing. Then development of algorithms which will result an accurate and automatic spatial overlaying of images is an emerging necessity. Such an algorithm is desired to be computationally efficient when huge volume of data is needed to be analyzed within a short period of time with a significant level of accuracy. In image processing, these methods or algorithms for overlaying images are very often referred to as image registration and over the years it has been an important topic of work for the researchers in this area.

1.2 Image Registration: A Background

For better understanding, this section has been divided into several subsections, viz., definition, examples, features, approach and last but not the least early works and scope of work in the area of image registration.

1.2.1 Definition

In short, image registration can be defined as the process of spatially overlaying images which are captured from the same scene but possess some geometric distortions. In general, there are two types of images in image registration: one reference image and one or more sensed images which are needed to be registered. The reference and sensed images again can be of following categories [1]:

- *Multitemporal*: images captured in different moments such as in different days, occasions or seasons.
- *Multiview*: images acquired from different viewpoints such as left focused, middle focused and right focused images of a scene.
- *Multimodal*: images captured by different mode settings of the image capturing instrument e.g., T1 and T2 mode images of MRI.
- *Multisensored*: images obtained from different sensors such as images captured by cameras sensitive to visual and infrared rays.

1.2.2 Examples

As mentioned earlier, registration is the mandatory first step in image fusion. For example, in the area of remote sensing, geology and cartography high resolution images such as Ikonos, Quick Bird, Orb View type images are needed to combined with low and medium images such as Landsat, IRS, Spot images [1]-[3]; and these images must be aligned before fusing them. In the field of medical imaging, commonly used imaging methods are computer tomography (CT), magnetic resonance imaging (MRI), single photon emission tomography (SPECT). The CT images can determine cancers, cardiovascular diseases, blood vessels, trauma and musculoskeletal disorders. Two commonly used modes in MRI are T1 weighted and T2 weighted MRI images. T1 weighted images demonstrate excellent anatomic detail whereas T2 weighted images provide outstanding contrast between normal and malignant tissues. The SPECT scan demonstrates the functional information about patient‟s specific organ; but do not show anatomical information like CT and MRI. When MRI, CT, SPECT or other medical images are to be fused into one image, the prior images are needed to be aligned exactly such that the fused image does not create any ambiguity [4]-[9]. Some other types of images such as for navigation and security purposes visual and infrared images [10], in printed circuit board (PCB) surface mount technology (SMT) assembly products inhomogenously illuminated circuit board images [11], for defect detection in circuits flexible printable circuit images [12], images captured with different focus points are needed to be registered and fused. Again, for wildlife preservation images of forests in different seasons are required to be aligned and then fused to provide better visualization.

Registration is used not only prior to the fusion of images but also in panoramic image construction [13] and 3D scene reconstruction [14]. When constructing panoramic image, several pieces of images capturing the different portions of a large scene are gathered and those pieces are overlaid to make a continuous image of the large scene. It is important to shift the consecutive pieces of images in proper amount so that the panoramic image does not contain any discontinuous or overlapping section. For example, recently a panoramic image of a 300-feet 1500 year old redwood tree in

California‟s Redwoods State Park has been composed from eighty-four images captured by three cameras and this process needed rigorous image registration [15]. This panoramic image construction is also needed in extensively used mapping software such as in Google map. CT colonography is a good example of 3D scene reconstruction [14]. In this process, after insufflating the abdomen with CO_2, CT scans are acquired both in the prone and supine position of a patient. But the remaining moving stool in the colon poses problems by creating empty spaces in the 3D CT colonography images. So, proper registration of the prone ant supine 3D CT scan images with some interpolation is applied here in order to obtain a total 3D view of the abdomen of the patient.

1.2.3 Issues of registration

In designing a registration algorithm, it is necessary that the algorithm to be not only highly accurate but also computationally efficient.

- Accuracy of registration is important in many fields such as in security purposes the images from different cameras or sensors are needed to be registered and analyzed very accurately. Otherwise it will make the security system futile. In synthetic aperture RADAR (SAR) images, accuracy is very important. As a small part in the map represent a large area on the Earth‟s surface, the registration process is needed to be highly accurate in this field.
- Computational efficiency of registration algorithm is a requirement in the fields, where fast analysis of huge volume of data is needed such as in remote sensing, analysis of large size high resolution images are needed to be registered within a short period of time. So, the algorithm should result a fast output within a certain amount of accuracy.

1.2.4 Common approaches

In general, there are two approaches for image registration: feature-based [16]-[22] and intensity-based [23]-[32]. In the fully-automated [17], [18] or semi-automated [16], [19]

feature-based registration processes at first, some feature or control points such as edges, lines and surfaces, are selected from the reference image and some matching points are selected from the sensed image. After that, control points and matching points are refined and a mapping function is estimated using which the sensed images are registered. Although in general these feature-based methods require a lower computational load by considering only a few number of selected features, the accuracy of such registration is lower as in these methods total pixels of entire images are not considered [16]-[18], [23]-[26].

In the intensity-based methods, at first a suitable geometric mapping function is chosen by observing the distortion between the reference and sensed images. The mapping function can be linear such as affine transform [33], [34] containing rotation, translation, scaling and shearing. It can also be piecewise-linear, polynomial, barrel or pin-cushion [35] type which generally bring arc or curve type distortions in images. Then, the sensed image is transformed using this selected mapping function. In order to set the parameters of the mapping function, an objective function has to be determined between the reference and the transformed sensed image which considers the pixel intensities of the whole image. At last, the sensed image is registered by using the calculated distortions parameters that optimizes the objective function. In general, the pixel-based or intensity-based methods provide a higher accuracy comparing to the feature-based methods. Because, unlike feature-based methods where a few feature points are considered, in the intensity-based registration algorithms pixel values of the entire images are considered. Due to this higher accuracy very often intensity-based registration methods are preferred to feature-based methods.

1.2.5 Related works and scope

Among the traditional objective functions used in the intensity-based image registration methods cross-correlation [17], [36], mutual information [26], [27], [29], [31] and joint-entropy [37] are worth mentioning. The problem of cross-correlation based image registration is that it gives unwanted peaks when calculating the value of the objective

function by changing the parameters of the mapping function. This problem is more visible where the pixel intensities of the image have a periodic nature. In between such periodic nature there exist some varying gray levels. In such a case the correlation becomes multimodal in nature. Hence, it becomes almost impossible to register images using cross-correlation. The objective functions such as mutual information (MI) and joint-entropy that uses probability model also has some limitations. Since the reference and the sensed images are captured from a same scene they have some sort of similarity and dependencies. The MI and joint-entropy based objective functions overlook the conditional dependency that may exist between the images. Moreover, the probability density functions (PDFs) [38] which are commonly used for calculating these objective functions are chosen heuristically without any justification. Now, another objective function that has been exploited is the cross-entropy [37]. In [37], for calculating the cross entropy two PDFs, namely, the actual joint PDF and an assumed prior estimated PDF among the pixel intensities of the images are required. Three unlikely conditions has been taken into consideration for assuming the prior PDF, viz., uniform PDF, independently related PDFs and joint PDF proportional to the marginal PDF. When optimizing the cross entropy from these three conditions it ultimately turns to the optimization of the conditional entropy. In this way this cross entropy procedure actually measures the conditional entropy in a difficult and indirect way. So in this thesis we intend to use the conditional entropy directly with a PDF verified by a standard statistical test of fit for constructing the objective function for image registration.

It is a general trend to carry out the image registration process in a suitable transform domain instead of the pixel domain in order to take the advantages of the properties of the transformations and thus improving the efficiency of the registration methods. Among these transformations the discrete wavelet transform (DWT) is the most popular [39]. The DWT based registration methods have been explored widely and showed a good performance in context of accuracy and processing time [31], [32], [40]-[42]. This is mainly due to the fact that the coefficients of a wavelet transform represent the edge and textures of images better than those of the discrete Fourier transform (DFT) and the discrete cosine transforms (DCT). Moreover, some selected subbands of the wavelet transform may be easily processed instead of the entire transformed data of the DFT and

DCT in order to reduce the processing time. But, the traditional wavelet transforms suffer from a property of poor directional selectivity. For example, the DWT can capture the edge and ridge features in an image in only four directions, viz., 0^0, 90^0 and $\pm45^0$. To improve the directional selectivity of the wavelet transforms, the complex wavelet transform (CWT) was introduced [26], [43]. The CWT can capture six directions, viz., $\pm15^0$, $\pm45^0$ and $\pm75^0$. But, it is hard to design complex wavelets with perfect reconstruction properties and good filter characteristics. Kingsbury proposed the dual-tree CWT [44] which enhanced the reconstruction problem of CWT. To improve the directional selectivity further, Cnadès and Donoho proposed an anisotropic geometric wavelet transform in 1999 and named it as the ridgelet transform [45], [46]. The ridgelet transform could optimally detect the straight-line singularities. But, in practical applications global straight-line singularities are rarely found. So, for analyzing curve singularities, the same authors proposed at first to consider a partition of the image, and then apply the ridgelet transform to the obtained sub-images [47]. This block-ridgelet transform was named as the curvelet transform. This so-called first-generation curvelet was facing problem as the geometry of the ridgelet was unclear and they were not true ridge functions in digital images. After that a considerably simpler second-generation curvelet transform was proposed based on frequency partition technique [48] and then the alternate second-generation curvelet transform was proposed by adding mirror extensions (ME) [49]. The curvelet transform has been proved its dominance in many different applications in image processing [50], [51]. Since, the curvelet transform extracts the image features efficiently and gives better directional sensitivity than previous wavelet-like transforms, it is expected that a suitable objective and mapping functions applied over the curvelet coefficients would give more accurate image registration results than existing methods. Traditional correlation, MI or joint entropy based objective functions may also be used for the curvelet coefficient to design an image registration algorithm. However, such an objective function will ignore the conditional dependencies that may exist between the reference and sensed images. So, there is good scope of work on the search of an objective function working on the curvelet coefficients of images and that will consider the conditional dependencies as well.

1.3 Objective

The objectives of this thesis are:

- To obtain better directional selectivity as well as lower computational complexity, the conditional entropies would be calculated for the coefficients of the approximate level curvelet transform of the reference and sensed images.
- To take into account the conditional dependencies among the reference and the sensed images, combination of the conditional entropies (CEs) would be taken into consideration for constructing the objective function.
- To calculate the CEs, a suitable probability density function is required. The probabilistic model for the objective function would be verified using a traditional test of fit.
- Finally, the performance of the proposed registration method would be investigated using commonly accepted performance metrics.

To achieve these objectives, at first a suitable PDF for the curvelet [17], [18] coefficients of image intensity values is chosen. This choice is verified by standard statistical tests of fit [19]. Using this PDF, an expression of the objective function is derived considering the CEs of the curvelet coefficients of images. Then the objective function is minimized over the experimentally selected subbands of the curvelet coefficients both locally and globally to find out the distortion parameters of the images. In order to verify the working capability of the proposed method, two images, namely, „reference image" and „sensed image" are chosen keeping in mind that it can be extended for a higher number of images also. For the purpose of experimentation, two types of sensed images are considered: (i) Distorted version of reference image using a known set of parameters of affine transformation. (ii) An image already aligned to the reference image but captured in a different mode, moment, view or sensor. Distorted version of this image will be found using a known set of parameters of affine transformation. These sensed images will be geometrically aligned or overlaid with the reference image by minimizing the entropy-based objective function of the curvelet coefficients of the images. The closeness of the estimated distortion parameters will be compared using the known distortion parameters. Finally, the performance of the proposed registration method will be compared with those of the existing methods using

commonly accepted metrics such as normalized cross correlation coefficient (NCCC), root mean squared deviation (RMSD), normalized root mean squared deviation (NRMSD) and percent root mean squared error (PRRMSE) [52].

1.4 Organization

This thesis is organized as follows. In Chapter 2, a brief introduction about the curvelet transform, differences of this transform with other wavelet-like transforms are given. The probabilistic test of fit for a suitable PDF of the curvelet coefficients of image pixel intensities has been presented in this chapter. In Chapter 3, a mathematical expression of the objective function of the proposed registration method is derived. Chapter 4 provides the experimental results along with the performance comparisons of the proposed algorithm with other existing methods. Finally, in Chapter 5, a general concluding discussion and future extension of this work is given.

CHAPTER 2: CURVELET TRANSFORM OF IMAGES

2.1 Introduction

In chapter one, the definition of image registration, its necessity, applications, techniques and scope of work are given. It was mentioned that a suitable transformation such as curvelet transform of the image pixel intensities would provide a better image registration algorithm as this transform will represent the points, edges and lines in the images in a better way. The curvelet transform is a multiscale directional transform that gives an optimal nonadaptive sparse representation of objects with edges in the images [47]-[49]. In recent years curvelet has proved its superiority in applied mathematics and signal processing. In this chapter a brief review on curvelet transform is given. Moreover, its history starting from wavelet and the relationship of the curvelet transform to other multiresolution transforms is discussed. In chapter one, it was mentioned that a statistical objective function of image registration require a suitable PDF for the coefficients of the curvelet transform. In this chapter, a PDF for the curvelet coefficients of image pixel intensities is chosen based on commonly used PDFs for other wavelet-like transforms. The suitability of such PDF of the curvelet coefficients is tested using a standard test of fit. At the end of this chapter, some objective functions that have been traditionally used for intensity-based image registration approach are given.

2.2 Curvelet Transform

In this section, at first a brief background of the curvelet transform is given. Following that mathematical expression for the curvelet transform is given. At the end of this section, the relationship between curvelet and other wavelet-like transforms is discussed.

2.2.1 A brief background

The natural images normally have discontinuities called line or curve singularities. Though the wavelet based applications have become increasingly popular in scientific

and engineering fields, traditional wavelets can only detect point singularities well. So wavelet based image registration, compression and denoising techniques have become computationally inefficient for geometric features with line and curve singularities [26]. So the evolvement of new transform having the quality of detecting the line and curve singularities is natural. Since Olshausen and Field‟s work in Nature [53], researchers have given importance about the similarity between the vison and multiscale image processing. The receptive fields of cells in the primary visual cortex can be characterized as being spatially localized, oriented, and bandpass, i.e., selective to structures at different spatial scales. Wavelets do not have good directional selectivity which is an important response property of simple cells and neurons at stages of the visual pathway. Therefore, a directional multiscale sparse coding has been desirable in this area. To extract the features from an image is one of the primary tasks in image processing. The features include points, lines, edges and textures. Linear scale-space filtering such as those done in multiresolution wavelet transform was widely used for extracting these features in early works. To overcome the poor directional selectivity of 2-D DWT, a multiresolution geometric analysis (MGA), named curvelet transform was proposed [47]-[49]. In images, the curvelet transform gives an almost sparse representation of objects with line or edge singularities. Moreover, the needle-shaped elements (as shown in figure 2.1 and 2.2) of curvelet transform possess very high directional sensitivity and anisotropy comparing to the isotropic elements of wavelet transform. If we compare the curvelet system with the conventional Fourier and wavelet analysis, the short-time Fourier transform uses shape-fixed rectangle in frequency domain (as shown in Figure 2.3a and Figure 2.3b) and the wavelet transform uses shape-changing but area fixed windows (as shown in Figure 2.4a and Figure 2.4b), whereas curvelet transform uses angles polar wedges or angled trapezoid windows in frequency domain (as shown in Figure 2.5) to resolve directional features.

2.2.2 Mathematical expression of the curvelet transforms

Curvelets are band-limited complex-valued functions $\boldsymbol{\Phi}_{\lambda\beta\Theta}: \mathbb{R}^2 \rightarrow \mathbb{C}$ parameterized in a scale ($\lambda > 0$), location ($\beta \in \mathbb{R}^2$) and rotation ($\Theta \in \mathbb{S}^1$) space. The graph of the modulus of a curvelet looks like a brush stroke (as shown in Figure 2.1) of a given thickness (as given by $\lambda > 0$), location on the canvas ($\beta \in \mathbb{R}^2$), and direction ($\Theta \in \mathbb{S}^1$).

Figure 2.1: Mesh plot of $|\boldsymbol{\Phi}_{\lambda\beta\Theta}|$; $\lambda = 2^{10}, \beta = (0,0), \Theta = 120^0$

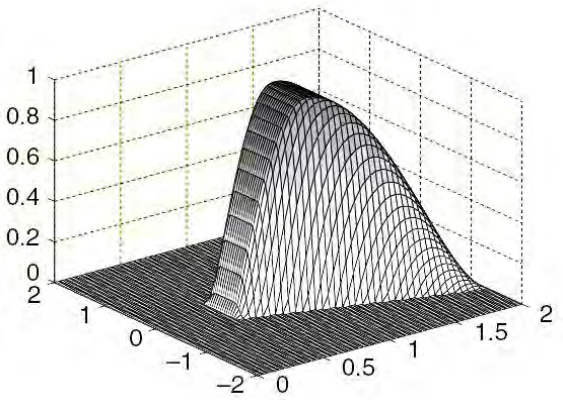

Figure 2.2: Basic curvelet $\boldsymbol{\Phi}_{n\kappa z}$, when calculating in Cartesian form

Let, $I(x,y) \in L_2(\mathbb{R}^2)$ be a pixel value of an image with spatial index (x,y). This square integrable function can be represented by discrete version of the curvelet transform as [48]

$$\gamma(i,j) = \langle I, \boldsymbol{\Phi}_{n\kappa z} \rangle = \sum_{n \in \mathbb{Z}} \sum_{\kappa=1}^{2\pi/\varphi_n} \sum_{z \in (x,y)} I(i-x, j-y) \boldsymbol{\Phi}_{n\kappa z} \tag{2.1}$$

Here, $\gamma(i,j)$ represent the curvelet coefficient. „n" is the scaling parameter, „κ" is the angle of rotation and „z" is the location of the curvelet $\boldsymbol{\Phi}_{n\kappa z}$. The basic curvelet in Cartesian form is shown in Figure 2.2. However, the inverse curvelet transform in discrete domain is given as [48]

$$I(x,y) = \sum_{n \in \mathbb{Z}} \sum_{\kappa=1}^{2\pi/\varphi_n} \sum_{z \in (i,j)} \gamma(i-x, j-y) \boldsymbol{\Phi}_{n\kappa z} \tag{2.2}$$

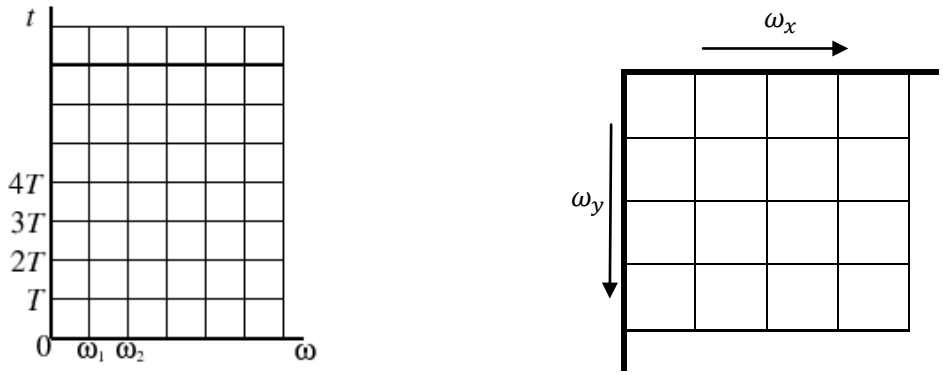

(a) (b)

Figure 2.3: (a) Time-frequency tiling (b) Frequency tiling for the 2-D short-term Fourier transform (STFT)

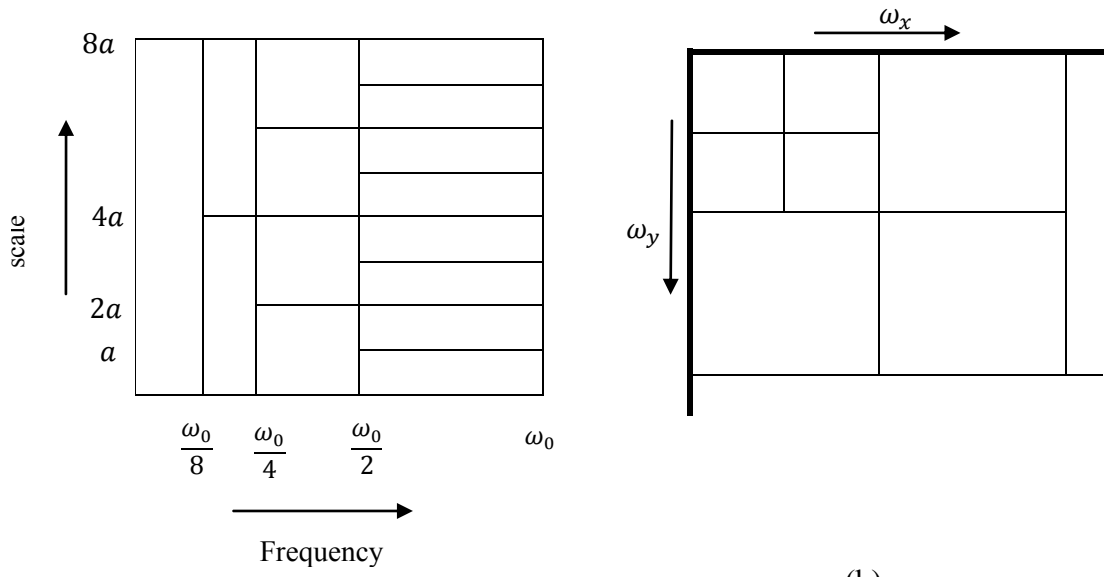

(a) (b)

Figure 2.4: (a) Scale-frequency tiling (b) Frequency tiling for the 2-D DWT

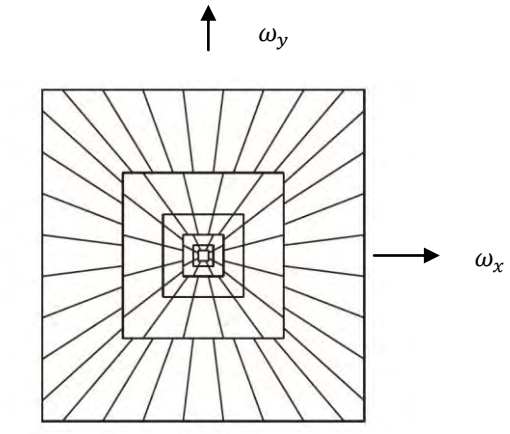

Figure 2.5: Frequency tiling for the curvelet transform , calculating in Cartesian form

2.2.3 Relationship between wavelet-like transforms

Over the years, several directional wavelet transforms have been developed to provide better directional selectivity. Among those systems, complex wavelets [26], [43], steerable wavelets [54], [55], Gabor wavelets [56], wedgelets [57], beamlets [58], contourlets [59], shearlets [60], wave atoms [61], platelets [62] and surfacelets [63] are worth mentioning. These directional wavelets are uniformly called X-lets. The steerable wavelets and Gabor wavelets can be seen as early directional wavelets. The steerable wavelets were built based on the directional derivative operators and Gabor wavelets were produced by a Gabor kernel that is a product of an elliptical Gaussian and a complex plane wave. The steerable wavelets give translation-invariance and rotation-invariance of the position and the orientation of considered image structures. Gabor wavelets were used for image classification and texture analysis. But unlike other X-lets, steerable wavelet and Gabor wavelet do not allow different number of directions in every scale. Do and Vetterli [59] proposed contourlets which form a discrete filter bank structure that can deal effectively with piecewise smooth images with smooth contours. This discrete transform can be connected to curvelet-like structures in the continuous domain. So the contourlet transform can be depicted as a discrete form of a particular curvelet transform. Curvelet constructions require a rotation operation and correspond to a partition of the 2-D frequency plane based on polar coordinates. Due to this property in continuous domain the idea of curvelet becomes simple but in discrete domain its implementation becomes difficult. Unfortunately, contourlet functions have less directional features than curvelets. Shearlets [60] form an affine transform system with a single generating mother shearlet function parameterized by a scaling, a shear and a translation parameter captures the direction of singularities. Both the curvelet and shearlet transforms are suited for approximation of piece-wise smooth images with singularities along smooth curves [47]-[49]. But the performance of curvelet transform is better than the shearlet transform as the curvelet transform can detect curve singularities in a better way [45]-[49].

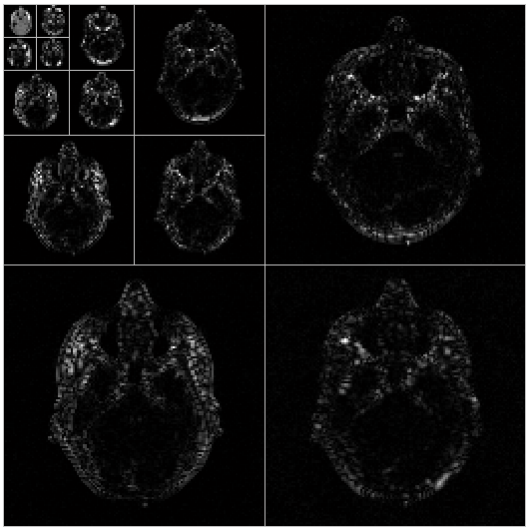

(a)

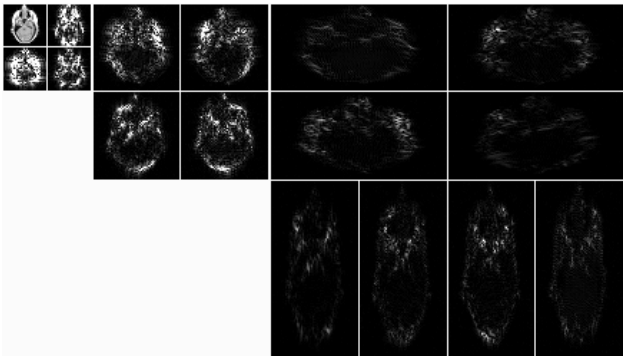

(b)

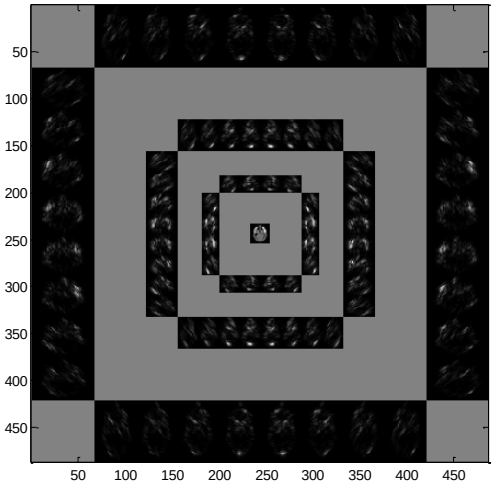

(c)

Figure 2.6: Coefficients of an MRI image for different multiresolution transforms (a) DWT coefficients (four level of decomposition) (b) Contourlet transform coefficients (three level of decomposition) (c) log of curvelet transform coefficients (Five numbers of scales and Sixteen number of angles)

In Figure 2.6 the wavelet, contourlet and curvelet coefficients of a MRI image are shown. The wavelet coefficients are found using the Daubechies 2 mother wavelet [39] and four levels of decomposition. The contourlet coefficients are found using the pyramidal directional filters and three levels of decomposition. The curvelet coefficients are found using Curvelab, version 2.1.2 which is available in (http://curvelab.org). For calculating curvelet coefficients, four number of scales ($n = 4$) and sixteen number of angles ($\beta = 16$) are used. If we compare the images in Figure 2.6, we observe that for the same scale number, curvelet transform gives more orientations. So, the curvelet transform gives better directional selectivity than that of the wavelet and contourlet transforms.

2.3 Test of Fit

In general, the wavelet-like transforms are locally stationary due to the fact that there remains an explicit intra-scale dependency among the coefficients of the sub bands [39]. Hence, the local processing of wavelet-like transform coefficients give better performance in images than global processing. This is why, the wavelet-like coefficients are probabilistically modeled using a local neighboring coefficients. In this thesis, we also prefer probabilistically model the curvelet coefficients using a local neighboring region as a scale. The Gaussian or normal PDF [64] is very often chosen as the probability model for DWT coefficients. It should be mentioned that, other wavelet-based image registration methods use only approximate band for registration. Moreover, the approximate level can be said as the miniature version of the original image and the computational load will be minimized if only this level is used for registratoin. Hence, we would like to use the approximate band of the curvelet coefficients of image for the registration. We choose the bivariate Gaussian or bivariate normal distribution [38], [64] to be the PDF for coefficients of the approximate level of the curvelet transform of images.

The probability density function for a single normally distributed variable, Γ, with mean μ and a standard deviation σ is given by [64]

$$p(\gamma) = \frac{1}{\sigma\sqrt{2\pi}}\exp[-(\gamma-\mu)^2/2\sigma^2] \qquad (2.3)$$
$$= \frac{1}{\sigma\sqrt{2\pi}}\exp[-0.5z^2]$$

where

$$z = \frac{\gamma-\mu}{\sigma} \qquad (2.4)$$

Here, z represents a standardized version of γ and γ is the sample value of the random variable (RV) Γ. The standardized random variable (RV), Z, follows a normal distribution with a mean zero and standard deviation one, or mathematically, $Z \sim \mathcal{N}(0,1)$. The appearance of $-z^2$, the negative of the squared scaled distance to the mean, in the exponential of the PDF is quite important. This squared scaled distance is the natural distance metric for normally distributed variables.

For the multivariate normal distribution, a vector of random variables (RVs) **Γ**, with a vector mean of $\boldsymbol{\mu}$ and a covariance matrix $\sum$ is considered. Each individual variable, Γ_i follows a normal distribution with a mean μ_i and a variance $\sigma_i^2 = \sum_{ii}$. The covariance between any pair of variables, Γ_i and Γ_j, is given by $\sum_{ij}$ and the corresponding correlation is given by [64]

$$\rho_{ij} = \frac{\sigma_{ij}}{\sqrt{\sigma_i^2\sigma_j^2}} \qquad (2.5)$$

Here, σ_{ij} is the covariance and σ^2 denote the variance. Now, the multivariate normal density function for **Γ** is given by [64]

$$p(\boldsymbol{\gamma}) = \frac{1}{\sqrt{(2\pi)^k\sqrt{|\sum|}}}\exp\left[-\frac{1}{2}(\boldsymbol{\gamma}-\boldsymbol{\mu})^T\sum^{-1}(\boldsymbol{\gamma}-\boldsymbol{\mu})\right] \qquad (2.6)$$

Where, k is the number of variables or the number of components of $\boldsymbol{\Gamma}$. The quadratic form

$$z^2 = (\boldsymbol{\gamma} - \boldsymbol{\mu})^T \sum^{-1} (\boldsymbol{\gamma} - \boldsymbol{\mu}) \tag{2.7}$$

represents the squared distance to the vector mean, scaled according to the variances and covariances specified in $\sum$. This is called the squared Mahalanobis distance (MD) to the vector mean [64]. We use this squared Mahalanobis distance (MD) and chi-squared quantile to check the deviation of the curvelet coefficients of the paired image"s distribution from the ideal bivariate normal distribution. The quantile indicates the point below which a given fraction of data remains [64]. For defining chi-square, let the probabilities of various classes in a distribution be $p_1, p_2, \ldots\ldots\ldots\ldots\ldots, p_k$with observed frequencies $m_1, m_2, \ldots\ldots\ldots, m_k$. Now, the quantity [64]

$$\chi_s^2 = \sum_{i=1}^{k} \frac{(m_i - Mp_i)^2}{Mp_i} \tag{2.8}$$

is therefore a measure of the deviation of a sample from mean or expectation, where M is the sample size.

In the multivariate case, each variable must be normally distributed for the entire set to follow a multivariate normal distribution. But, normality of the individual variables does not guarantee multivariate normality. If the data do follow a multivariate normal distribution, then the squared MD from the data points to the centroid (mean) should follow a chi-squared distribution with k degrees of freedom [64]. For this purpose we construct a quantile-quantile plot of the observed squared M.D."s versus chi-squared quantile. The closeness of this plot to the $\tan 45^0$ line is the measure of closeness of the distribution to the multivariate normal distribution. The more the closeness, the higher the accuracy of the data follows the normal distribution. Figure 2.7 and Figure 2.8 show the MD versus χ^2 quantile for the approximate curvelet coefficients of four pair of chosen test images with mask sizes 5×5 and 7×7 respectively. The test images used here Toy (image 1 and 2), Room, SAR1, and MRI for 5×5 window and Toy (image 1

and 3), Room, SAR2, and MRI for7×7 window. These test images are given in the appendix. Here, for the calculation of chi-square quantile 2-degrees of freedom is used. From Figure 2.7 and Figure 2.8, it is observed that for both 5×5 and 7×7 windows the squared distance versus chi-squared quantile approximately follow the $\tan 45^0$ line with negligible amount of deviation. The percent squared error of the test line from the ideal Bivariate PDF line for each case is less that 10%. This means that, the test line is very close to the ideal line. Hence, for designing a probabilistic objective function using the approximate curvelet coefficients of images for registration purposes, the bivariate Gaussian distribution can be used.

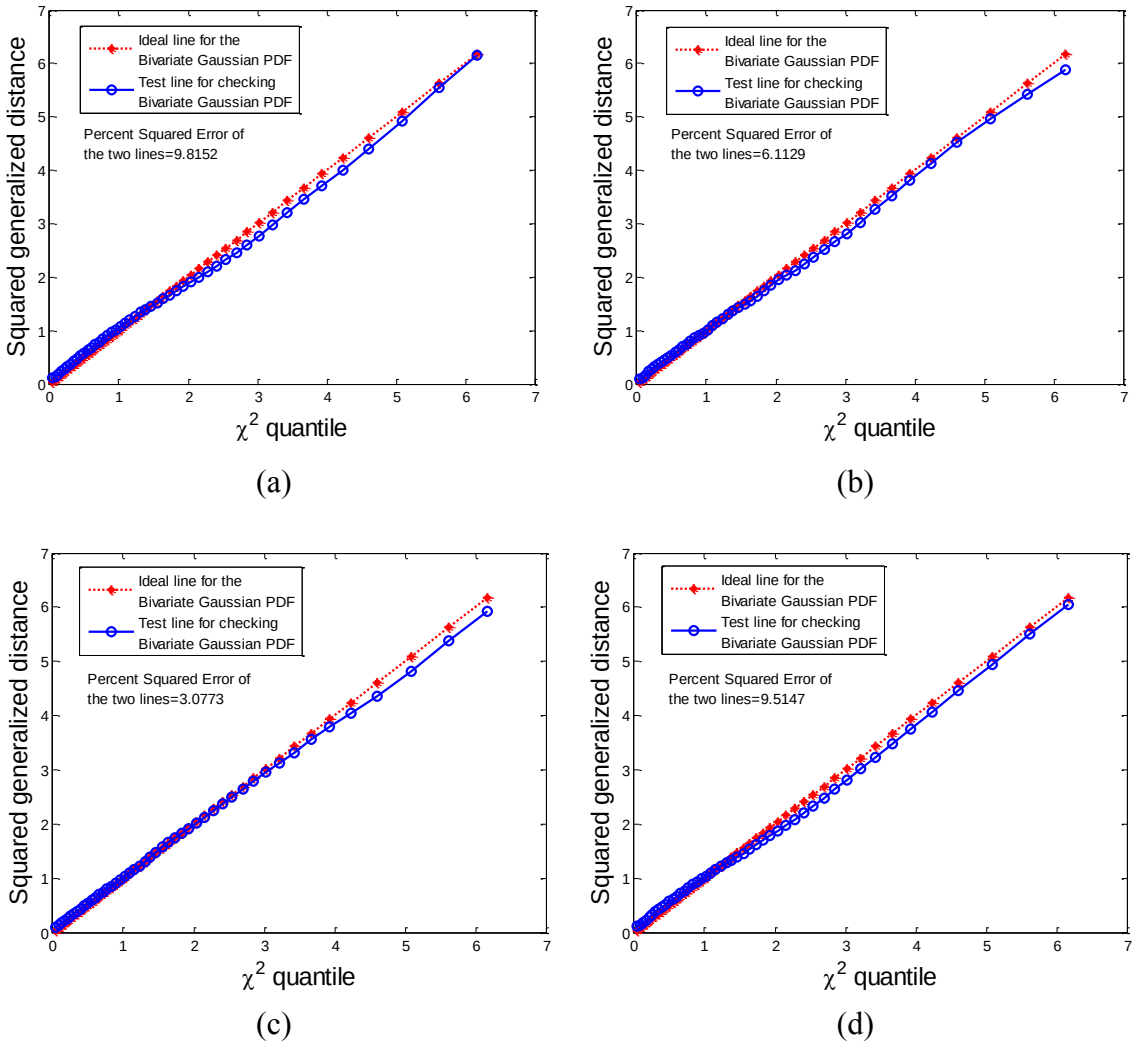

Figure 2.7: χ^2 plot using 5×5 window. The test images are: (a) Toy (images 1 and 2) (b) Room (c) SAR1 (d) MRI

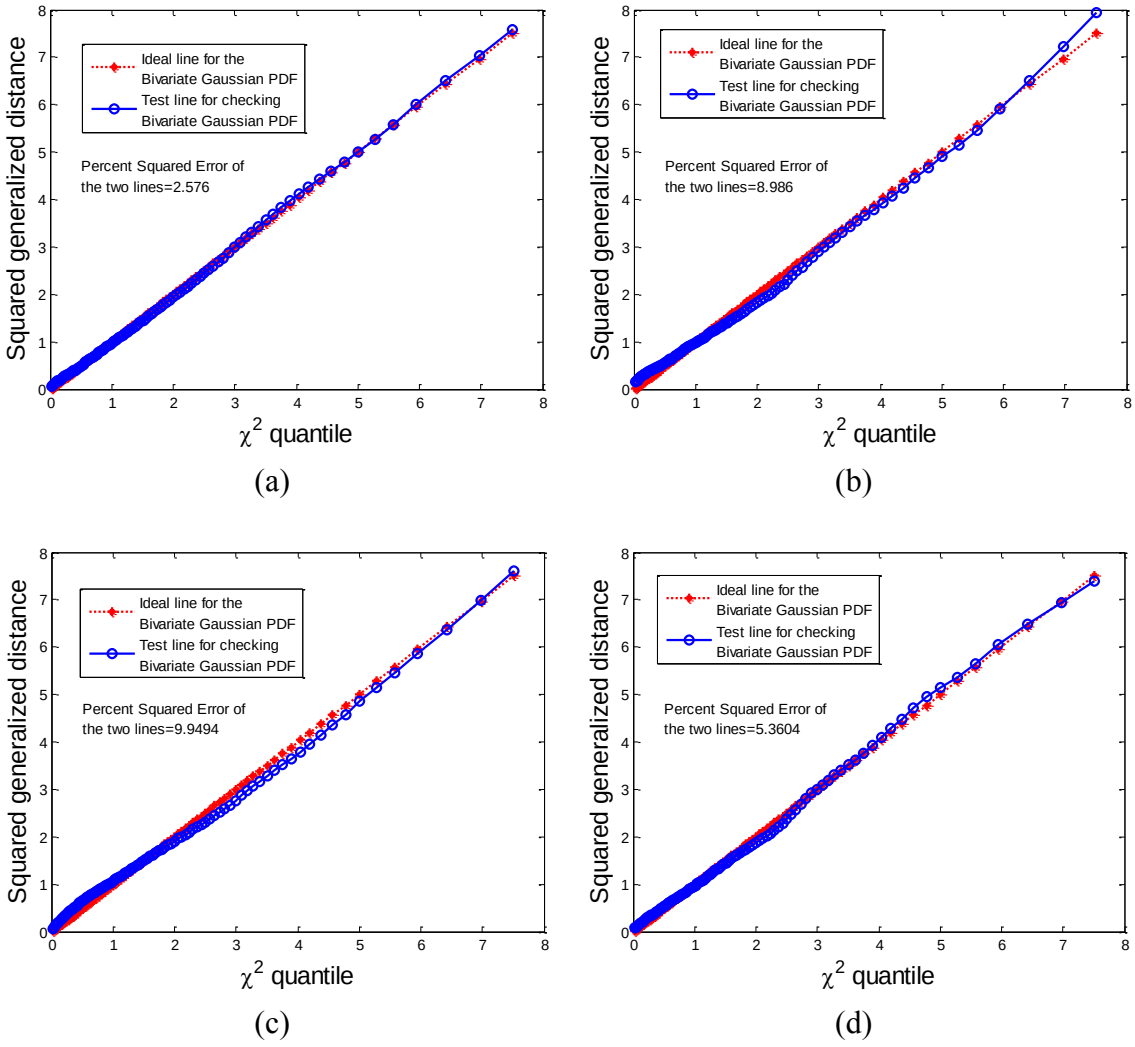

Figure 2.8: χ^2 plot using 7×7 window. The test images are: (a) Toy (images 1 and 3) (b) Room (c) SAR2 (d) MRI

2.4 Traditional Objective Functions

In the previous sections of this chapter, the curvelet transform and the statistical choice of PDF for the curvelet coefficients of images with standard test of fit has been discussed. Now for the purpose of modeling of objective function using this curvelet transform coefficient of images, we intend to recall some objective function traditionally used in intensity-based registration methods. These objective functions include cross correlation [17], [36], mutual information [26], [27], [29], [31] and joint-entropy [37]. Let γ_r, γ_s be the curvelet coefficients in the approximate level and Γ_r, Γ_s

denote their random variables (RVs) for reference and sensed images respectively. Let the reference and registered images are of size $X \times Y$. Let the curvelet coefficients in approximate level are of size $D_x \times D_y$.

2.4.1 Cross correlation

The formula of the cross-correlation computation is [17] the equation of cross correlation coefficient

$$\rho = \frac{\sum_{i=1}^{D_x}\sum_{j=1}^{D_y}\{[\gamma_r(i,j) - \mu_R][\gamma_s(i,j) - \mu_s]\}}{\sqrt{\sum_{i=1}^{D_x}\sum_{j=1}^{D_y}[\gamma_r(i,j) - \mu_R]^2 \sum_{i=1}^{D_x}\sum_{j=1}^{D_y}[\gamma_s(i,j) - \mu_s]^2}} \tag{2.9}$$

where μ_r and μ_s denote the mean of the approximate curvelet coefficients of the reference and sensed images respectively. The problem of this objective function is that cross correlation gives unwanted peaks when calculating the value of the objective function by changing the parameters of the mapping function. This problem becomes more visible when the image has periodicity. So it becomes difficult to determine the required or desired registration parameters using the cross correlation method.

2.4.2 Mutual information

The mutual information among the RVs Γ_r and Γ_s is given as [26], [27], [29], [31]

$$MI = \int_{-\infty}^{\infty}\int_{-\infty}^{\infty} p_{rs}(\gamma_r, \gamma_s) \ln\left[\frac{p_{rs}(\gamma_r, \gamma_s)}{p_r(\gamma_r)p_s(\gamma_s)}\right] d\gamma_r d\gamma_s \tag{2.10}$$

where $p_{rs}(\gamma_r, \gamma_s)$ is the joint PDF and $p_r(\gamma_r), p_s(\gamma_s)$ are the marginal PDFs of the coefficients of the approximate level of the curvelet transform of the reference and sensed images. The mutual information calculates the mutual dependency or joint dependency that remains among the images needed to be registered. In this context it performs better than the cross correlation-based methods. But mutual information does

not consider the conditional dependency that may exist among the images. This is to be noted that, it is likely to have conditional dependency among the images as they are captured from the same scene but may be captured in different modes or by different sensors or in different times.

2.4.3 Joint entropy

The joint entropy of two random variables Γ_r and Γ_s is given as [65], [66]

$$H(\Gamma_r, \Gamma_s) = -\int_{-\infty}^{+\infty}\int_{-\infty}^{+\infty} p_{rs}(\gamma_r, \gamma_s)\, ln[p_{rs}(\gamma_r, \gamma_s)]\, d\gamma_r d\gamma_s \qquad (2.11).$$

This objective function considers the joint dependency among the images but ignores the conditional dependency that may exist among them. Moreover, in the previous methods that used joint entropy or mutual information, the required PDF was never verified by statistical test of fit.

In this thesis, we intend to form an objective function that will consider the conditional dependency that may remain among the images. Here in this thesis we intend to use conditional entropy to form the objective function.

2.5 Conclusion

In this chapter, the curvelet transform and the probabilistic modeling of the approximate level curvelet coefficients are discussed. Here, the backgrounds of the curvelet transform, mathematical expression, relationship with other wavelet-like transforms are described. Moreover, it has been verified by chi-square plot that for local neighboring region of curvelet coefficients, the bivariate Gaussian density function can be used for constructing the probabilistic objective function for image registration purposes. At the end of the chapter traditional objective functions for image registration has been discussed.

CHAPTER 3: PROPOSED REGISTRATION METHOD

3.1 Introduction

In Chapter 1, it has been mentioned that the curvelet coefficients of the image can detect the curve and line singularities very efficiently. The approximate level of the curvelet transform represents the significant edge and line features of an image. Thus such coefficients of the approximate level are adequate for developing a curvelet based registration algorithm with a lower computational load. Now, from the χ^2 test in Chapter 2, it has been found that the bivariate normal distribution can be used for probabilistic modeling of the local neighboring region of the approximate curvelet coefficients of images. This PDF may be used to develop the conditional entropy based registration algorithm. For this purpose, in this chapter, an analytical form of conditional entropies between the approximate curvelet coefficients of the reference and sensed images is determined by considering that their joint PDF follows the bivariate Gaussian distribution. The distortions considered are obtained by using the affine transform, which considers different geometric distortions, viz., rotation, translation, scaling and shearing of images. Expressions of the affine transformation matrix and the parameters of this transform are also given at the end of this chapter.

3.2 Conditional Entropy-Based Objective Function

Let I_r, I_s and I_g be the reference, sensed and registered images. Here, the subscript „r" denotes the reference image and the subscript „s" denotes the sensed image. Now, prior to develop the CE based objective function; at first the connotations of different symbols used in the following discussions are given below:

$S(i,j)$: a square-shaped local window centered at (i,j) position in the approximate level of the curvelet transform of the images

$\Gamma_r(i,j)$: index dependent random variable (RV) in the approximate curvelet coefficients of the reference image

$\Gamma_s(i,j)$: index dependent RV in the approximate curvelet coefficients of the sensed image

$\gamma_r(i,j)$: sample value of the RV $\Gamma_r(i,j)$ in $S(i,j)$

$\gamma_s(i,j)$: sample value of the RV $\Gamma_s(i,j)$ in $S(i,j)$

If stated otherwise, here after in this thesis, the index (i,j) will be suppressed from the RVs $\Gamma_r(i,j)$ and $\Gamma_s(i,j)$ for notational convenience. Let the joint PDF of the RVs Γ_r and Γ_s be expressed in terms of the bivariate Gaussian distribution as [64]

$$p_{rs}(\gamma_r,\gamma_s) = \frac{1}{2\pi\sigma_r\sigma_s\sqrt{1-\rho^2}}\exp\left[-\frac{Z}{(1-\rho^2)}\right] \tag{3.1}$$

where

$$Z \equiv \frac{(\gamma_r-\mu_r)^2}{\sigma_r^2} - \frac{2\rho(\gamma_r-\mu_r)(\gamma_s-\mu_s)}{\sigma_r\sigma_s} + \frac{(\gamma_s-\mu_s)^2}{\sigma_s^2}$$

and

$$\rho = \frac{E[(\Gamma_r-\mu_r)(\Gamma_s-\mu_s)]}{\sigma_r\sigma_s}$$

where, $\rho\ (-1 \le \rho \le 1)$ is the correlation coefficient [64]; μ_r, μ_s are the means; $\sigma_r, \sigma_s\ (\sigma_s \ge 0, \sigma_r \ge 0)$ are the standard deviations of the RVs Γ_r and Γ_s, respectively and $E[\cdot]$ denotes the mathematical expectation. Now, the joint entropy of the two RVs Γ_r and Γ_s having joint PDF $p_{rs}(\Gamma_r,\Gamma_s)$ is given by the following equation [65], [66]

$$H(\Gamma_r,\Gamma_s) = -\int_{-\infty}^{+\infty}\int_{-\infty}^{+\infty} p_{rs}(\gamma_r,\gamma_s)\, ln[p_{rs}(\gamma_r,\gamma_s)]\, d\gamma_r d\gamma_s \tag{3.2}.$$

For the bivariate Gaussian PDF, the differential joint entropy given in (3.2) can be expressed as [67]

$$H(\Gamma_r,\Gamma_s) = \frac{1}{2} ln\{(2\pi e)^2|\sum_2|\} \tag{3.3}$$

where $\sum_2$ is the covariance matrix between the RVs Γ_r and Γ_s and is given by [64]

$$\sum_2 = \begin{bmatrix} \sigma_r^2 & \rho\sigma_r\sigma_s \\ \rho\sigma_r\sigma_s & \sigma_s^2 \end{bmatrix}$$
$$= \begin{bmatrix} E[(\Gamma_r - \mu_r)(\Gamma_r - \mu_r)] & E[(\Gamma_r - \mu_r)(\Gamma_s - \mu_s)] \\ E[(\Gamma_r - \mu_r)(\Gamma_s - \mu_s)] & E[(\Gamma_s - \mu_s)(\Gamma_s - \mu_s)] \end{bmatrix} \quad (3.4).$$

Now, the conditional entropy (CE) of two RVs Γ_r and Γ_s can be found as [68]

$$H(\Gamma_s|\Gamma_r) = \int_{-\infty}^{\infty} p_r(\gamma_r) h(\Gamma_s|\Gamma_r = \gamma_r)\, d\gamma_r$$
$$= \int_{-\infty}^{\infty} p_r(\gamma_r) \left[- \int_{-\infty}^{\infty} p_s(\gamma_s|\gamma_r)\, ln[p_s(\gamma_s|\gamma_r)]\, d\gamma_s \right] d\gamma_r$$
$$= - \int_{-\infty}^{\infty} \int_{-\infty}^{\infty} p_r(\gamma_r) p_s(\gamma_s|\gamma_r)\, ln[p_s(\gamma_s|\gamma_r)]\, d\gamma_r d\gamma_s$$
$$= - \int_{-\infty}^{\infty} \int_{-\infty}^{\infty} p_{rs}(\gamma_r, \gamma_s)\, ln\left[\frac{p_{rs}(\gamma_r, \gamma_s)}{p_r(\gamma_r)}\right] d\gamma_r d\gamma_s$$
$$= - \int_{-\infty}^{\infty} \int_{-\infty}^{\infty} p_{rs}(\gamma_r, \gamma_s)\, ln[p_{rs}(\gamma_r, \gamma_s)]\, d\gamma_r d\gamma_s$$
$$+ \int_{-\infty}^{\infty} \int_{-\infty}^{\infty} p_{rs}(\gamma_r, \gamma_s)\, ln[p_r(\gamma_r)]\, d\gamma_r d\gamma_s$$
$$= - \int_{-\infty}^{\infty} \int_{-\infty}^{\infty} p_{rs}(\gamma_r, \gamma_s)\, ln[p_{rs}(\gamma_r, \gamma_s)]\, d\gamma_r d\gamma_s$$
$$+ \int_{-\infty}^{\infty} \left[\int_{-\infty}^{\infty} p_{rs}(\gamma_r, \gamma_s) d\gamma_s \right] ln[p_r(\gamma_r)]\, d\gamma_r$$
$$= - \int_{-\infty}^{\infty} \int_{-\infty}^{\infty} p_{rs}(\gamma_r, \gamma_s)\, ln[p_{rs}(\gamma_r, \gamma_s)]\, d\gamma_r d\gamma_s + \int_{-\infty}^{\infty} p_r(\gamma_r)\, ln[p_r(\gamma_r)]\, d\gamma_r$$

$$= H(\Gamma_r, \Gamma_s) - H(\Gamma_r) \quad (3.5).$$

In the similar fashion, it can be shown that

$$H(\Gamma_r|\Gamma_s) = H(\Gamma_r, \Gamma_s) - H(\Gamma_s) \quad (3.6).$$

Thus, CE can be expressed as the difference between the joint and the marginal entropies. So the dependence of one RV is deducted to find the conditional entropy of other RV. Now, if the marginal distributions of RVs Γ_r and Γ_s follow the univariate Gaussian distribution, the entropy for single variable can be evaluated as [64], [65]

$$H(\Gamma_r) = -\int_{-\infty}^{\infty} p_r(\gamma_r)\, ln[p_r(\gamma_r)] d\gamma_r$$

$$= \frac{1}{2} ln(2\pi\sigma_r^2) + \frac{1}{2} E\left[\frac{(\Gamma_r - \mu_r)^2}{\sigma_r^2}\right] \quad (3.7).$$

Since, $E\left[\frac{(\Gamma_r-\mu_r)^2}{\sigma_r^2}\right] = 1$, from equation (3.7) we obtain

$$H(\Gamma_r) = \frac{1}{2}\{ln(2\pi\sigma_r^2) + 1\} \quad (3.8).$$

In the similar fashion, we obtain

$$H(\Gamma_s) = \frac{1}{2}\{ln(2\pi\sigma_s^2) + 1\} \quad (3.9).$$

From equations (3.8) and (3.9), it can be found that if the variance σ_r^2 or σ_s^2 increases, the entropy $H(\Gamma_r)$ or $H(\Gamma_s)$ increases. Now, from the above equations the CEs between $\Gamma_r$and Γ_s can be expressed as

$$H(\Gamma_s|\Gamma_r) = H(\Gamma_r, \Gamma_s) - H(\Gamma_r)$$

or

$$H(\Gamma_s|\Gamma_r) = \frac{1}{2} ln\{(2\pi e)^2|\sum_2|\} - \frac{1}{2}\{ln(2\pi\sigma_r^2) + 1\} \quad (3.10)$$

and

$$H(\Gamma_r|\Gamma_s) = H(\Gamma_r, \Gamma_s) - H(\Gamma_s)$$

or,

$$H(\Gamma_r|\Gamma_s) = \frac{1}{2} ln\{(2\pi e)^2|\sum_2|\} - \frac{1}{2}\{ln(2\pi\sigma_s^2) + 1\} \qquad (3.11).$$

The independent variable in equations (3.10) and (3.11) is $\sum_2$. From equation (3.4) it is seen that the determinant of this covariance matrix is actually the difference between the product of the variances and the product of the correlation coefficient with the covariances of the RVs Γ_r and Γ_s. In other words, this determinant is the measure of similarity of the RVs Γ_r and Γ_s. As the reference and sensed images are aligned properly, the curvelet coefficients of them become closer and the RVs Γ_r and Γ_s become closer. So the value of the determinant of the covariance matrix, $|\sum_2|$ becomes lower and subsequently, the conditional entropies $H(\Gamma_r|\Gamma_s)$ or $H(\Gamma_r|\Gamma_s)$ become lower.

Now, the reference and the sensed images must have a linear dependency as they are captured from the same scene. Again, in this thesis, linear geometric distortion is considered for the sensed image. Hence, the objective function may be formed as the minimization of a linear combination of CEs. It is noted that the RVs, viz., Γ_r and Γ_s considered here are indexed dependent. Hence, the CEs from the equations (3.10) and (3.11) are combined to construct the indexed dependent objective function given by

$$F(i,j) = \alpha \cdot H(\Gamma_r|\Gamma_s) + (1-\alpha) \cdot H(\Gamma_s|\Gamma_r) \qquad (3.12)$$

where α $(0 \leq \alpha \leq 1)$ is the weight parameter. If the reference image is given more importance comparing to the sensed image, α approaches 1. Again if the sensed image is given more importance than the reference image, α approaches 0. In general, α may be set as 0.5 to give equal importance to both of the reference and sensed images. Now all the $F(i,j)$ found for the entire coefficients of the approximate level of the curvelet transform are summed up to calculate the final value of the objective function which is given by

$$F = \sum_{i=1}^{D_x} \sum_{j=1}^{D_y} F(i,j) \qquad (3.13).$$

3.3 Parameter Estimation

In order to register the images, the index dependent objective function $F(i,j)$ is needed to be estimated. This function is a linear combination of conditional entropies between the approximate curvelet coefficients of reference and sensed images. For determining the value of this index dependent objective function, the following parameters are needed to be calculated for each of the coefficient. Each of the following parameters are defined around the neighboring region of point (i,j) defined by square window $S(i,j)$.

$\mu_r(i,j)$: Arithmetic mean of the coefficients of the approximate level of the curvelet transform of the reference image

$\mu_r(i,j)$: Arithmetic mean of the coefficients of the approximate level of the curvelet transform of the sensed image

$\sigma_r(i,j)$: Standard deviation of the coefficients of the approximate level of the curvelet transform of the reference image

$\sigma_s(i,j)$: Standard deviation of the coefficients of the approximate level of the curvelet transform of the sensed image

$\rho_{rs}(i,j)$: Correlation coefficient between the coefficients of the approximate level of the curvelet transform of the reference and the sensed images

By using maximum likelihood (ML) estimation [64] method, the parameters are defined as following [64]

$$\mu_r(i,j) = \frac{1}{M} \sum_{(k,l)\in S(i,j)} \gamma_r(k,l) \qquad (3.14)$$

$$\mu_s(i,j) = \frac{1}{M} \sum_{(k,l)\in S(i,j)} \gamma_s(k,l) \qquad (3.15)$$

$$\sigma_r^2(i,j) = \max\left(\frac{1}{M}\sum_{(k,l)\in S(i,j)}[\gamma_r(k,l) - \mu_r(i,j)]^2\ , 0\right) \tag{3.16}$$

$$\sigma_s^2(i,j) = \max\left(\frac{1}{M}\sum_{(k,l)\in S(i,j)}[\gamma_s(k,l) - \mu_s(i,j)]^2\ , 0\right) \tag{3.17}$$

$$\rho_{rs}(i,j) = \min\left(\max\left(\frac{\sigma_{rs}(i,j)}{\sigma_r(i,j)\sigma_s(i,j)}, -1\right), 1\right) \tag{3.18}$$

where

$$\sigma_{rs}(i,j) = \frac{1}{M}\sum_{(k,l)\in S(i,j)} \begin{aligned}&[\gamma_r(k,l)\gamma_s(k,l) - \gamma_r(k,l)\mu_s(i,j) - \\ &\gamma_s(k,l)\mu_r(i,j) + \mu_r(i,j)\mu_s(i,j)]\end{aligned}$$

where M is the total number of coefficients in the local neighboring region in $S(i,j)$.

3.4 Distortion Function

In order to obtain synthetically distorted images, linear distortion function is applied over the images uniformly. We choose the linear distortion function, viz., the affine transform because it gives a low computational load; at the same time most of the practical distortions may be realized by this transformation. In this thesis, the distortion function is applied uniformly over the image. It is to be noted that such a uniform distortion may be applied locally where nonuniform or piecewise-linear distortion is considered. Let (x', y') be the geometrically distorted location of the index (x, y). The affine transform is then given by the following equation [33], [34]

$$\begin{bmatrix} x' \\ y' \\ 1 \end{bmatrix} = A \cdot \begin{bmatrix} x \\ y \\ 1 \end{bmatrix} \tag{3.19}$$

where

$$A = \begin{bmatrix} \cos\theta & \sin\theta & 0 \\ -\sin\theta & \cos\theta & 0 \\ 0 & 0 & 1 \end{bmatrix} \cdot \begin{bmatrix} c_x & 0 & 0 \\ 0 & c_y & 0 \\ 0 & 0 & 1 \end{bmatrix} \cdot \begin{bmatrix} 1 & s_h & 0 \\ 0 & 1 & 0 \\ 0 & 0 & 1 \end{bmatrix} \cdot \begin{bmatrix} 1 & 0 & 0 \\ s_v & 1 & 0 \\ 0 & 0 & 1 \end{bmatrix} \cdot \begin{bmatrix} 1 & 0 & t_x \\ 0 & 1 & t_y \\ 0 & 0 & 1 \end{bmatrix} \quad (3.20).$$

Here, θ is the angle of rotation, c_x is the horizontal scaling parameter, c_y is the vertical scaling parameter, s_h is the horizontal shearing parameter, s_v is the vertical shearing parameter, t_x is the translation in x-direction and t_y is the translation in y-direction.

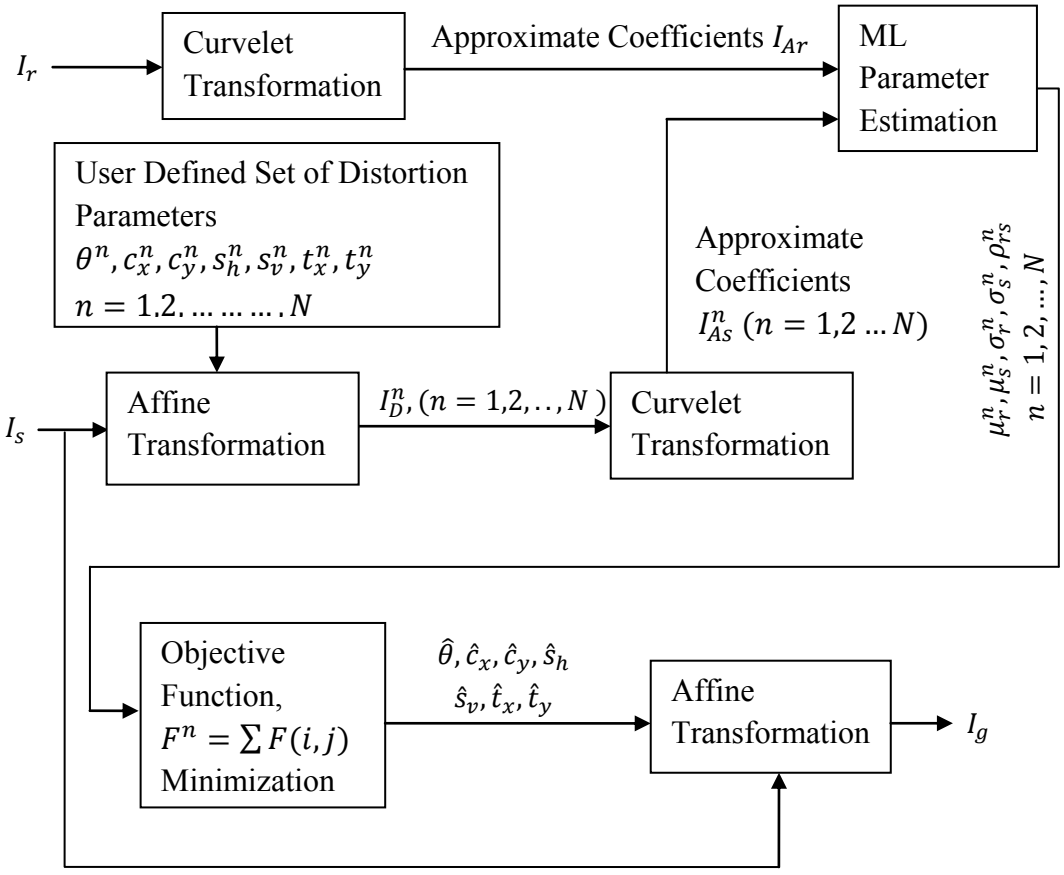

Figure 3.1: Block diagram of the proposed algorithm

In the proposed algorithm at first, a user defined set of distortions is carried out on the sensed image (I_s) using the affine transform and N sets of the parameter grid, viz., $\theta^n, c_x^n, c_y^n, s_h^n, s_v^n, t_x^n, t_y^n$ $(n = 1,2, \dots \dots \dots, N)$. Thus, the distorted images $I_D^n (n = 1,2, \dots \dots, N)$ are found. Now, the reference image (I_r) as well as all the distorted images (I_D^n) are gone through curvelet transform. Then, the approximate level coefficients (I_{Ar}) of the curvelet transform of the reference image and approximate level coefficients

($I_{As}^n, n = 1,2, \dots \dots, N$) of all the distorted images are sent to the ML estimator which estimates N set of statistical parameters ($\mu_r^n, \mu_s^n, \sigma_r^n, \sigma_s^n, \rho_{rs}^n, n = 1,2, \dots \dots, N$). After that the values of the objective function ($F^n, n = 1,2, \dots \dots, N$) for all the sets of statistical parameters are calculated. Then, the lowest of all the N values of the objective function is calculated and the corresponding distortion parameters give the desired distortion parameters ($\hat{\theta}, \hat{c}_x, \hat{c}_y, \hat{s}_h, \hat{s}_v, \hat{t}_x, \hat{t}_y$). Using these desired distortion parameters the affine transform is carried out on the sensed image (I_s) which gives the registered image I_g. A simple block diagram of this algorithm is shown in the Figure 3.1.

Some points are to be noted about this registration algorithm:

- The computational load depends on the number of sets of distortion parameters (N) in the parameter grid used in the algorithm. If N increases, the computational load increases.
- In the proposed algorithm discrete values in the entire search space of the parameter grid are considered, and hence the best local minima of the objective function may be chosen for finding the desired distortion parameters. In this regard, the proposed algorithm may not provide an optimal registration performance, but it is ensured to provide the best suboptimal result.
- Another thing is to be noted that the ML detection is done only on the approximate level of the curvelet transform. This is due to the fact that, previous wavelet-like methods also used only the approximate level and in this thesis, we also followed that approach. Moreover, the detailed level coefficients of the curvelet transform are complex valued. So the calculation of objective function using detailed level coefficients is mathematically difficult. Using only the real valued approximate level coefficients decrease the computational complexity and register the images with good performance.
- There are two linear blocks in the block diagram of the proposed method namely „Affine Transform“ and „Curvelet Transformation“. These two blocks are placed one after another. As these boxes are linear, they could have been placed by swapping their position. In that case the sensed image I_s would have been at first curvelet transformed and then the approximate level coefficients would have been sent to the „Affine Transform“ block. So the set of parameters in the grid

would have been applied on the coefficients of the approximate level of the curvelet transform of the sensed image. This position change could have saved some computational load as the dimension of the approximate curvelet level is smaller than that of the original image. But there is a problem in this process. We can consider the approximate level of the curvelet transform as a miniature version of the total image. So every coefficient of the approximate level represents a large area in the pixel domain. That means slight geometrical change in the coefficients of the approximate level would indicate a large change in the pixel domain. So it would be difficult to detect slight geometrical changes in the pixel domain if affine transform is carried out on the approximate level curvelet coefficients rather than on the pixel domain. Hence, the affine transform is first carried out on the sensed image and then the curvelet transform is carried out on the distorted images.

- Another thing should be mentioned that the algorithm could be arranged in an iterative process, in which the objective function would have to be checked in every iteration and depending on the change in the objective function the value of the parameter set would have to be updated. But, there is no guarantee that changing the distortion parameter would monotonically decrease the value of the objective function and ultimately converge to an optimal result. Moreover, if there are several lower regions in the plot of the distortion versus objective function, the iterative process may produce wrong result by finding the solution in a local lower point instead of finding the solution in global lower point.

3.5 Conclusion

In this chapter, the analysis of the proposed registration method has been presented. At the beginning of this chapter, the objective function for the image registration algorithm is obtained using the conditional entropies among the approximate curvelet coefficients of the reference and sensed images. Afterwards, the parameters are estimated using ML estimator. The distortion function used for the proposed registration algorithm is given with necessary equations. At last, the block diagram of the proposed algorithm with necessary explanations is presented.

CHAPTER 4: EXPERIMENTAL RESULTS

4.1 Introduction

In order to evaluate the performance of the algorithm proposed in Chapter 3, experiments are carried out on commonly used test images. Both subjective and objective evaluations of the distorted and registered images are done. The subjective evaluation is done through visualization of the reference, sensed and registered images. On the other hand, the objective evaluation is done by the comparison of the values of some traditional performance metrics. The performance metrics include the root mean square distortion (RMSD), normalized root mean square distortion (NRMSD), normalized cross correlation coefficient (NCCC) and percent relative root mean square error (PRRMSE) [52], [69]. The distortions considered in this thesis are rotation, scaling, translation, and shearing of images. Both the single and combination of distortions are considered here. To calculate the objective function from the local neighboring region of the approximate level curvelet coefficients the experiments are carried out using local windows of sizes $3 \times 3, 5 \times 5$ and 7×7. In the following sections of this chapter, details of the test data, mathematical definitions of the performance metrics, entropy curves for the objective functions of the proposed algorithm, reference and registered images and comparison with three existing methods are presented and the performance of the proposed method for real registration case will be discussed.

4.2 Test Data and Distortions

In this thesis, two types of sensed images are considered:

(i) Distorted version of reference image using a known set of parameters of affine transformation.

(ii) Distorted version of images captured in different modes, moments, views or sensors, using a known set of parameters.

All the test images are available in different sources given in www.imagefusion.org and a few of these images are shown in Appendix A. In the case of „single distortion", rotation, translation, shearing and scaling is taken into account separately. While in „combination of distortions" four types of distortions are considered namely,

(i) Translations in both x and y axes,
(ii) Translation in y-axis along with rotation,
(iii) Translation in x-axis along with horizontal shear, and
(iv) Translations in both x and y axes along with rotation.

4.3 Performance Metrics

The mathematical expressions of the performance metrics, viz., RMSD, NRMSD, NCCC and PRRMSE considered in this thesis are as follow [52], [69]

$$RMSD = \sqrt{\frac{\sum_{x,y}\left[I_r - I_g\right]^2}{X \times Y}} \tag{4.1}$$

$$NRMSD = \frac{RMSD}{I_{max} - I_{min}} \tag{4.2}$$

$$NCCC = \frac{\sum_{x,y}[I_r(x,y) - \bar{I}_r][I_g(x,y) - \bar{I}_g]}{\left\{\sum_{x,y}[I_r(x,y) - \bar{I}_r]^2 \ \sum_{x,y}\left[I_g(x,y) - \bar{I}_g\right]^2\right\}^{0.5}} \tag{4.3}$$

$$PRRMSE = \sqrt{\frac{\frac{1}{XY}\sum_{x=1}^{X}\sum_{y=1}^{Y}\left(I_g(x,y) - I_r(x,y)\right)^2}{\sum_{x=1}^{X}\sum_{y=1}^{Y} I_r(x,y)}} \tag{4.4}$$

where $I_r(x,y)$ denotes the pixel intensity of the reference image at spatial index (x,y), $I_g(x,y)$ denotes the pixel intensity of the registered image at that location, I_{max} and

I_{min} are the maximum and minimum pixel value in the entire image. $\bar{I}_r$ and $\overline{I_g}$ are the mean of the pixel values of the reference and sensed images.

Each of the performance metrics mentioned above has different significance concerning the registration performance. The RMSD, NRMSD and PRRMSE are the measure of the distortion of the registered image from the reference image. As the reference and sensed images may be obtained in different modes, they already have dissimilarity even if they are aligned. So depending upon the registration algorithm, the more the two images is properly aligned, the lower the value of the RMSD, NRMSD and PRRMSE will be. On the other hand, the NCCC measure the closeness of the reference and registered images. The more the two images are properly overlaid, the higher the NCCC becomes.

4.4 Single Distortion

In this section, the experimental results considering the image registration for rotation, translation in single direction, shearing in horizontal or vertical direction and scaling in x or y direction in the sensed images are given.

4.4.1 Rotation

Figures 4.1 and 4.2 show the variation in the value of objective function F due to the variation in the angle of rotation θ for image of same modality and images of different modalities respectively. It may be observed that in Figure 4.1 (a) the minimum value of the objective function is in -15^0 of angle of rotation. It means that the sensed image has a clockwise rotation of 15^0 and a counterclockwise rotation of -15^0 would register it. In a similar fashion, the other figures of the objective function can be interpreted. Moreover, for all window sizes the lowest value of the objective function occur at the same angle of rotation. In Figures 4.3 and 4.4, the reference, sensed and registered images are shown. It can be seen from these figures that the sensed images are registered properly.

4.4.2 Translation in x or y direction

Figures 4.5 and 4.6 show the variation in the value of objective function F due to the variation in the translation in x or y direction for image of same modality and images of different modalities, respectively. It may be observed that in Figure 4.5 (a) the minimum value of the objective function is in -30 pixels of translation in x direction (t_x). It means that the sensed image has a translation in $+x$ direction of 30 pixels and a translation of 30 pixels in $-x$ direction would register it. In a similar fashion, the other figures of the objective function can be interpreted. Moreover, for all window sizes the lowest value of the objective function occur at the translation (t_x or t_y) required for registration. In Figures 4.7 and 4.8, the reference, sensed and registered images are shown. It can be seen from these figures that the sensed images are registered properly.

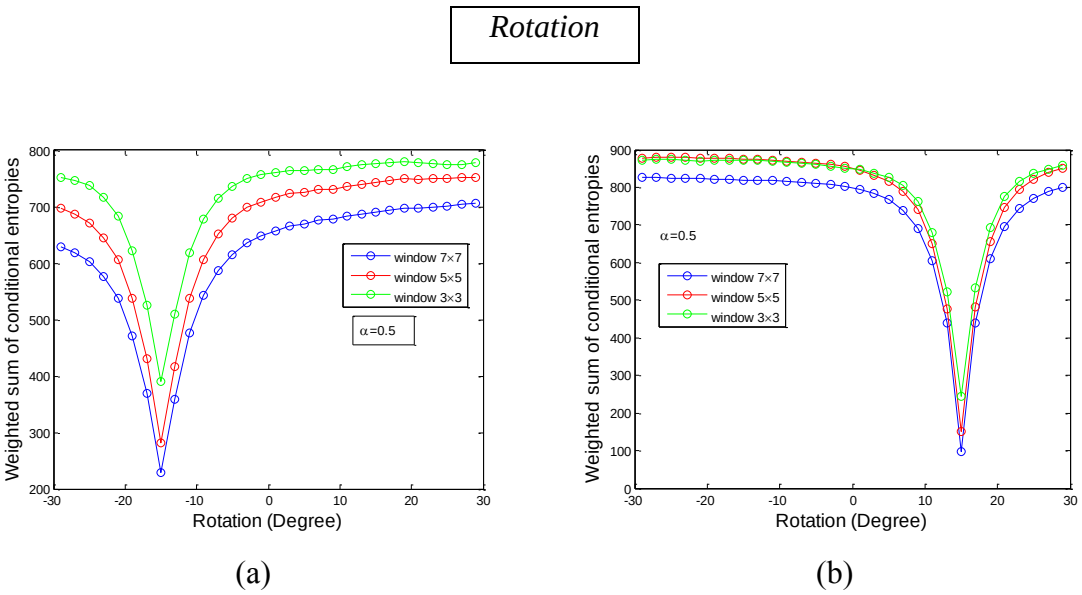

Figure 4.1: Objective function versus the angle of rotation (θ) for images of same modality (a) Toy (image 1) (b) SAR1 (image 1)

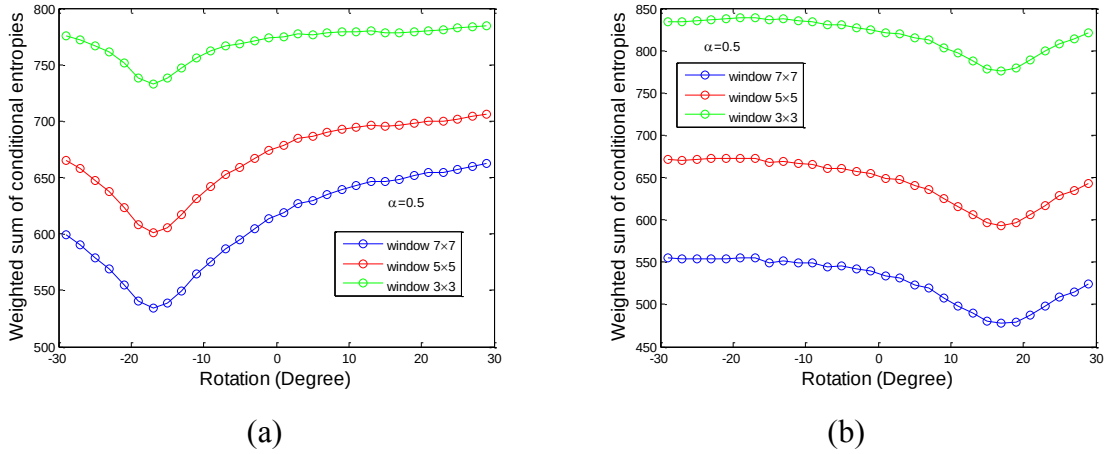

Figure 4.2: Objective function versus the angle of rotation (θ) for images of different modalities (a) Navigation (images 1 and 2) (b) MRI

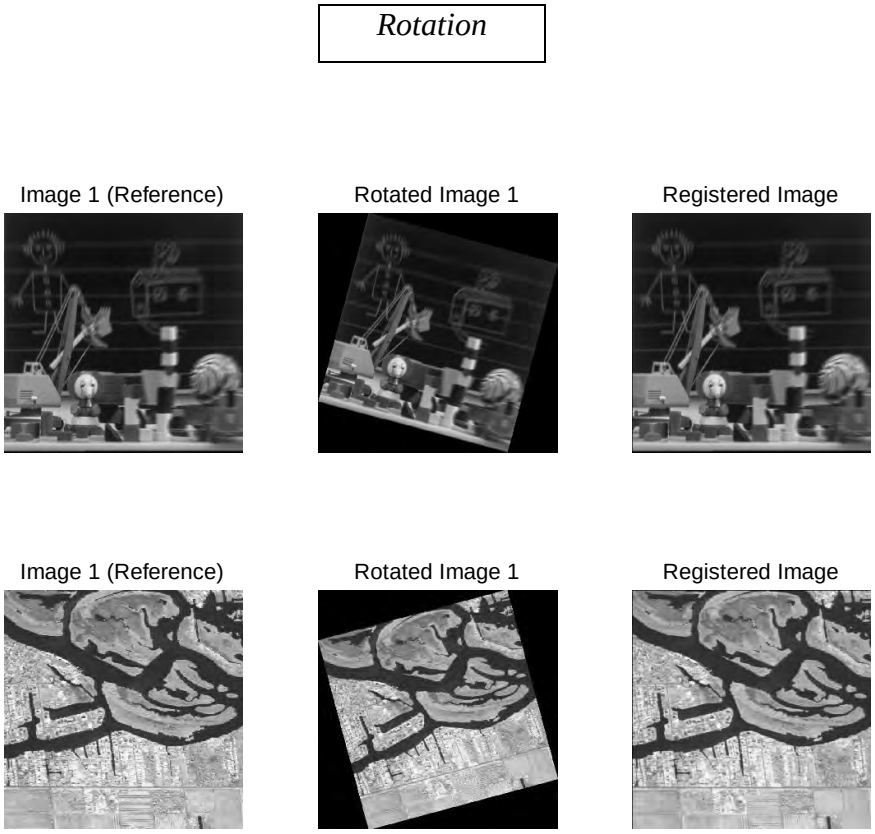

Figure 4.3: Reference, sensed (rotated) and registered images for images of same modality (a) Toy (image 1) (b) SAR1 (image 1)

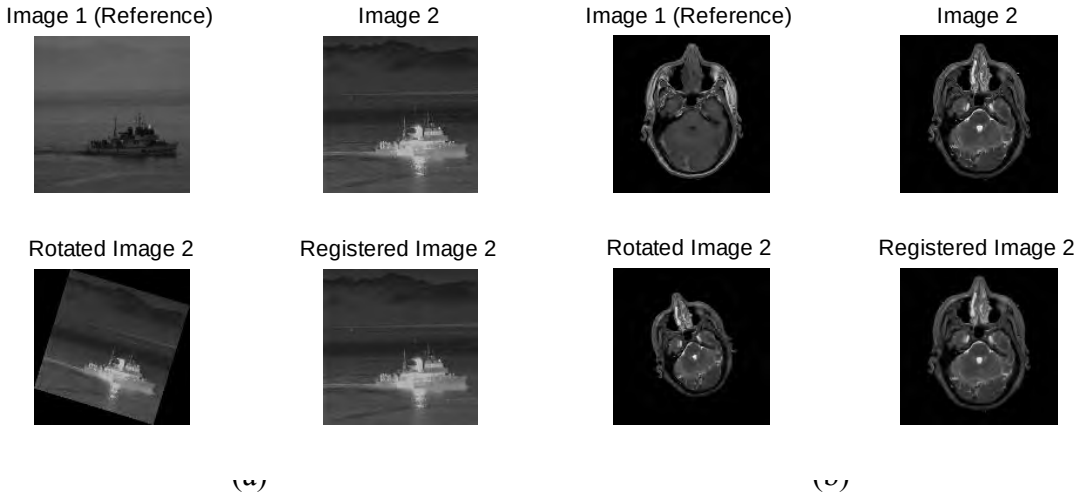

(a) (b)

Figure 4.4: Reference, sensed (rotated) and registered images for images of different modalities (a) Navigation (images 1 and 2) (b) MRI

Translation in x or y direction

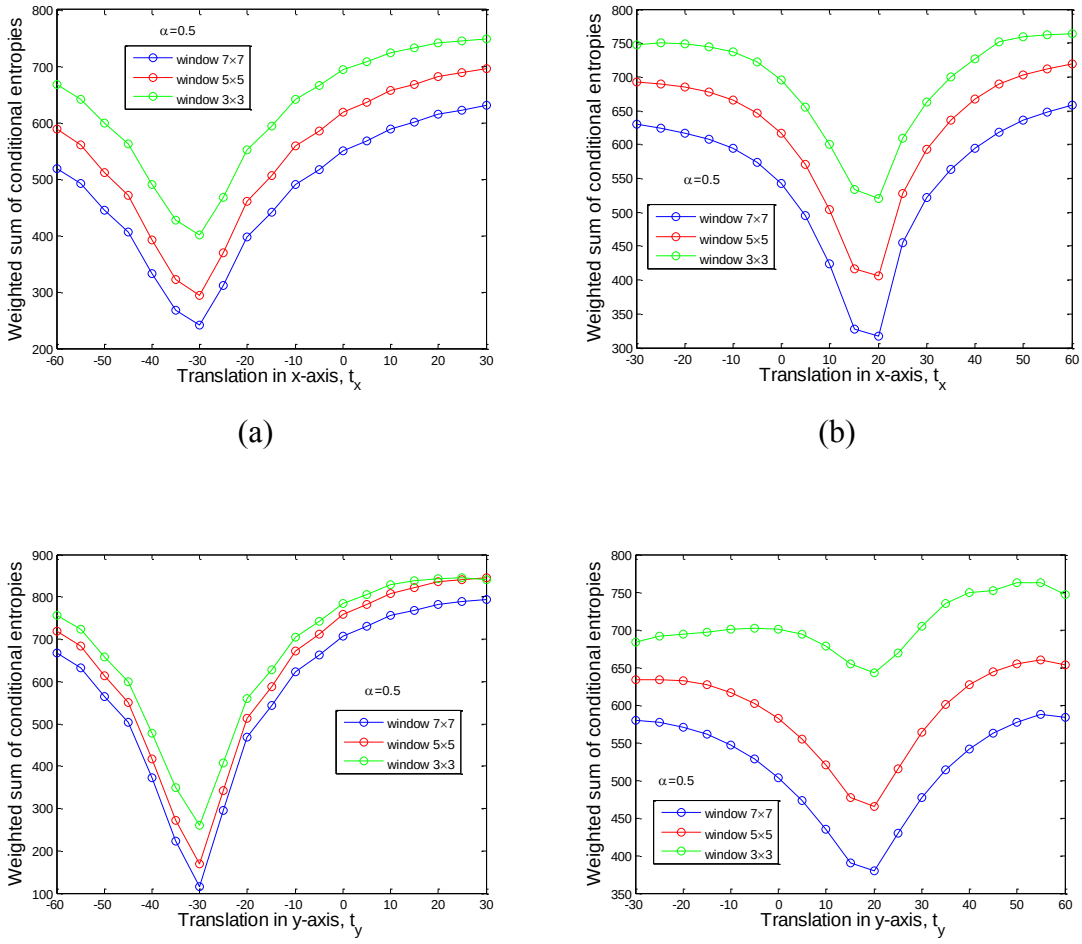

Figure 4.5: Objective function versus translation in x-axis (t_x) or translation in y-axis (t_y) for images of same modality (a) Toy (image 1) (b) Room (image 1) (c) SAR1 (image 1) (d) Navigation (image 1)

Translation in x or y direction

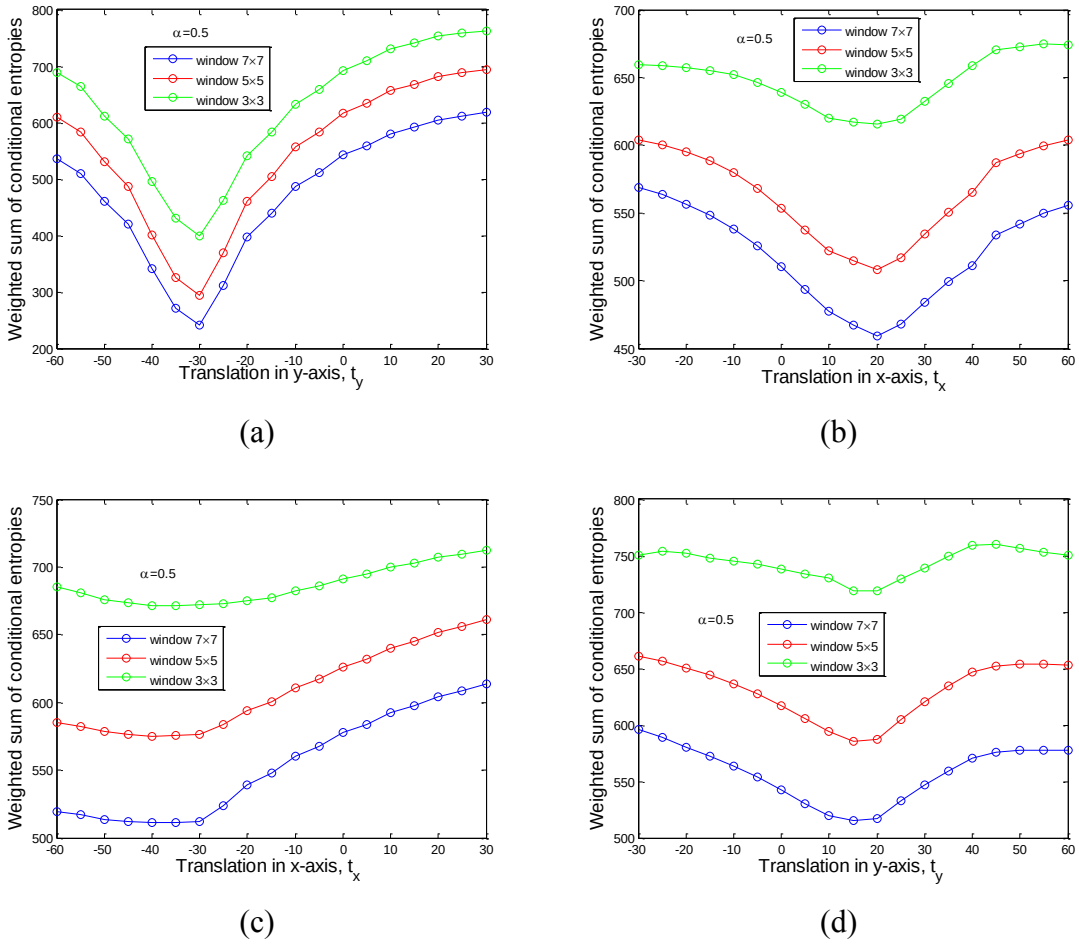

Figure 4.6: Objective function versus translation in x-axis (t_x) or translation in y-axis (t_y) for images of different modalities (a) Toy (images 1 and 3) (b) Room (c) SAR2 (d) Navigation (images 1 and 2)

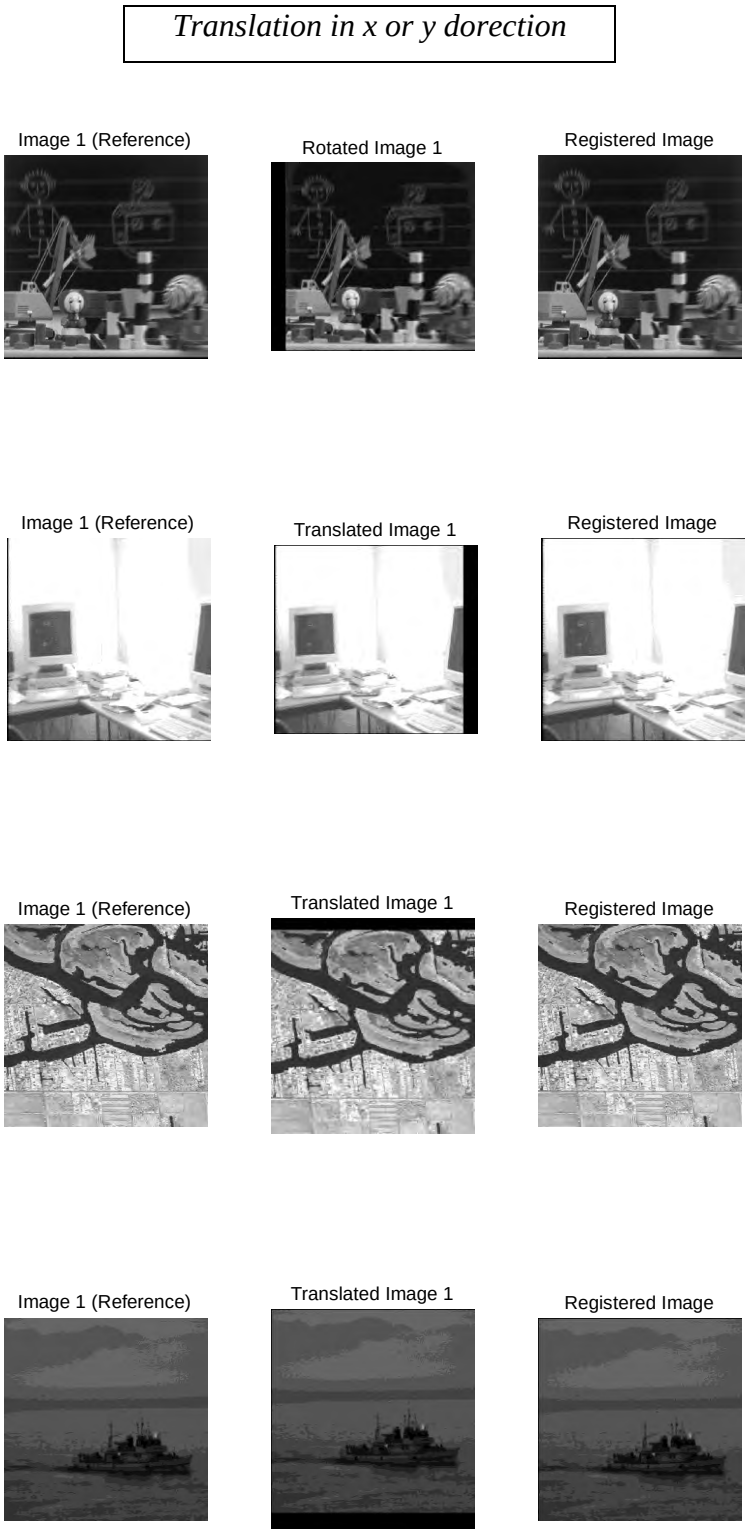

Figure 4.7: Reference, sensed (translated in x or y direction) and registered images for images of same modality (a) Toy (image 1) (b) Room (image 1) (c) SAR1 (image 1) (d) Navigation (image 1)

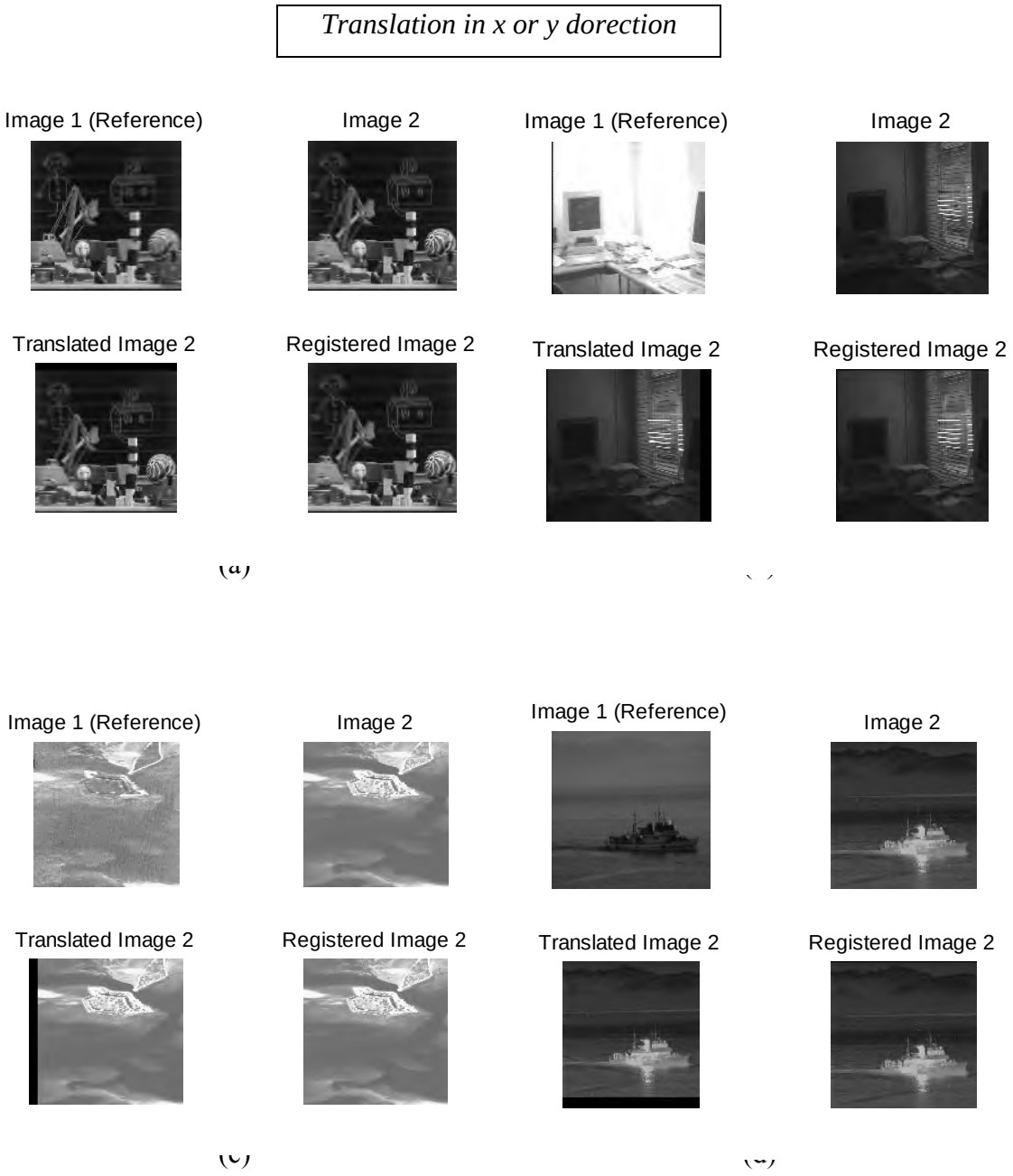

Figure 4.8: Reference, sensed (translated in x or y direction) and registered images for images of different modalities (a) Toy (images 1 and 3) (b) Room (c) SAR2 (d) Navigation (images 1 and 2)

4.4.3 Horizontal or vertical shearing

Figures 4.9 and 4.10 show the variation in the value of objective function F due to the variation in shear in horizontal (s_h) or shear in vertical (s_v) direction for image of same modality and images of different modalities, respectively. It may be observed that in Figure 4.9 (a) the minimum value of the objective function is in -0.5 of shear in horizontal direction. It means that the sensed image has a shear of 0.5 in horizontal direction and a opposite shear of -0.5 in horizontal direction would register it. In the similar fashion, the other figures of the objective function can be interpreted. Moreover, for all window sizes the lowest value of the objective function occur at the shearing parameter (s_h or s_v) required for the registration. In Figures 4.11 and 4.12, the reference, sensed and registered images are shown. It can be seen from these figures that the sensed images are registered properly.

4.4.4 Scaling in x or y axis

Figures 4.13 and 4.14 show the variation in the value of objective function F due to the variation in scale in x-axis (c_x) or scale in y-axis (c_y) for image of same modality and images of different modalities, respectively. It may be observed that in Figure 4.13 (a) the minimum value of the objective function is found in scaling on x-direction, $c_x = 2$. It means that the sensed image has a scaling of 0.5 (inverse of 2) in horizontal direction and an opposite shear of $c_x = 2$ in x-axis would register it. In the similar fashion, the other figures of the objective function can be interpreted. Moreover, for all window sizes the lowest value of the objective function occur at the scaling parameter (c_x or c_y) required for the registration. In Figures 4.15 and 4.16, the reference, sensed and registered images are shown. It can be seen from these figures that the sensed images are registered properly.

Horizontal or vertical shearing

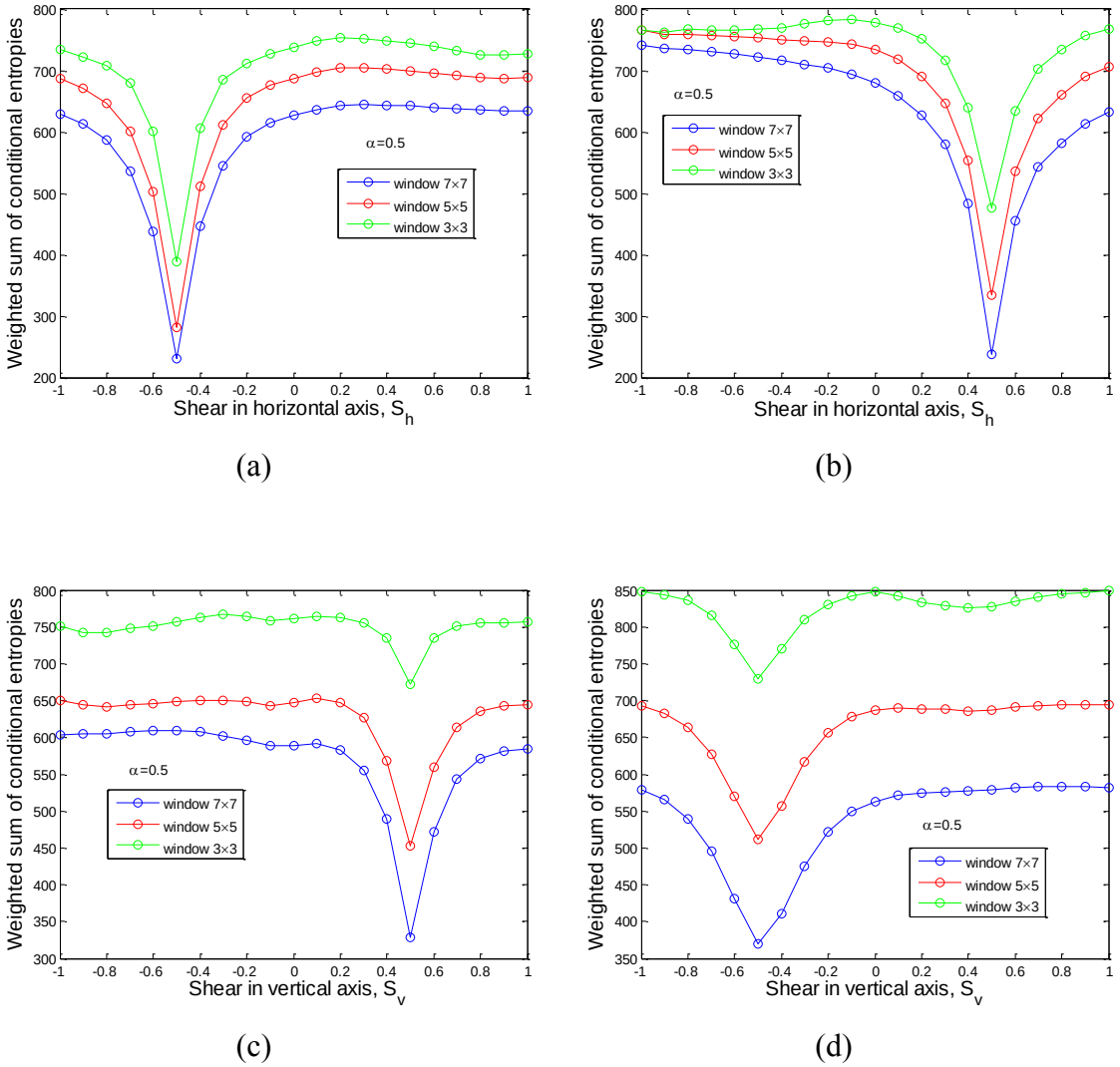

Figure 4.9: Objective function versus shear in horizontal direction (S_h) or shear in vertical direction (S_v) for images of same modality (a) Toy (image 1) (b) Room (image 1) (c) Tree (image 1) (d) MRI (image 1)

Horizontal or vertical shearing

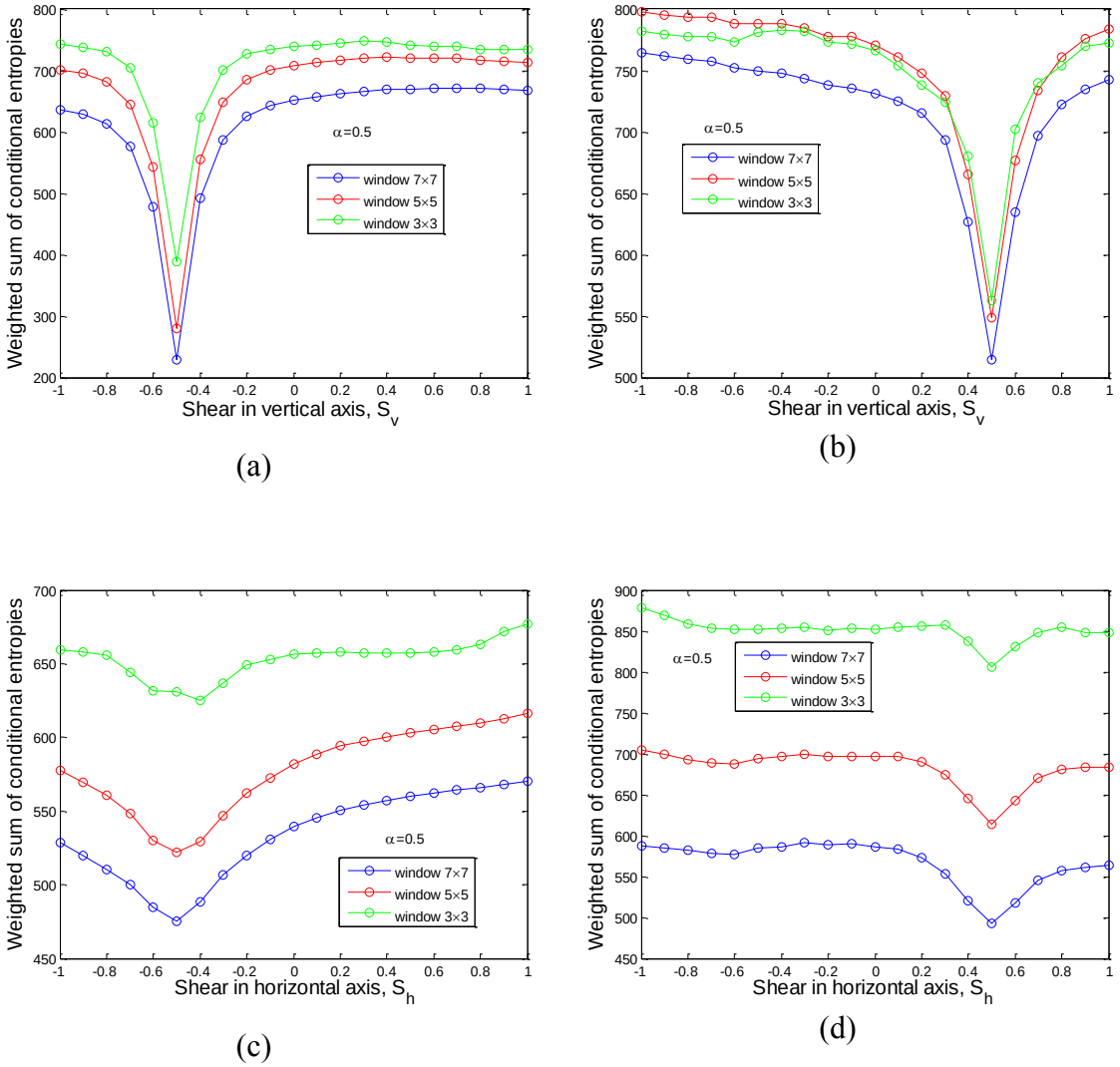

Figure 4.10: Objective function versus shear in horizontal direction (S_h) or shear in vertical direction (S_v) for images of different modalities (a) Toy (images 1 and 2) (b) SAR2 (c) Navigation (images 1 and 3) (d) MRI

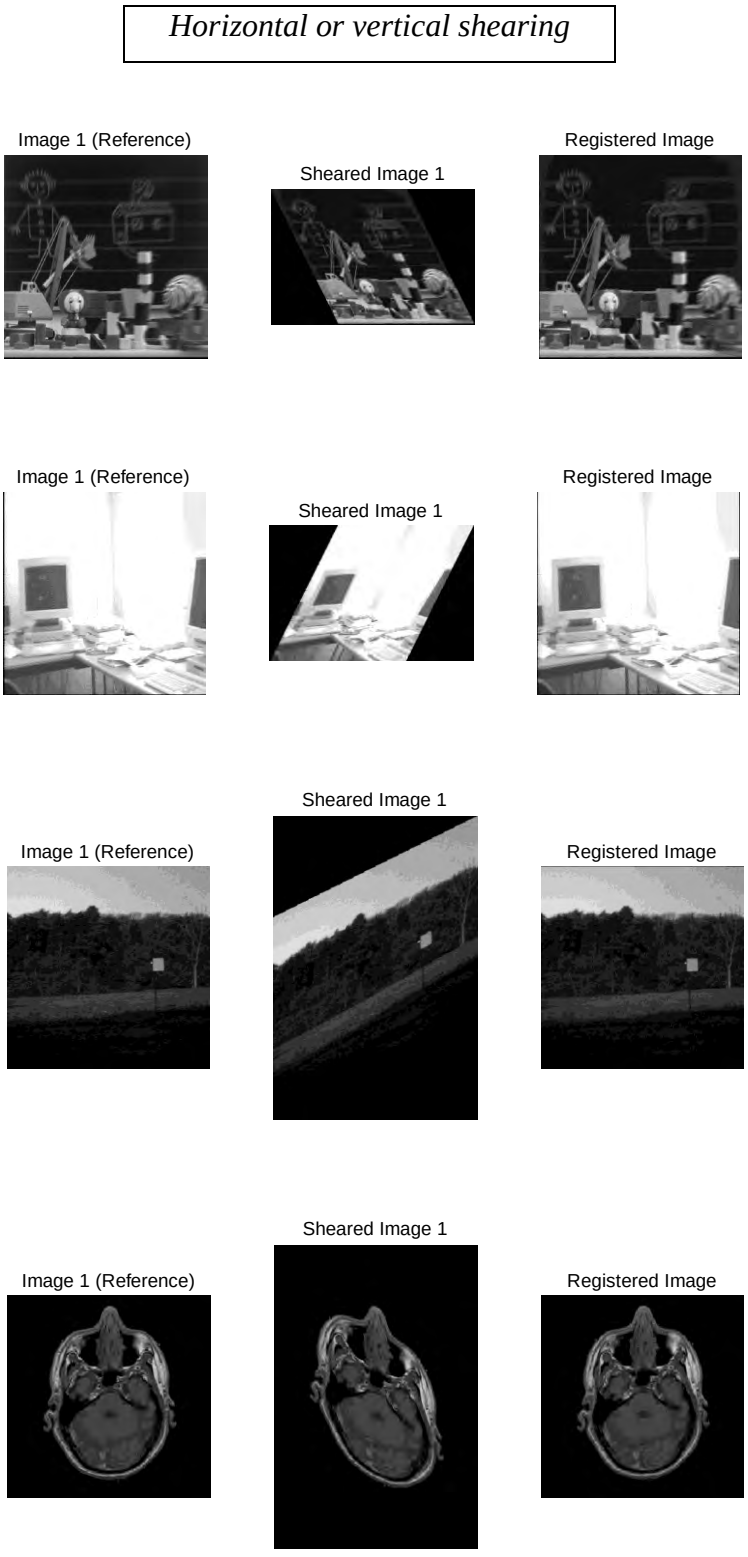

Figure 4.11: Reference, sensed (sheared in horizontal or vertical direction) and registered images for images of same modality (a) Toy (image 1) (b) Room (image 1) (c) Tree (image 1) (d) MRI (image 1)

Horizontal or vertical shearing

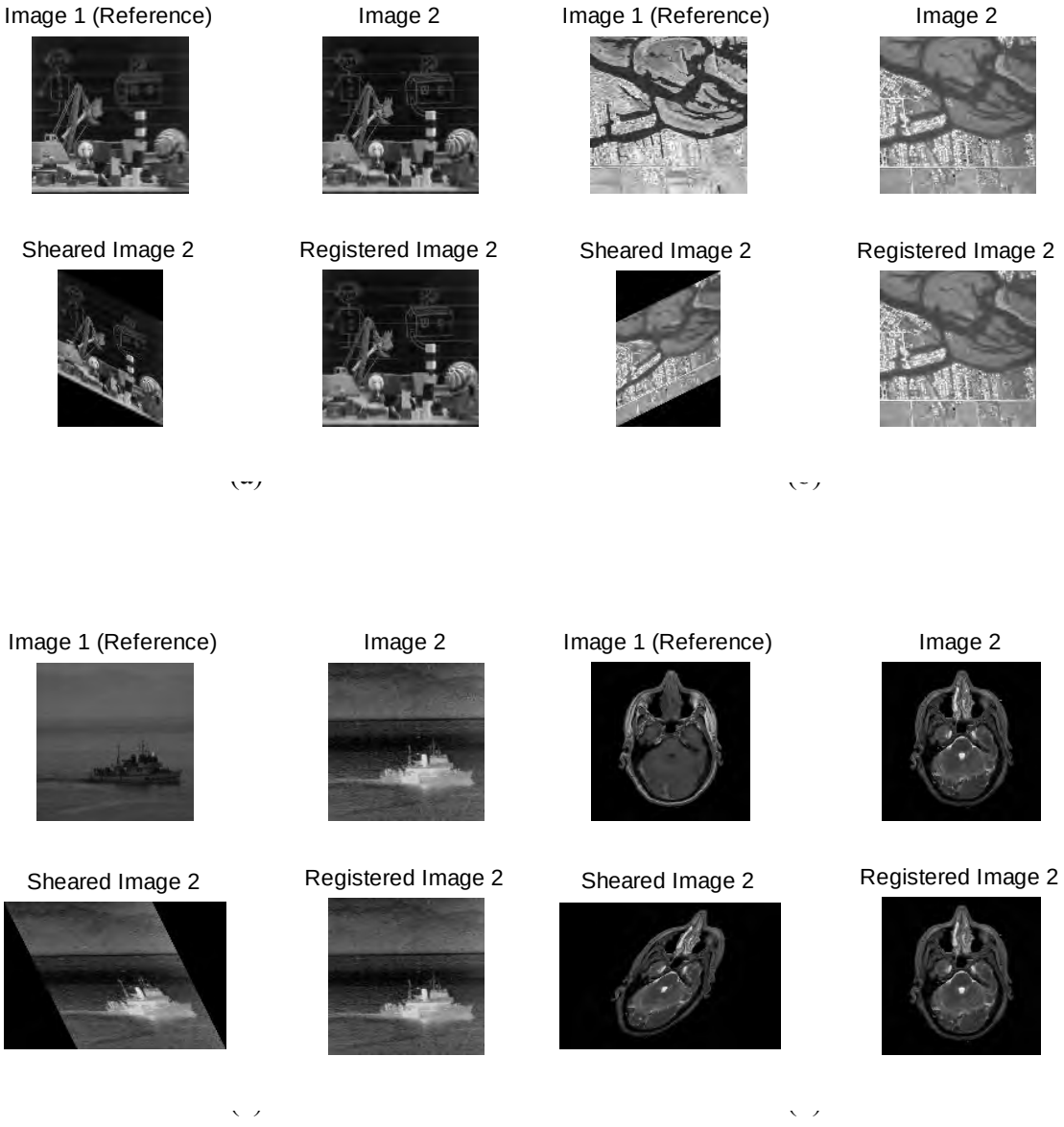

Figure 4.12: Reference, sensed (sheared in horizontal or vertical direction) and registered images for images of different modalities (a) Toy (images 1 and 2) (b) SAR 2 (c) Navigation (images 1 and 3) (d) MRI

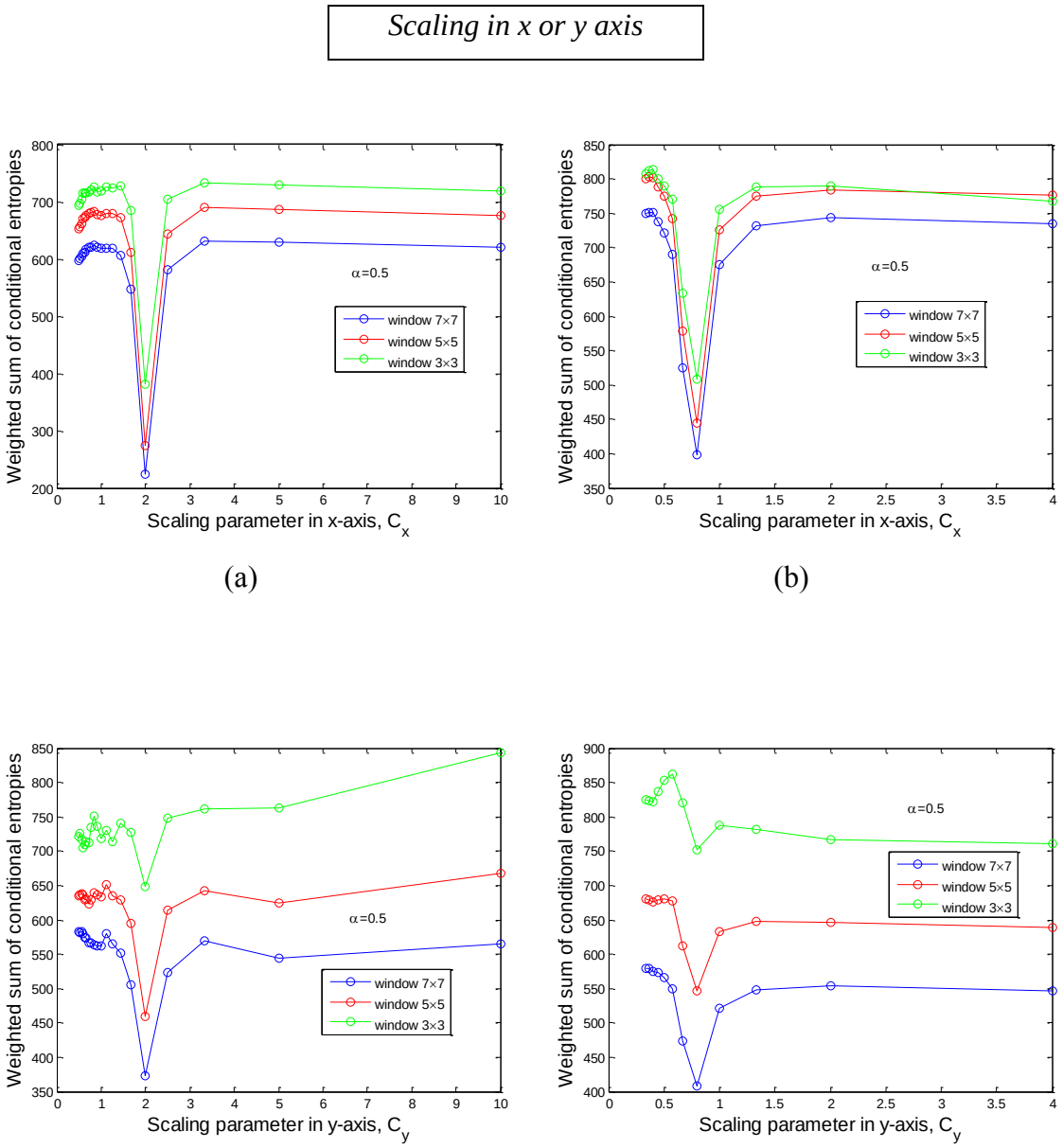

Figure 4.13: Objective function versus scale in x-axis (c_x) or scale in y-axis (c_y) for images of same modality (a) Toy (image 1) (b) SAR1 (image 1) (c) Navigation (image 1) (d) MRI (image 1)

Scaling in x or y axis

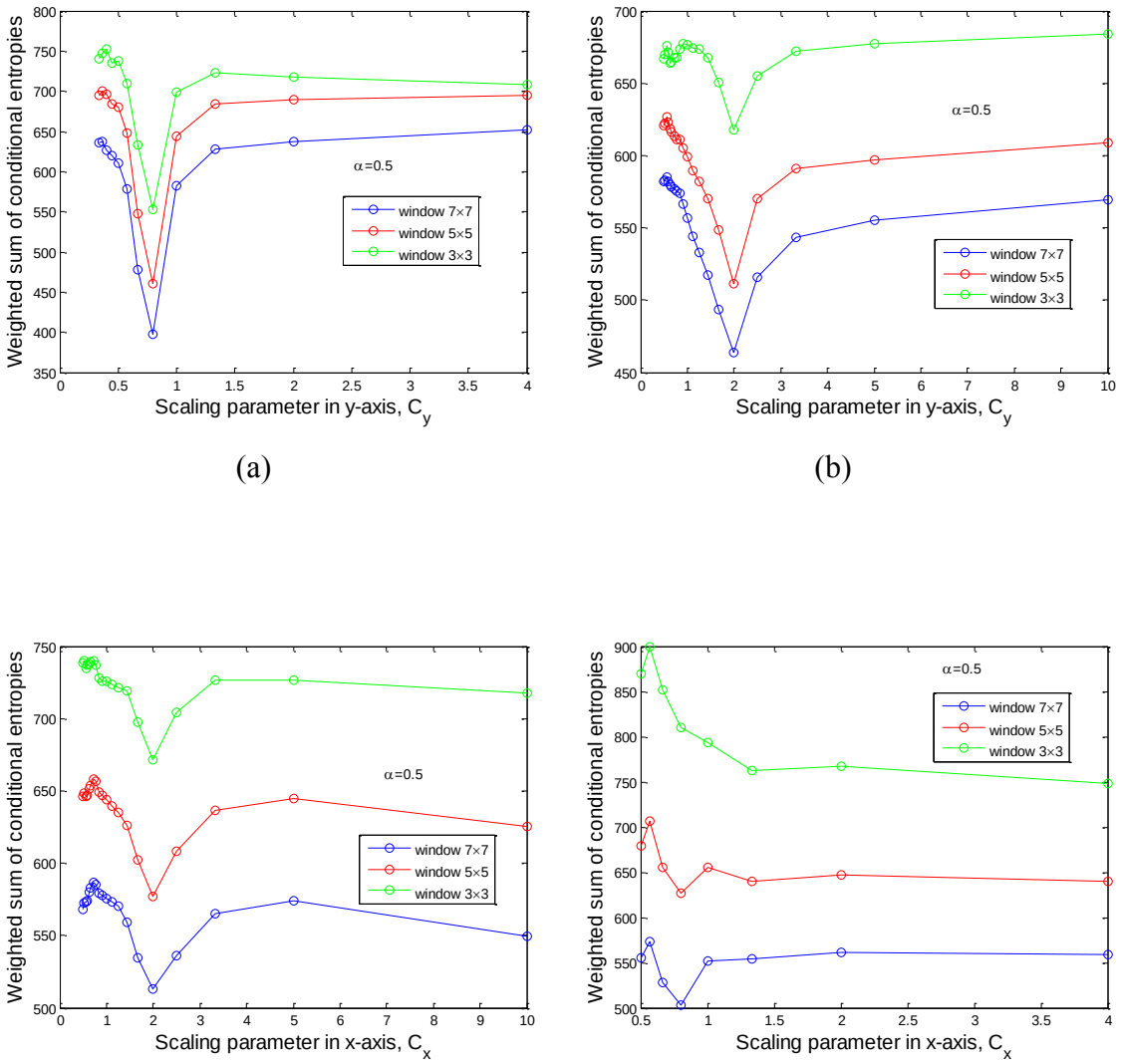

Figure 4.14: Objective function versus scale in x-axis (c_x) or scale in y-axis (c_y) for images of different modalities (a) Toy (images 1 and 3) (b) Room (c) SAR2 (d) MRI

Scaling in x or y axis

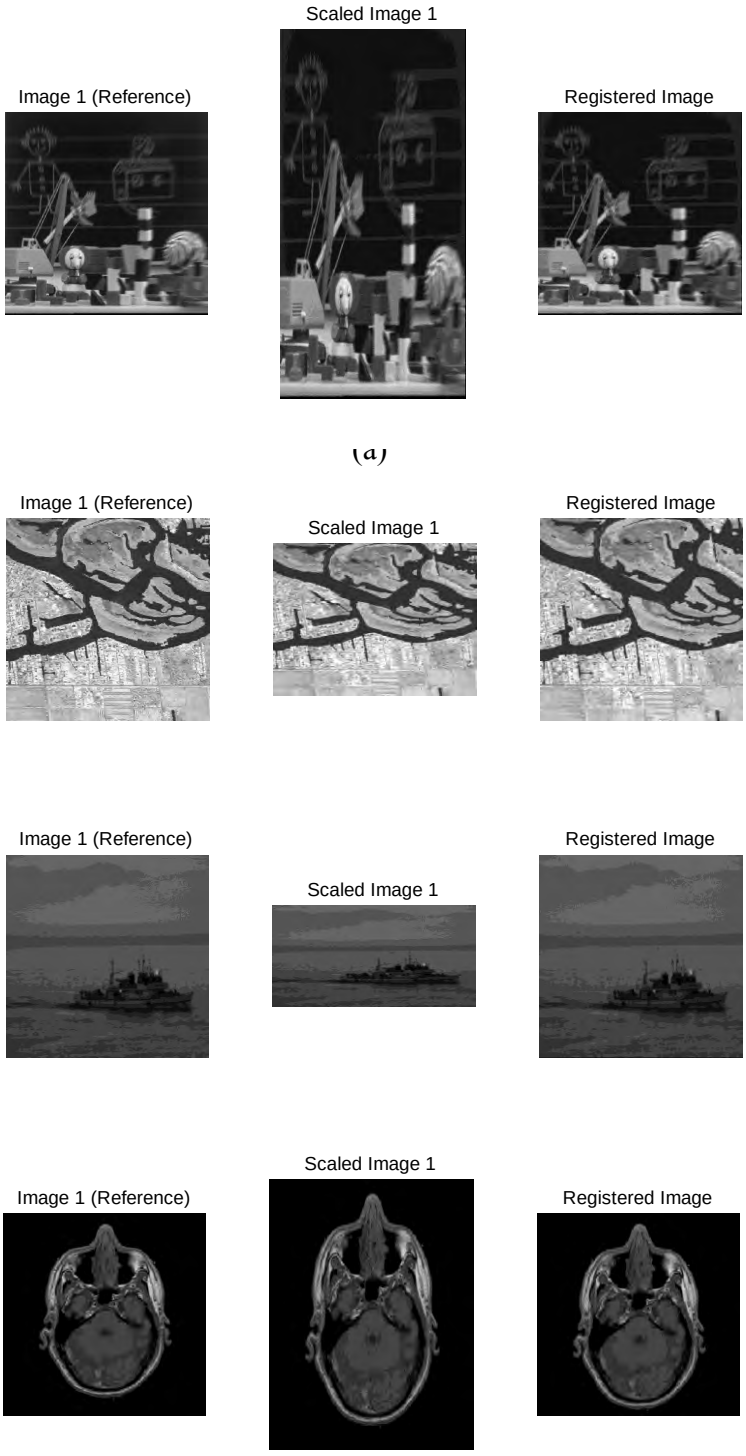

Figure 4.15 Reference, sensed (scaled in x or y direction) and registered images for images of same modality (a) Toy (image 1) (b) SAR1 (image 1) (c) Navigation (image 1) (d) MRI (image 1)

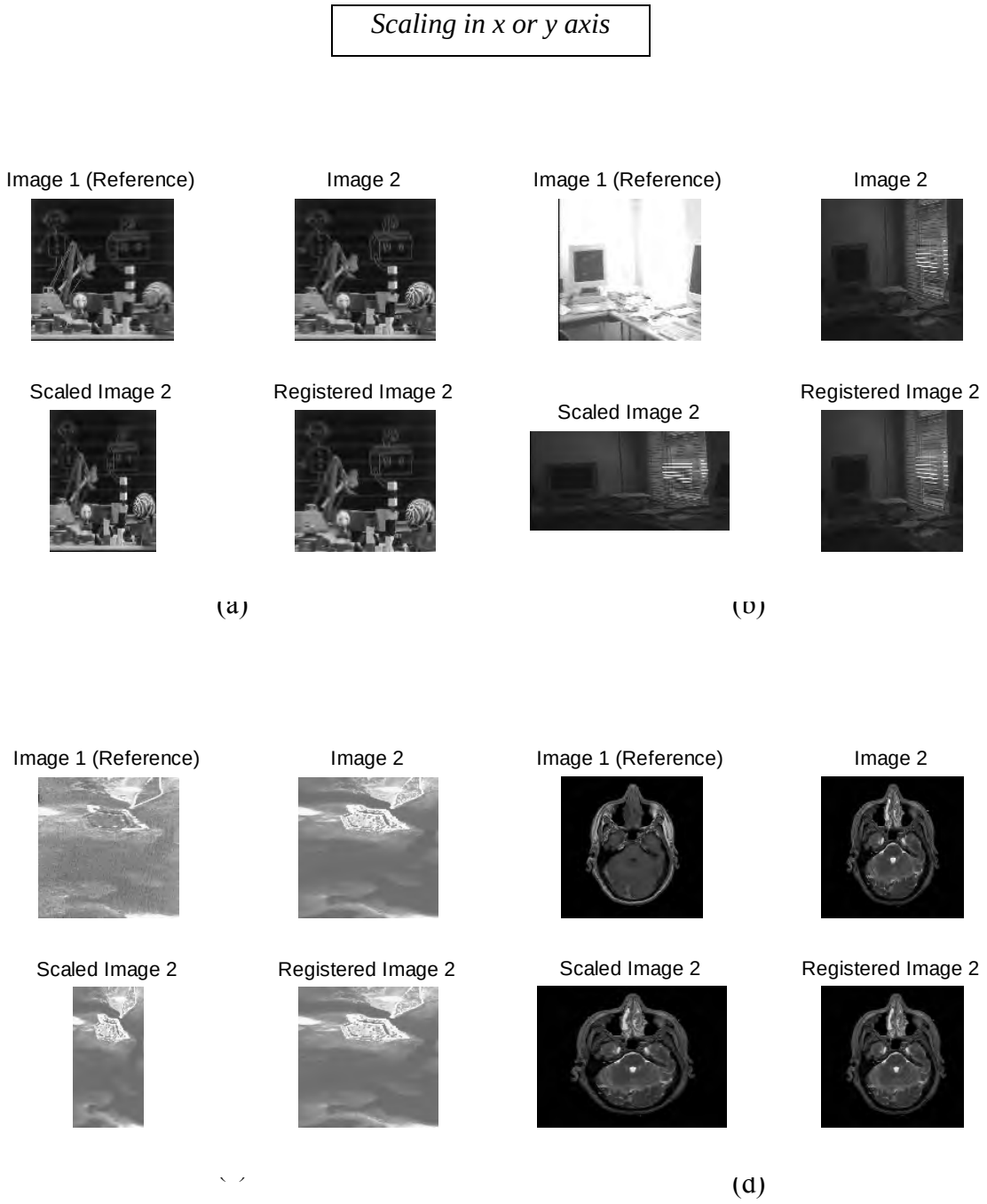

Figure 4.16: Reference, sensed (scaled in x or y direction) and registered images for images of different modalities (a) Toy (images 1 and 3) (b) Room (c) SAR2 (d) MRI

4.5 Combinations of Distortions

Experimental results concerning image registration for four types of combinations of distortions, viz., rotation, shearing and translation are presented in this section.

4.5.1 Translations in both x and y axes

Figures 4.17 show the variation in the value of objective function F due to the variation in translation both in x-axis (t_x) and in y-axis (t_y) for image of different modalities. It may be observed that in Figure 4.17 (a) the minimum value of the objective function is found at around $t_x = -20$ and $t_y = -30$. It means that the sensed image has a translation in $+x$ direction of 20 pixels and a translation in $+y$ direction of 30 pixels. So a translation on 20 pixels in $-x$ direction and a translation of 30 pixels in $-y$ direction would register it. In the similar fashion, the other figures of the objective function can be interpreted. In Figure 4.18, the reference, sensed and registered images are shown. It can be seen from this figure that the sensed images are registered properly.

4.5.2 Translation in y-axis along with rotation

Figure 4.19 show the variation in the value of objective function F due to the variation in translation in y-axis (t_y) along with angle of rotation (θ) for image of different modalities. It may be observed that in Figure 4.19 (a) the minimum value of the objective function is found at around $t_y = -30$ and $\theta = -10^0$. It means that the sensed image has a translation in $+y$ direction of 30 pixels and a rotation of 10^0 in clockwise direction. So a translation of 30 pixels in $-y$ direction and a rotation of 10^0 in the counterclockwise direction would register it. In the similar fashion, the other figures of the objective function can be interpreted. In Figure 4.20, the reference, sensed and registered images are shown. It can be seen from this figure that the sensed images are registered properly.

4.5.3 Translation in x-axis along with horizontal shear

Figure 4.21 show the variation in the value of objective function F due to the variation in translation in x-axis (t_x) along with shear in horizontal direction (s_h) for image of different modality. It may be observed that in Figure 4.21 (a) the minimum value of the objective function is found at around $t_x = -30$ and $s_h = -0.6$. It means that the sensed image has a translation in $+x$ direction of 30 pixels and a shear, $s_h = 0.6$ in horizontal direction. So a translation of 30 pixels in $-x$ direction and a shear, $s_h = -0.6$ in the horizontal direction would register it. In the similar fashion, the other figures of the objective function can be interpreted. In Figure 4.22, the reference, sensed and registered images are shown. It can be seen from this figure that the sensed images are registered properly.

Translation in both x and y axes

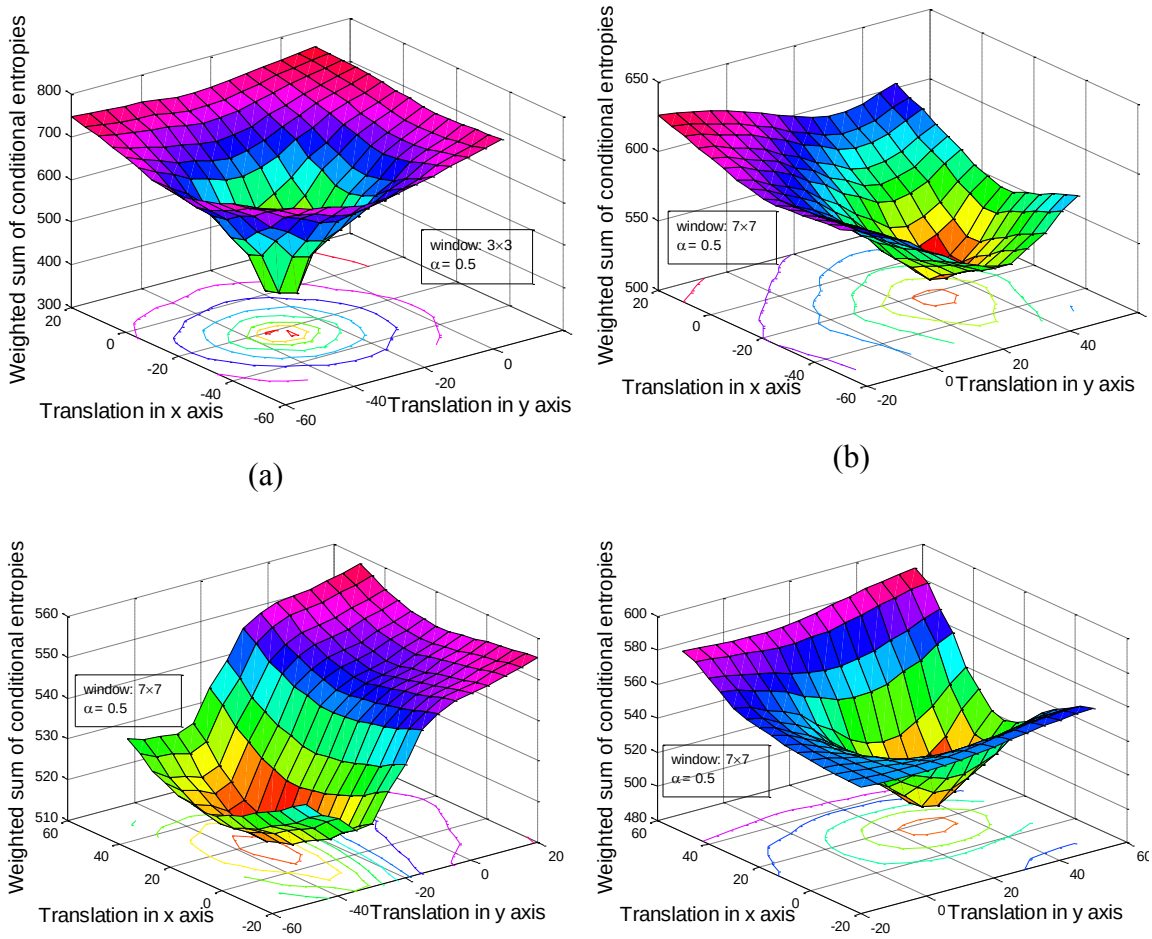

Figure 4.17: Objective function versus translation in x-axis (t_x) and translation in y-axis (t_y) for images of different modalities (a) Toy (images 1 and 2) (b) SAR2 (c) Navigation (images 1 and 2) (d) MRI

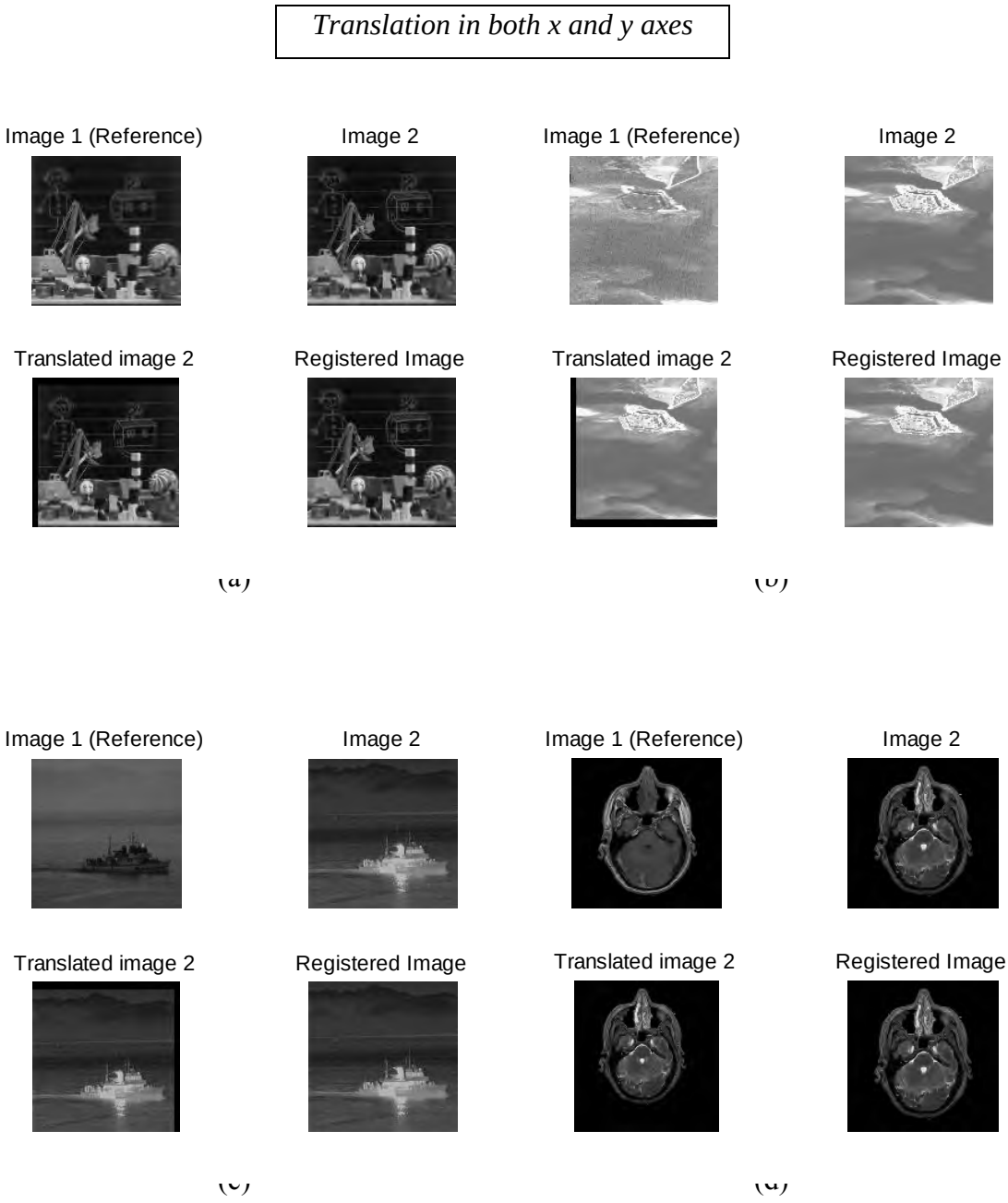

Figure 4.18: Reference, sensed (translated in both x and y direction) and registered images for images of different modalities (a) Toy (images 1 and 2) (b) SAR2 (c) Navigation (images 1 and 2) (d) MRI

Translation in y-axis along with rotation

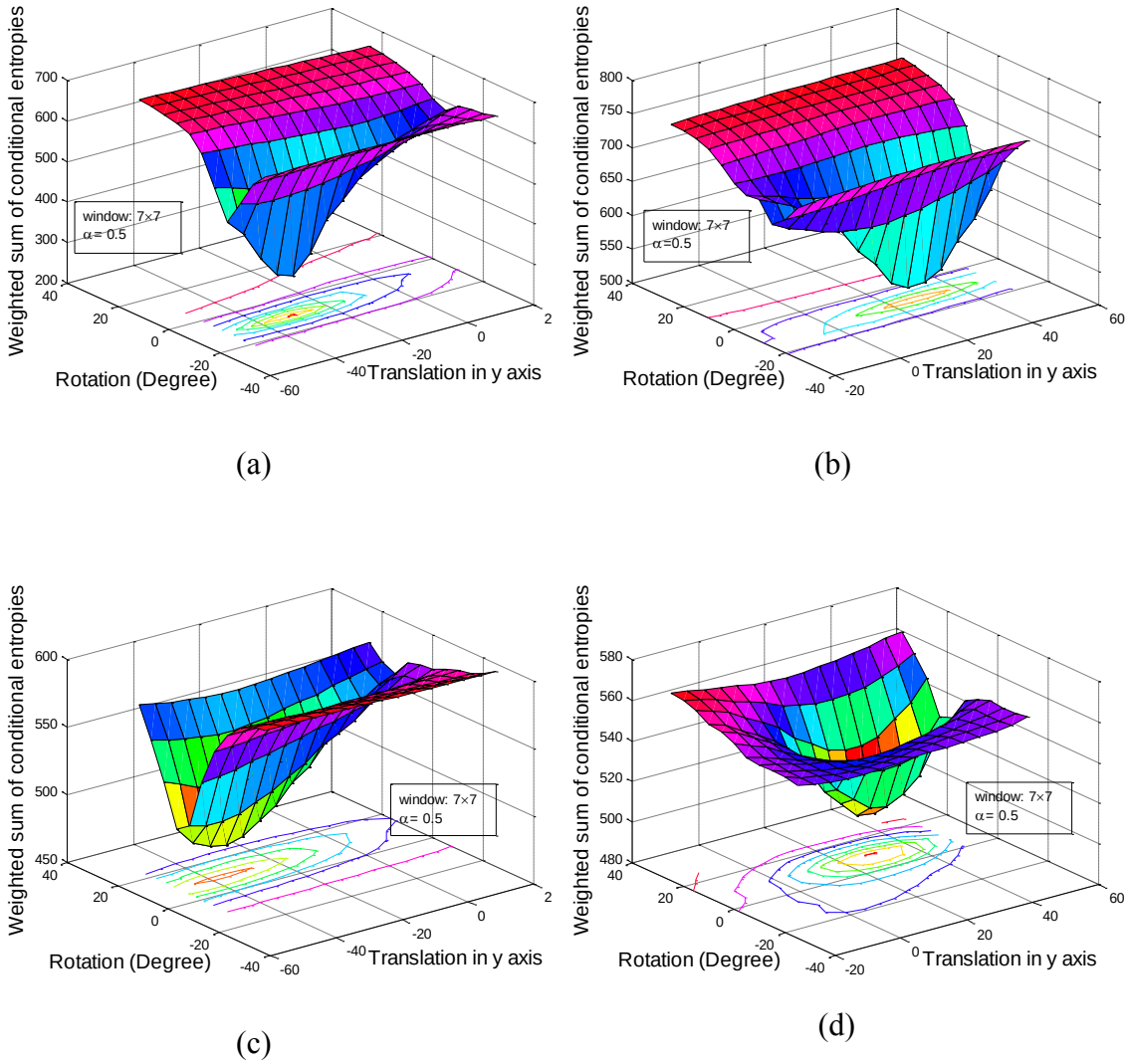

Figure 4.19: Objective function versus translation in y-axis (t_y) and angle of rotation (θ) for images of different modalities (a) Toy (images 1 and 3) (b) SAR1 (c) Navigation (images 1 and 3) (d) MRI

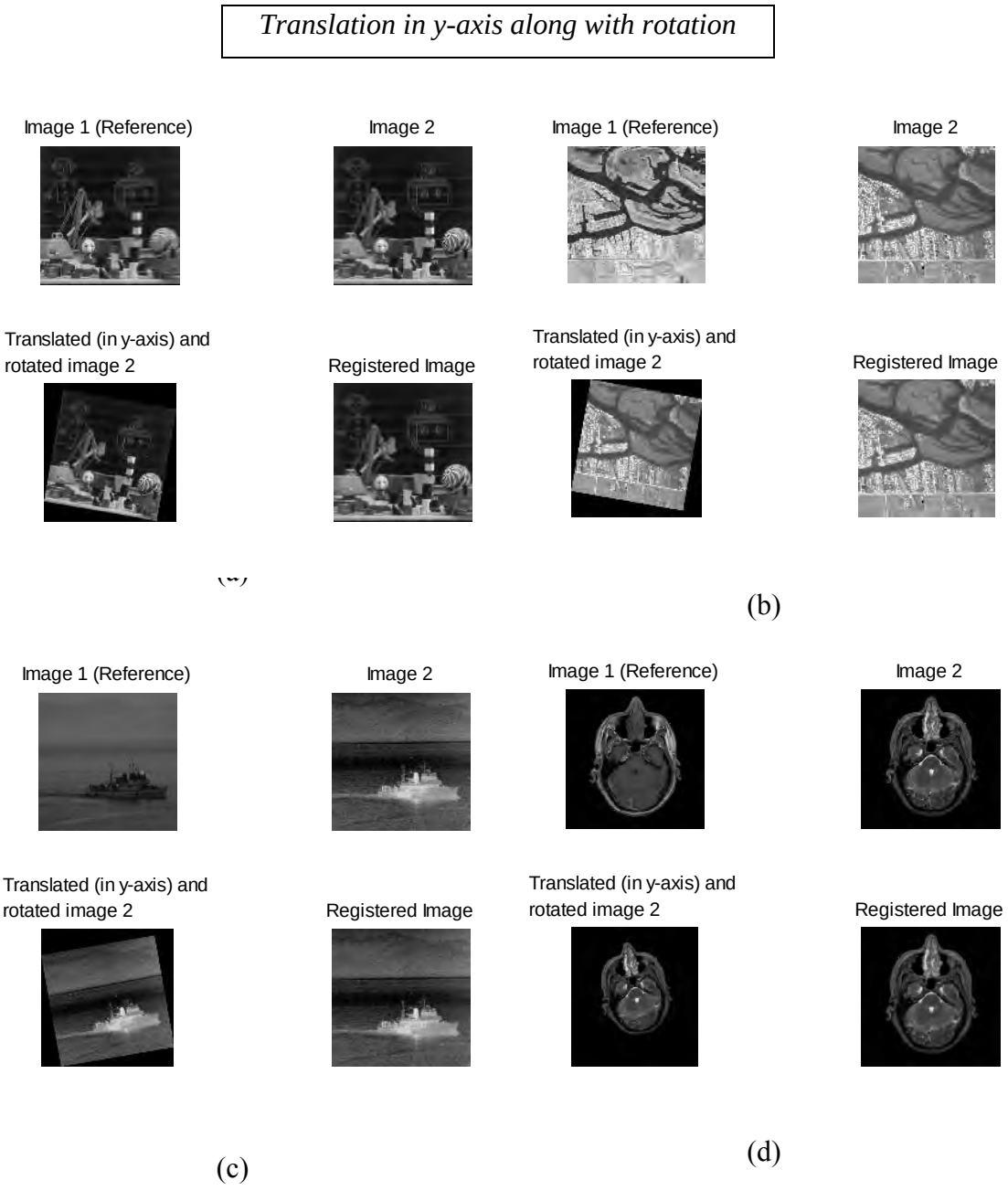

Figure 4.20: Reference, sensed (translated in *y*-axis and rotated) and registered images for images of different modalities (a) Toy (images 1 and 3) (b) SAR 1 (c) Navigation (images 1 and 3) (d) MRI

Translation in x-axis along with horizontal shear

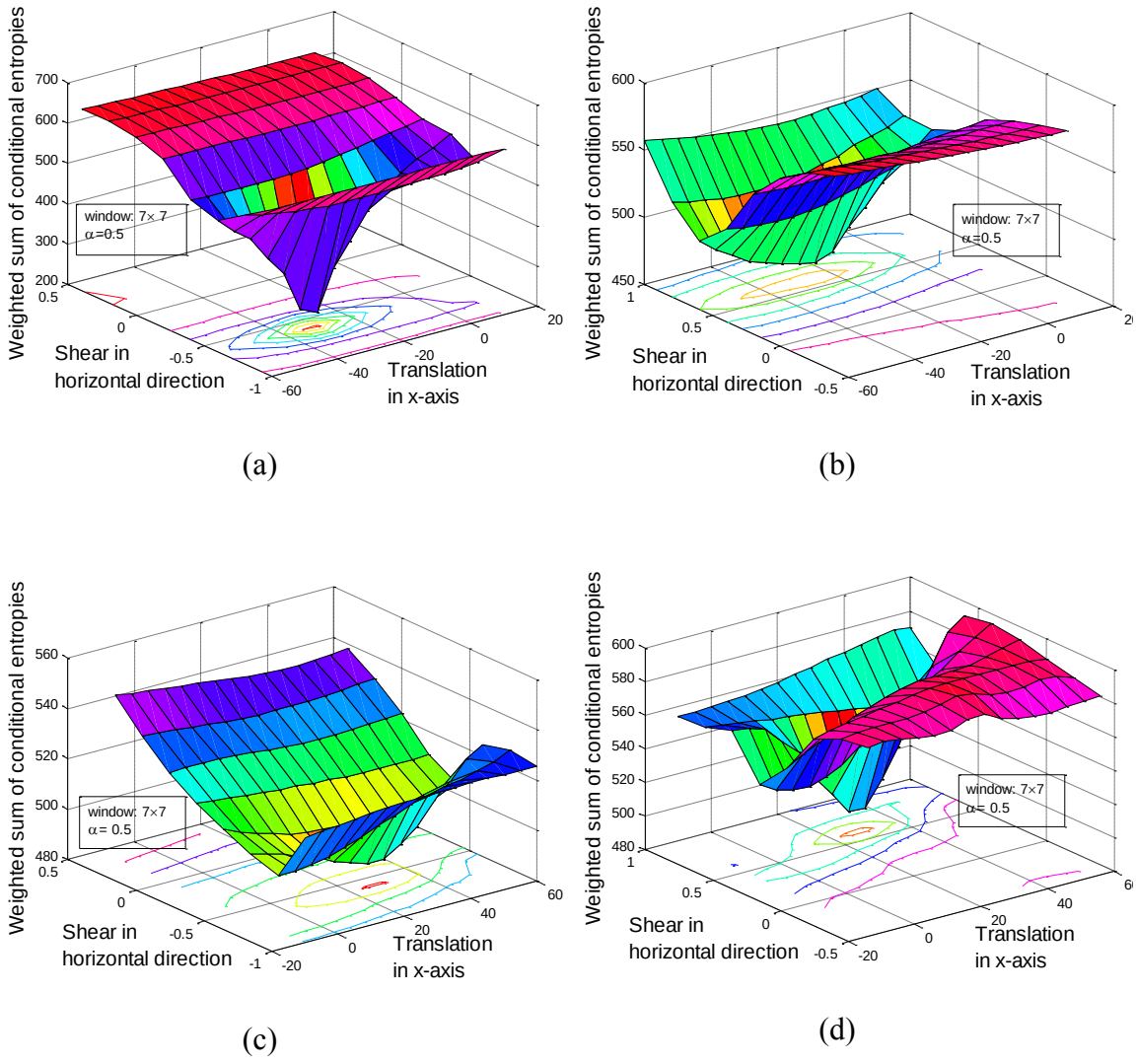

Figure 4.21: Objective function versus translation in x-axis (t_x) and shear in horizontal direction (S_h) for images of different modalities (a) Toy (images 1 and 2) (b) Room (c) Tree (d) MRI

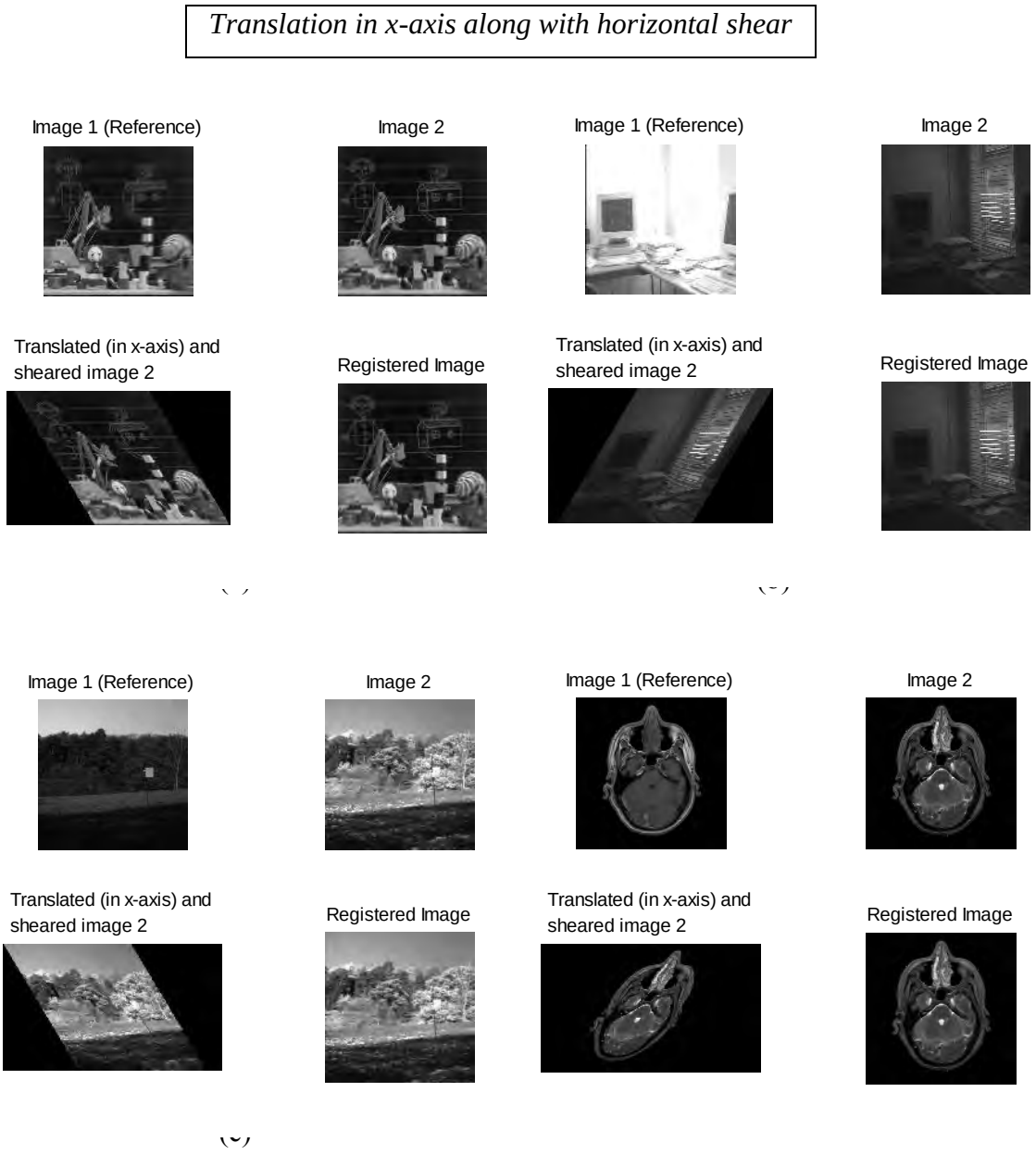

Figure 4.22: Reference, sensed (translated in x-axis and sheared in horizontal direction) and registered images for image of different modalities (a) Toy (images 1 and 2) (b) Room (c) Tree (d) MRI

4.5.4 Translations in both x and y axes along with rotation

Figures 4.23a, 4.23b and 4.23c show the variation in the value of objective function F due to the variation in translation in x-axis (t_x), translation in y-axis (t_y) along with angle of rotation (θ) for image of different modality. It may be observed that in Figure 4.23a the minimum value of the objective function is found at $\theta = -10^0$ $t_x = 30$ and $t_y = 40$. It means that the sensed image has a rotation of 10^0 in clockwise direction, a translation in $-x$ direction of 30 pixels and a translation in $-y$ direction of 40 pixels. So a rotation of 10^0 in the counterclockwise direction along with a translation of 30 pixels in $+x$ direction and a translation of 40 pixels in $+y$ direction would register it. In the similar fashion, the other figures of the objective function can be interpreted. In Figures 4.24a, 4.24b and 4.24c, the reference, sensed and registered images are shown. It can be seen from these figures that the sensed images are registered properly.

Translation in both x and y axes along with rotation

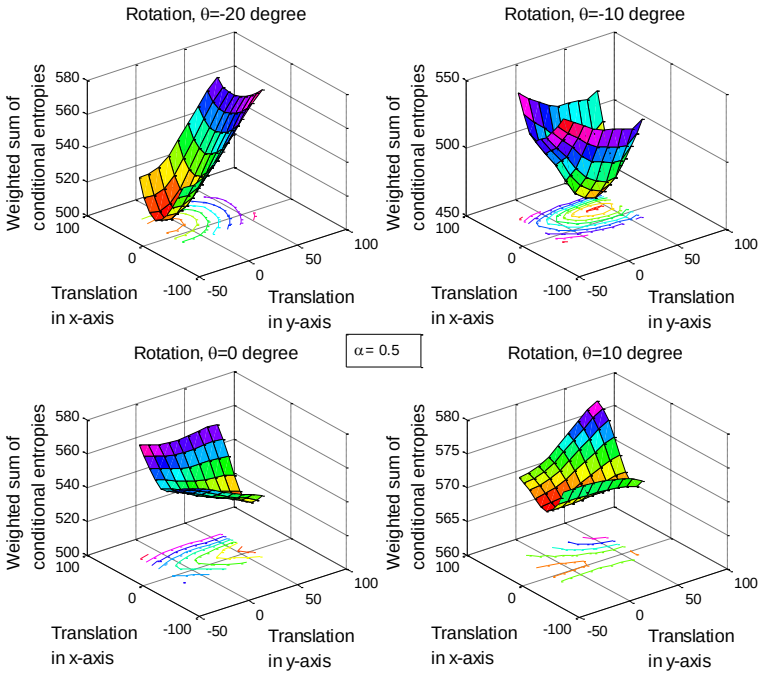

(i)

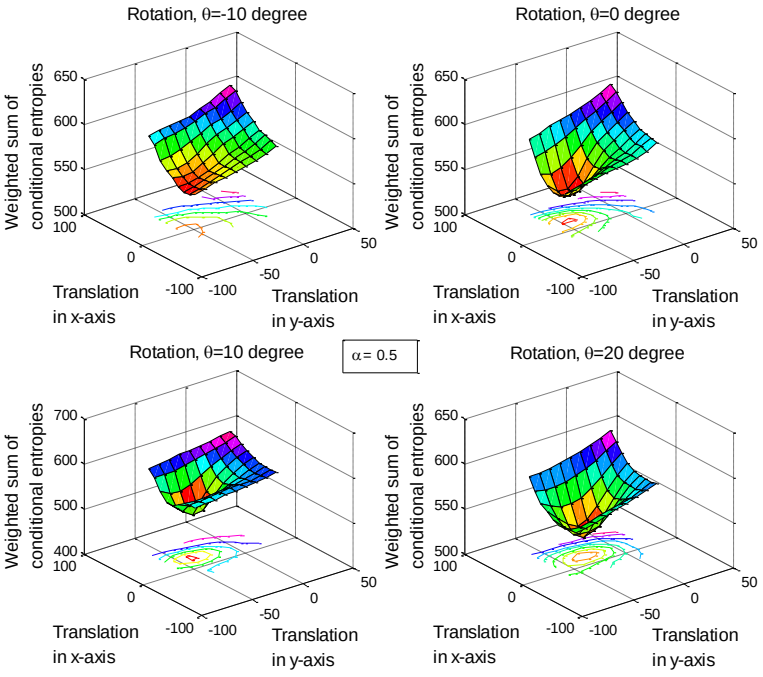

(ii)

Figure 4.23a: Objective function versus translation in x-axis (t_x) and translation in y-axis (t_y) with different angle of rotation (θ) for images of different modalities (i) Room (ii) MRI

Translation in both x and y axes along with rotation

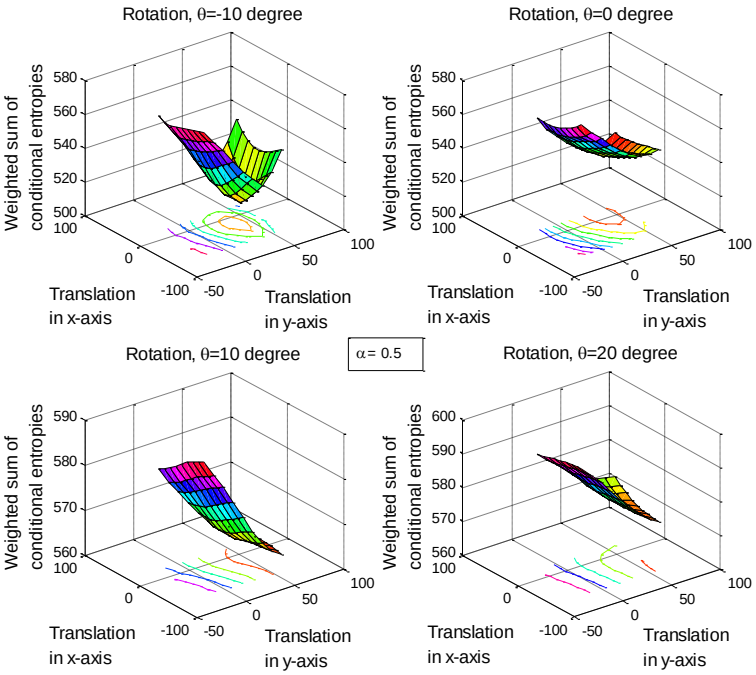

(i)

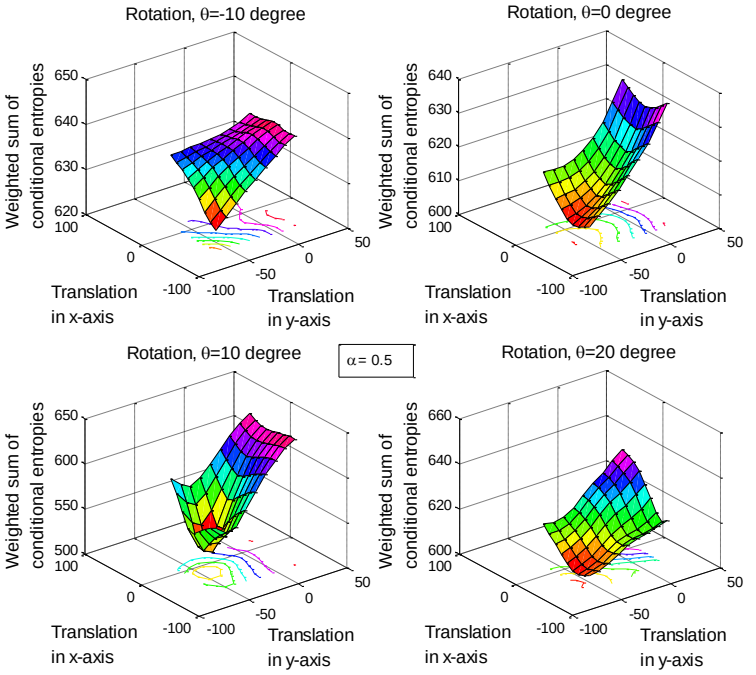

(ii)

Figure 4.23b: Objective function versus translation in x-axis (t_x) and translation in y-axis (t_y) with different angle of rotation (θ) for images of different modalities (i) Navigation (images 1 and 2) (ii) SAR2

Translation in both x and y axes along with rotation

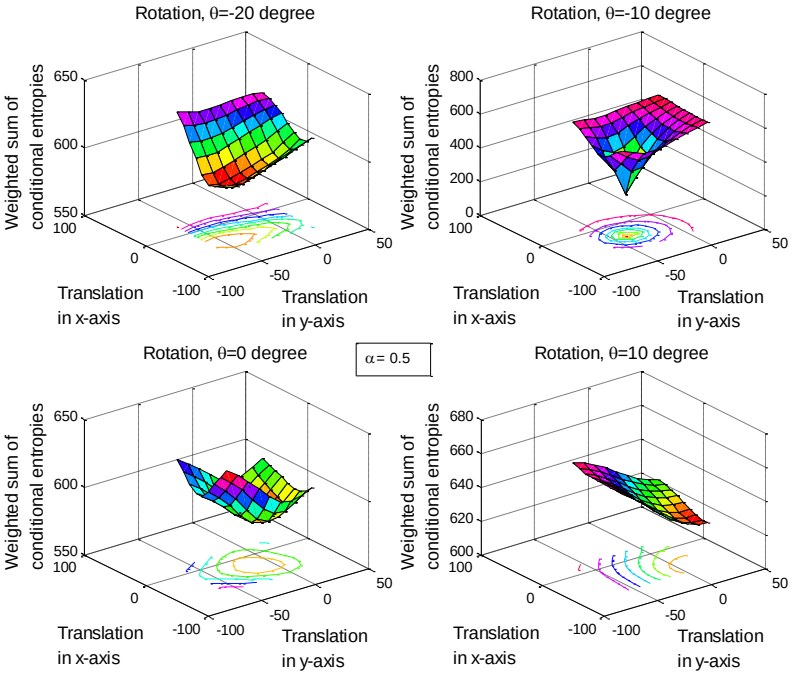

(i)

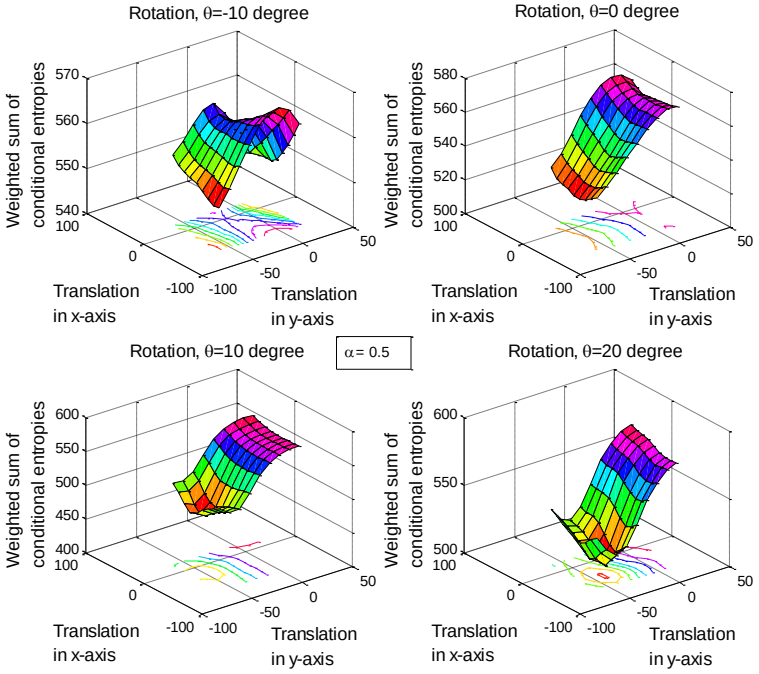

(ii)

Figure 4.23c: Objective function versus translation in x-axis (t_x) and translation in y-axis (t_y) with different angle of rotation (θ) for images of different modalities (i) Toy (images 1 and 2) (ii) Tree

Translation in both x and y axes along with rotation

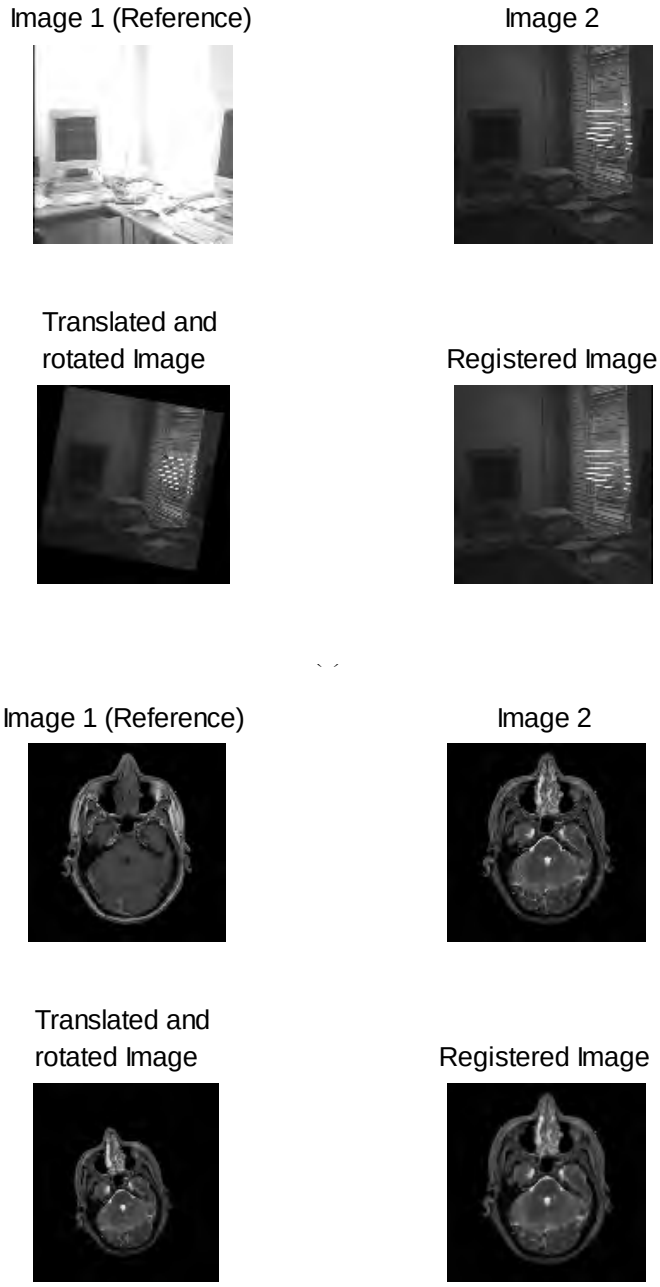

Figure 4.24a: Reference, sensed (translated in both x and y-axes along with rotation) and registered images for images of different modalities (i) Room (ii) MRI

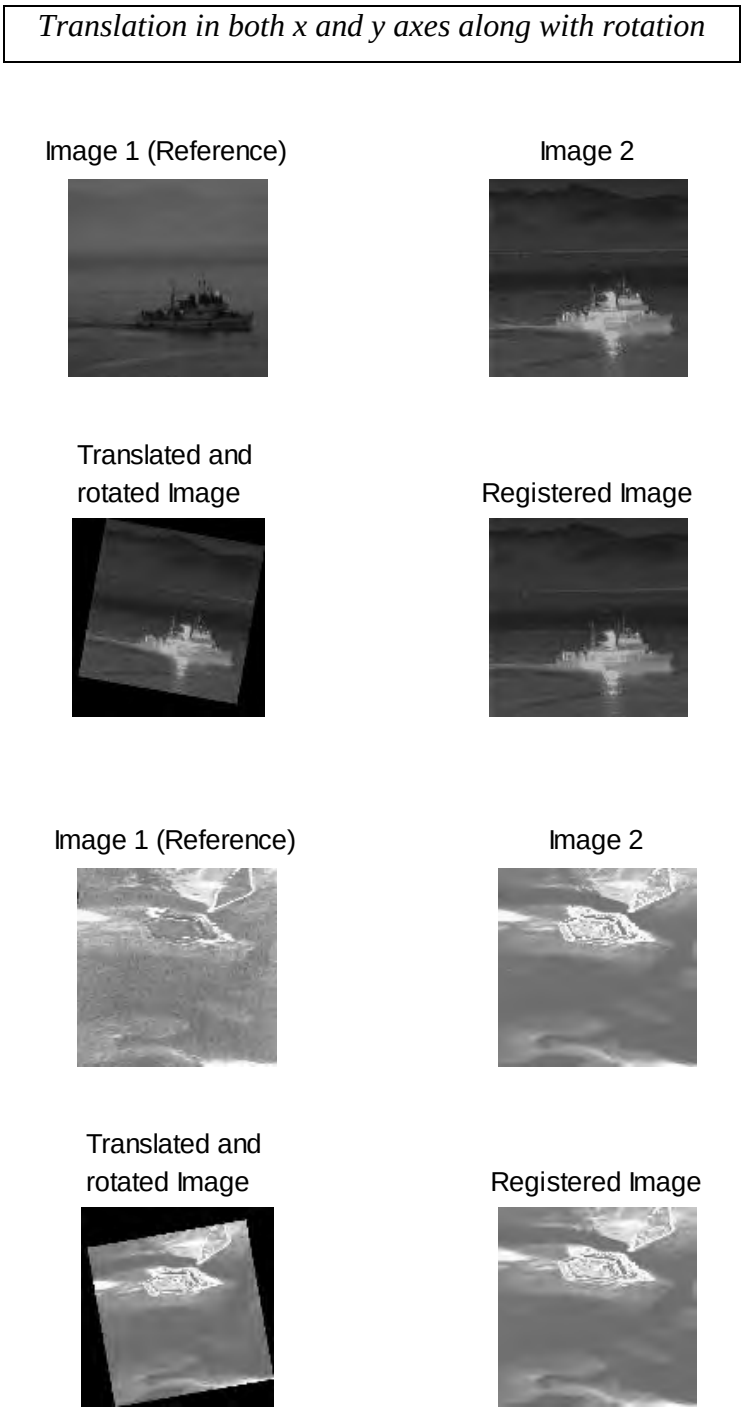

Figure 4.24b: Reference, sensed (translated in both x and y-axes along with rotation) and registered images for images of different modalities (i) Navigation (images 1 and 2) (ii) SAR2

Translation in both x and y axes along with rotation

Figure 4.24c: Reference, sensed (translated in both x and y-axes along with rotation)and registered images for images of different modalities (i) Toy (images 1 and 2) (ii) Tree

4.6 Comparisons with Other Methods

The proposed method is compared with three other existing intensity-based methods where the probabilistic objective function either in the wavelet domain or pixel domain is used. The comparison is shown with the context of four standard performance metrics. Here, the values of the performance metrics are calculated only for „combination of distortions". Because, the performance of the proposed registration algorithm can be realized properly by the values of the performance metrics calculated for „combination of distortions". Moreover, by observing these values for combination of distortions, the performance due to single distortion can be easily realized. The three existing methods with which the proposed algorithm is compared are briefly described below.

Method 1[41]: Here the objective function is the mutual information of the coefficients of the approximate level of DWT of the reference and sensed image. Where the mutual information of the approximate wavelet coefficients gets highest the desired distortion there is found there. Similar registration algorithm is also used in [31].

Method 2 [42]: The objective function in this method is the normalized cross correlation coefficient of the approximate DWT coefficients estimated at different levels of the reference and sensed image. The approximate coefficient of a given level are thresholded to the 50% of the maximum value at that level and the next level"s coefficients are threshold to the 40% of the maximum value in that level. The desired distortion is found where the normalized cross correlation coefficient becomes the highest.

Method 3 [10]: In this method the objective function is the mutual information of the pixel intensities of the reference and sensed image [70]. The desired distortion is found where the mutual information becomes the highest. Similar registration algorithm is used also in [70].

The values of the performance metrics for four combinations of distortions and for five sets of images, viz., Toy, Room, SAR2, Tree and MRI are shown in tables 4.1, 4.2, 4.3 and 4.4. The best result is shown in bold for the test images and each of the performance metrics. A close observation reveals that for most of the cases the proposed method gives the best performance as compared to the other methods. In the cases, where the proposed method does not give the best result, the difference between the values of the metrics for the best and for the proposed method is negligible. Thus, it can be concluded that the proposed method performs better than the similar existing methods with the context of the mentioned performance metrics.

Table 4.1 Results concerning the performance metrics for translation in both x and y-axes

Image	**Methods**	**RMSD**	**NRMSD**	**NCCC**	**PRRMSE**
Toy (Image 1 and 2)	Method 1	26.5063	0.1183	0.2616	0.0067
	Method 2	49.0427	0.2189	0.2394	0.0134
	Method 3	19.8472	0.0827	**0.2664**	0.0050
	Proposed	**10.9576**	**0.0457**	0.2617	**0.0028**
Room	Method 1	167.5459	0.6570	0.0020	0.0225
	Method 2	173.4010	0.6800	0.0102	0.0236
	Method 3	167.5459	0.6570	0.0020	0.0225
	Proposed	**166.7243**	**0.6538**	**0.0021**	**0.0223**
SAR 2	Method 1	30.0326	0.1615	0.0554	0.0048
	Method 2	37.4100	0.2011	**0.0536**	0.0062
	Method 3	30.0326	0.1615	0.0554	0.0048
	Proposed	**26.0410**	**0.1400**	**0.0536**	**0.0041**
Tree	Method 1	79.8601	0.3427	0.2482	0.0394
	Method 2	79.8301	0.3426	0.2395	0.0392
	Method 3	74.1598	0.3169	0.2405	0.0364
	Proposed	**73.7378**	**0.3151**	**0.2316**	**0.0359**
MRI	Method 1	25.0563	0.1165	**0.1872**	0.0195
	Method 2	41.7196	0.1940	0.1778	0.0327
	Method 3	25.0563	0.1165	**0.1872**	0.0195
	Proposed	**24.0689**	**0.1119**	0.1871	**0.0188**

Table 4.2 Results concerning the performance metrics for translation in y-axis and rotation

Image	**Methods**	**RMSD**	**NRMSD**	**NCCC**	**PRRMSE**
Toy (Image 1 and 2)	Method 1	14.8429	0.0628	0.2471	0.0037
	Method 2	14.8519	0.0618	**0.2662**	0.0038
	Method 3	14.8559	0.0617	0.2651	0.0039
	Proposed	**12.2350**	**0.0510**	0.2550	**0.0031**
Room	Method 1	166.9185	0.6551	0.0083	**0.0223**
	Method 2	187.8198	0.7365	**0.0089**	0.0251
	Method 3	166.9174	**0.6546**	0.0084	**0.0223**
	Proposed	**166.9104**	**0.6546**	0.0078	**0.0223**
SAR 2	Method 1	32.1065	0.1728	0.0271	0.0052
	Method 2	54.2317	0.2916	0.0421	0.0086
	Method 3	**32.1062**	**0.1726**	0.0430	**0.0051**
	Proposed	46.3639	0.2342	**0.0433**	0.0075
Tree	Method 1	83.1587	0.3375	0.0178	0.0378
	Method 2	87.5612	0.3847	0.0212	0.0425
	Method 3	86.2132	0.3684	0.0199	0.0419
	Proposed	**72.8155**	**0.3112**	**0.2363**	**0.0354**
MRI	Method 1	24.2991	0.1141	0.1911	0.0190
	Method 2	33.9082	0.1577	**0.1921**	0.0264
	Method 3	24.2984	0.1130	0.1914	0.0189
	Proposed	**23.3756**	**0.1087**	0.1918	**0.0182**

Table 4.3 Results concerning the performance metrics for translation in x-axis and shear in horizontal direction

Image	**Methods**	**RMSD**	**NRMSD**	**NCCC**	**PRRMSE**
Toy (Image 1 and 2)	Method 1	21.8523	0.0845	0.2524	0.0066
	Method 2	30.5769	0.1548	0.2146	0.0089
	Method 3	22.6931	0.0946	0.2534	0.0057
	Proposed	**11.2929**	**0.0471**	**0.2610**	**0.0028**
Room	Method 1	167.1371	0.6556	1.8237e-004	0.0225
	Method 2	191.6020	0.7514	0.1275	0.0256
	Method 3	167.1369	0.6554	1.8234e-004	0.0224
	Proposed	**166.9185**	**0.6546**	**0.0027**	**0.0223**
SAR 2	Method 1	54.1554	0.2737	0.0430	0.0088
	Method 2	57.6431	0.2785	0.04301	0.0092
	Method 3	54.1553	0.2735	0.0431	0.0088
	Proposed	**46.8098**	**0.2364**	**0.0695**	**0.0076**
Tree	Method 1	74.0438	0.3164	0.1975	0.0360
	Method 2	76.3241	0.3219	0.1975	0.0362
	Method 3	75.3040	0.3218	0.1974	0.0366
	Proposed	**73.6977**	**0.3149**	**0.2259**	**0.0358**
MRI	Method 1	26.2495	0.1222	0.1861	0.0206
	Method 2	45.7609	0.2128	0.1032	0.0357
	Method 3	26.2486	0.1221	**0.1897**	0.0205
	Proposed	**23.6884**	**0.1102**	0.1896	**0.0185**

Table 4.4 Results concerning the performance metrics for translation in x-axis, translation in y-axis, and rotation

Image	Methods	RMSD	NRMSD	NCCC	PRRMSE
Toy (Image 1 and 2)	Method 1	12.3114	0.0513	0.2540	**0.0031**
	Method 2	13.4589	0.0523	0.2501	0.0032
	Method 3	12.3015	0.0513	0.2541	**0.0031**
	Proposed	**12.2861**	**0.0512**	**0.2543**	**0.0031**
Room	Method 1	166.9182	0.6550	0.0081	**0.0222**
	Method 2	187.8194	0.7363	**0.0087**	0.0250
	Method 3	**166.9104**	**0.6546**	0.0058	0.0223
	Proposed	**166.9104**	**0.6546**	0.0058	0.0223
SAR 2	Method 1	26.2513	0.1414	0.0502	0.0042
	Method 2	28.5498	0.1424	0.0507	**0.0041**
	Method 3	26.2223	0.1410	0.0509	0.0042
	Proposed	**26.1651**	**0.1407**	**0.0511**	**0.0041**
Tree	Method 1	82.2456	0.3134	0.0178	0.0378
	Method 2	86.8576	0.3762	0.0201	0.0420
	Method 3	85.9534	0.3542	0.0174	0.0402
	Proposed	**71.4548**	**0.3014**	**0.2241**	**0.0345**
MRI	Method 1	34.0312	0.1583	**0.1921**	0.0265
	Method 2	34.0312	0.1583	**0.1921**	0.0265
	Method 3	**23.8300**	**0.1108**	0.1918	**0.0186**
	Proposed	24.0503	0.1119	0.1918	0.0187

4.7 Registration in Real Cases

Up to the previous section of this chapter, all the sensed images were synthetically generated. In real cases the sensed image is already misaligned with respect to the reference image. In this section two sets of images will be considered. The sensed image in each of the case is geometrically in misaligned position with respect to the reference image. Here, the sensed image is not found by synthetic distortion function.

The images shown in figure 4.25(a) and 4.25(b) are the reference and sensed images of Doll image. The reference image is middle focused and sensed image is left focused. The two images vary in dimension and the sensed image is translated in both axes with respect to the reference image. By using the proposed registration algorithm the sensed image registered. In 4.25 (c), it is observed that there is a dark line at the right and

bottom of the image. This means a translation in x an y axes. The objective function surface is shown in figure 4.26.

(a)

(b)

(c)

Figure 4.25 Doll (a) reference (b) sensed (c) registered image

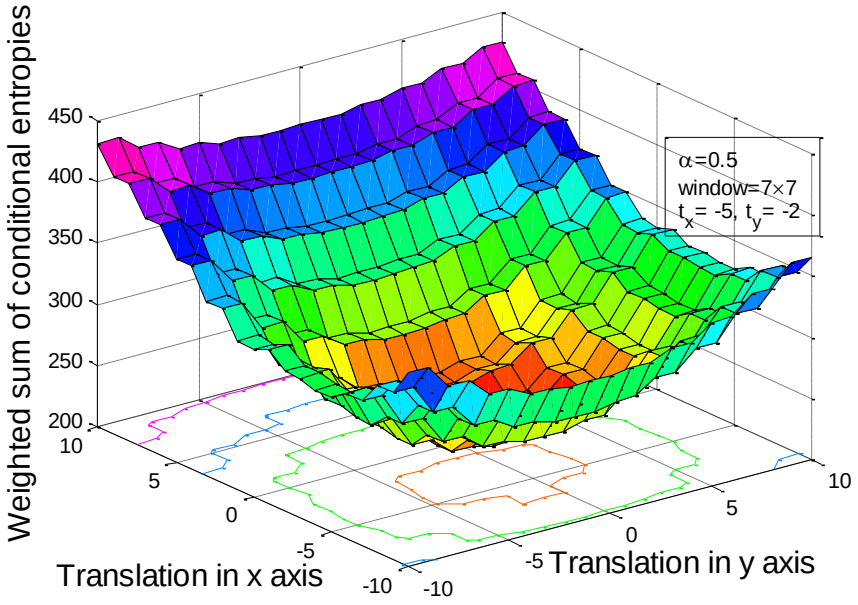

Figure 4.26: Objective function versus translation in x-axis (t_x) and translation in y-axis (t_y) for Doll

Another set of image consist of two SAR images (SAR3). In figure 4.27(a) and figure 4.72(b) the reference and sensed images are shown. It is easily observed that the sensed image has rotational distortion with respect to the reference image. The building and highways in the sensed image are rotationally different to the reference image.

(a) (b)

Figure 4.27 SAR3 (a) reference (b) sensed image

Using the proposed registration algorithm, the angle of rotation versus the objective function is plotted in figure 4.28. The lowest value of the objective function occurs at 15^0 of rotation. This gives the required or desired distortion parameter. Using this parameter the sensed image is affine transformed and thus the registered image is found.

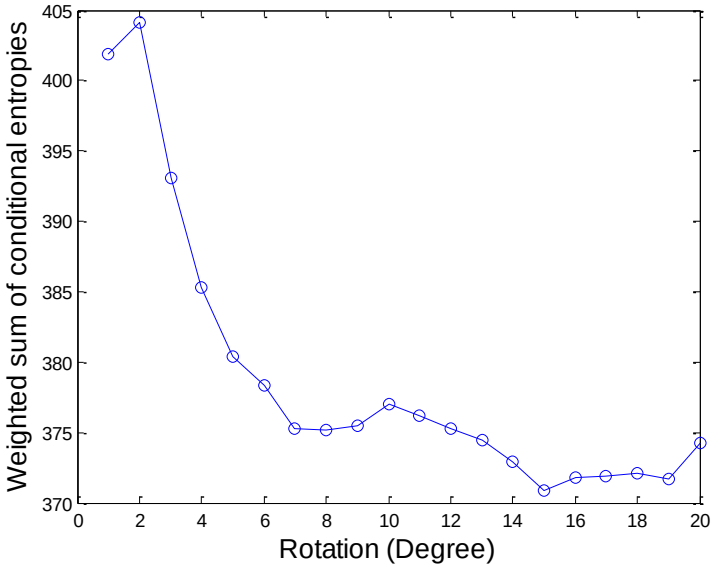

Figure 4.28: Objective function versus angle of rotation (θ) for SAR3

(a) (b)

Figure 4.29 SAR3 (a) reference (b) registered image

The reference and registered images are shown in figure 4.29(a) and 4.29(b). If we observe this figure, we find that the highways and building structures are now properly aligned with respect to the reference image. Upon our subjective evaluation it can be said that the proposed method works well for real registration problems.

4.7 Conclusion

In this chapter, the performance of the proposed registration algorithm is evaluated in terms of visual representation and the values of performance metrics. Distortion which is linear and uniform is used here. Both single and combination of distortions are considered for the distortion of the sensed image. The performance of the proposed method is compared with three existing methods with the context of four standard performance metrics. Moreover, the performance of the proposed registration algorithm has been checked for real registration problems. From these evaluations, it is found that the proposed method gives a better performance than existing methods.

CHAPTER 5: CONCLUSION

5.1 Conclusion and Discussion

In many real world applications, integration of information from different sources is becoming more and more important. In the field of image processing also such integration is also increasingly used. In medical diagnostic, remote sensing, panoramic image construction and security purposes this integration of images is very important. It is prerequisite that the images are geometrically aligned before their integration and this aligning process is called „image registration".

In general, two approaches are followed for registering images, namely, feature-based and intensity-based methods. The latter give better accuracy than the former as the latter methods consider the pixel intensities of the entire image. In this thesis, an intensity-based image registration algorithm has been developed using the conditional dependencies that may exist between the curvelet coefficients of images. Only the coefficients of the approximate level of the curvelet transform have been taken into account and hence, the computational load has been reduced significantly. The objective function is a linear combination of the conditional entropies of the approximate level curvelet coefficients of reference and sensed images. The functional value of the objective function has been evaluated from the values obtained from local neighboring approximate curvelet coefficients. This is due to the fact that the curvelet coefficients of images are locally stationary. For calculating the conditional entropies, it has been considered that the local neighboring approximate curvelet coefficients follow the bivariate Gaussian distribution. This consideration has been verified by using the standard statistical χ^2 test of fit.

Here, images taken from the same scene but captured in different modes or by different sensors or in different viewpoints are selected as test images. The alignment of images are carried out by using a distortion function which is linear and uniform namely, the affine transformation that possesses a low computational complexity. The images are

registered both for single and a combination of distortions. From the visual inspection of the distorted and registered images, it has been found that the proposed algorithm is capable of geometrically align the distorted images with the reference image. Moreover, the proposed algorithm has been compared with three other existing methods those are similar to the proposed method in terms of standard performance metrics. From the calculated performance metrics, it can be observed that for most of the cases the proposed algorithm performs better than the other methods. Thus, the proposed registration algorithm is expected to play a significant role in automatic image registration used in practice.

5.2 Scope of Further Work

There are a number of scopes to extend the research done in the thesis. Some possible avenues include:

- The performance of the registration algorithm may be evaluated for noisy images.
- The registration algorithm can be implemented for nonlinear distortions such as the barrel or polynomial type distortions.
- A general form of Gaussian PDF may be used for determining the objective function.

REFERENCES

[1] Arévalo, V., and González, J., "An Experimental Evaluation of Non-rigid Registration Techniques on Quickbird Satellite Imagery," *International Journal of Remote Sensing*, vol. 29, no. 2, pp. 513-527, 20 Jan. 2008.

[2] Suri, S., and Reinartz, P., "Mutual-Information-Based Registration of TerraSAR-X and Ikonos Imagery in Urban Areas," *IEEE Transactions on Geoscience and Remote Sensing*, vol. 48, no. 2, pp. 939-949, Feb. 2010.

[3] Zhang, C., and Fraser, C. P., "Automated Registration of High-Resolution Satellite Images," *The Photogrammetric Record*, vol. 22, no. 117, pp. 75-87, Mar. 2007.

[4] Wang, X., and Dagan, F. D., "Automatic Elastic Medical Image Registration Based on Image Intensity," *International Journal of Image and Graphics*, vol. 5, no. 2, pp. 351-369, Apr. 2005.

[5] Ramprasad, P., Nagaraj, H. C., Parasuram, M. K., and Shubha, M., "Multi Resolution Based Image Registration Technique for Matching Dental X-rays," *Journal of Mechanics in Medicine and Biology*, vol. 9, no. 4, pp. 621-632, Dec. 2009.

[6] Schmitt, O., Modersitzki, J., Heldmann, S., and Wirtz, S., "Image Registration of Sectioned Brains," *International Journal of Computer Vision*, vol. 73, no. 1, pp. 5-39, 2007.

[7] Hogea, C., Davatzikos, C., and Biros, G., "Brain-Tumor Interaction Biophysical Models for Medical Image Registration," *Siam Journal of Scientific Computing*, vol. 30, no. 6, pp. 3050-3072, Dec. 2008.

[8] Chanwimaluang, T., Fan, G., and Fransen, S. R., "Hybrid Retinal Image Registration," *IEEE Transactions on Information Technology in Biomedicine*, vol. 10, no. 1, pp. 129-142, Jan. 2006.

[9] Wachinger, C., and Navab, N., "Structural image representation for image

registration," in *IEEE Computer Society Conference on Computer Vision and Pattern Recognition Workshops*, San Fransisco, Jun. 2010, pp. 23-30.

[10] Zhaoying, L., Fugen, Z., Xiangzhi, B., Hui, W., and Dongjie, T., "Multi-modal image registration by mutual information based on optimal region selection," in *IEEE International Conference on Information Networking and Automation*, Kunming, Oct. 2010, pp. v2-249-v253.

[11] Luo, B., and Gan, J.-Y., "Inhomogenous illuminated images registration based on wavelet decomposition," in *International Conference on Wavelet Analysis and Pattern Recognition*, Baoding, Jul. 2009, pp. 365-368.

[12] Huang, J.-X., Li, D., Ye, F., and Dong, Z.-J., "Flexible printed circuit defective detection based on image registration," in *2010 3rd International Congress on Image and Signal Processing*, Yantai, Oct. 2010, pp. 2570-2574.

[13] Brown, M., and Lowe, D. G., "Automatic Panoramic Image Stitching Using Invariant Features," *International Journal of Computer Vision*, vol. 74, no. 1, pp. 59-73, 2007.

[14] Suh, J. W., and Wyatt, C. L., "Registration Under Topological Change for CT Colonoscopy," *IEEE Transactions on Biomedical Engineering*, vol. 58, no. 5, pp. 1403-1411, May 2011.

[15] Available in website of national geographic magazine in: „http://ngm.nationalgeographic.com/redwoods/gatefold-image".

[16] Ton, J., Jain, and A. K., "Registering Landsat Images by Point Matching," *IEEE transactions on Geoscience and Remote Sensing*, vol. 27, no. 5, pp. 642-651, Sep. 1989.

[17] Heo, J., Kim, J. H., Eo, Y. D., and Sohn, H.-G., "Automated TM/ETM+ Image Co-registration Using Pre-Qualified Area Matching and Studentized Outlier Detection," *The Imaging Science Journal*, vol. 57, no. 2, pp. 69-78, Apr. 2009.

[18] Rignot, E., Kowk, R., Curlander, J. C., and Pang, S. S., "Automated Multisensor Registration: Requirements and Techniques," *Photogrammetric Engineering and*

Remote Sensing, vol. 57, pp. 1029-1038, 1991.

[19] Habib, A. F., and Al-Ruzouq, R. I., "Semi-Automatic Registration and Change Detection Using Multi-Source Imagery With Varying and Radiometric Properties," *Photogrammetric Engineering and Remote Sensing*, vol. 71, no. 3, pp. 325-332, 2005.

[20] Flusser, J., and Suk, T., "A Moment-Based Approach to Registration of Images with Affine Geometric Distortion," *IEEE Transaction on Geoscience and Remote Sensing*, vol. 32, no. 2, pp. 382-387, Mar. 1994.

[21] Dai, X., and Khorram, S., "A Feature-Based Image Registration Algorithm Using Improved Chain-Code Representation Combined with Invariant Moments," *IEEE Transaction on Geoscience and Remote Sensing*, vol. 37, no. 5, pp. 2351-2362, Sep. 1999.

[22] Kwak, T.-S., Kim, Y.-I., Yu, K.-Y., and Lee, B.-K., "Registration of Aerial Imagery and Aerial LiDar Data Using Centroids of Plane Roof Surfaces as Control Information," *KSCE Journal of Civil Engineering*, vol. 10, no. 5, pp. 365-370, 2006.

[23] Kim, J., and Fessler, J.A., "Intensity-Based Image Registration Using Robust Correlation Coefficients," *IEEE Transactions of Medical Imaging*, vol. 23, no. 11, pp. 1430-1444, Nov. 2004.

[24] Rohde, G. K., Aldroubi, A., and Dawant, B. M., "The Adaptive Bases Algorithm for Intensity-Based Nonrigid Image Registration," *IEEE Transactions of Medical Imaging*, vol. 22, no. 11, pp. 1470-1479, Nov. 2003.

[25] Myroneko, A., and Song, X., "Intensity-Based Image Registration by Minimizing Residual Complexity," *IEEE Transactions of Medical Imaging*, vol. 29, no. 11, pp. 1882-1891, Nov. 2010.

[26] Ghantous, M., Ghosh, S. and Bayoumi, M., "A multi-modal automatic image registration technique based on complex wavelets," in *16th IEEE International Conference on Image Processing*, Cairo, Nov. 2009, pp. 173-176.

[27] Corsini, M., Dellapiane, M., Ponchio, F. and Scopigno, R., "Image-to-Geometry Registration: A Mutual Information Method Exploiting Illumination-Related Geometric Properties," *Computer Graphics Forum*, vol. 28, no. 7, pp. 1755-1764, Dec. 2009.

[28] Wang, F., and Vemuri, B. C., "Non-Rigid Multi-Modal Image Registration Using Cross-Cumulative Residual Entropy," *International Journal of Computer Vision*, vol. 74, no. 2, pp. 201-215, Aug. 2007.

[29] Maes, F., Collignon, A., Vandermeulen, D., Marchal, G., and Suetens, P., "Multimodality Image Registration by Maximization of Mutual Information," *IEEE Transaction of Medical Imaging*, vol. 16, no. 2, pp. 187-198, Apr. 1997.

[30] Qin, B., Gu, Z., Sun, X., and Lv, Y., "Registration of Images with Outliers Using Joint Saliency Map," *IEEE Signal Processing Letters*, vol. 17, no. 1, pp. 91-94, Jan. 2010.

[31] Malviya, A., and Bhirud, S.G., "Wavelet based image registration using mutual information," in *International Conference on Emerging Trends in Electronic and Photonic Devices and Systems*, Varanasai, Dec. 2009, pp. 241-244.

[32] Shi, H., and Luo, S., "Image registration using the shift-insensitive discrete wavelet transformation," in *International Conference on Medical Image Analysis and Clinical Applications*, Guangdong, Jun. 2010, pp. 46-49.

[33] Jain A. K. (1986) *Fundamentals of digital image processing*. Prentice-Hall, Inc., New Jersey.

[34] Gonzalez, R. C., and Woods, R. E. (2002) *Digital image processing*. Prentice-Hall, Inc., New Jersey.

[35] Szeliski, R. (2011) *Computer vision algorithms and applications.* Springer, New York.

[36] Yang, Z., Shen, G., Wang, W., Qian, Z., and Ke, Y., "Spatial-spectral cross correlation for reliable multispectral image registration," in *2009 IEEE Applied Imagery Pattern Recognition Workshop*, Oct. 2009, pp. 1-8.

[37] Zhu, Y.-M., "Volume Image Registration by Cross Entropy Optimization," *IEEE Transactions of Medical Imaging*, vol. 21, no. 2, pp. 174-180, Feb. 2002.

[38] Balakrishnan, N., and Lai, C.-D. (2009) *Continuous bivariate distributions.* Springer, New York.

[39] Mallat, S. (1998) *Wavelet tour of signal processing.* Academic Press, California.

[40] Peter, A. M., and Rangarajan, A., "Maximum Likelihood Wavelet Density Estimation With Applications and Shape Matching," *IEEE Transactions on Image Processing*, vol. 17, no. 4, pp. 458-468, Apr. 2008.

[41] Du, Q., and Chen, L., "An image registration method based on wavelet transform," in *International Conference on Computer, Mechatronics, Control and Electronic Engineering*, Changchun, Aug. 2010, pp. 158-160.

[42] Hongli, S., and Bo, H., "Image registration using a new scheme of wavelet decomposition," in *IEEE Instrumentation and Measurement technology Conference*, Victoria, British Columbia, May 2008, pp. 235-239.

[43] Gao, X. Q., Nguyen, T. Q., and Strang, G., "A Study of Two-Channel Complex-Valued Filter Banks and Wavelets with Orthogonality and Symmetry Properties," *IEEE Transactions on Signal Processing*, vol. 50, no. 4, pp. 824-833, Apr. 2002.

[44] Kingsbury, N., "Image Processing with Complex Wavelets," *Philosophical Transaction Society of London, Applied Mathematics Physical Science,* vol. 357, no. 1760, pp. 2543-2560, 1999.

[45] Candés, E. J., "Harmonic Analysis of Neural Networks," *Applied and Computational Harmonic Analysis*, vol. 6, no. 2, pp. 197-218, Mar. 1999.

[46] Candés, E. J., and Donoho, D., "Ridgelets: A Key to higher-dimensional intermittency?," *Philosophical Transaction of Royal Society of London Applied Mathematics Physics English Science*, vol. 357, no. 1760, pp. 2495-2509, 1999.

[47] Candés, E. J., and Donoho, D., "Curvelets-A Surprisingly Efffective Nonadaptive Representation for Objectives with Edges," in A. Cohen, C. Rabut and L.

Schumaker (eds.). *Curves and Surface Fitting: Saint-Malo 1999,* pp. 105-120, Vanderbilt University Press, Nashville, 2000.

[48] Candés, E. J., and Donoho, D., "New Tight Frames of Curvelets and Optimal Representations of Object with Piecewise C^2 Singularities," *Communication Pure Applied Mathematics,* pp. 219-266, vol. 57, no. 2, Feb. 2004.

[49] Demanet, L., and Ying, L., "Curvelets and wave atoms for mirror-extended images," in *SPIE Wavelets XII,* San Diego, vol. 6701, Aug. 2007, pp. 67010J.

[50] Chauris, H., and Nguyen, T., "Seismic Demigration/Migratoin in the Curvelet Domain," *Geophysics*, vol. 73, no. 2, pp. 4203-4215, Mar.-Apr. 2005.

[51] Choi, M., Kim, R. Y., Nam, M.-R., and Kim, H. O., "Fusion of Multispectral and Panchromatic Satellite Images Using the Curvelet Transform," *IEEE Geoscience and Remote Sensing Letters*, vol. 2, no. 2, pp. 136-140, Apr. 2005.

[52] Mekky, N. E., Abou-Chadi, F. E., and Kishk, S., "A new dental panoramic X-ray image registration technique using hybrid and hierarchical strategies," in *International Conference on Computer Engineering and Systems*, Cairo, Dec. 2010, pp. 361-367.

[53] Olshausen, B., and Field, D., "Emergence of Simple-Cell Receptive Field Properties by Learning a Sparse Code for Natural Images," *Nature*, vol. 381, no. 6583, pp. 607-609, 1996.

[54] Freeman, W. T., and Adelson, E. H., "The Design and Use of Steerable Filters," *IEEE Transactions on Pattern Analysis and Machine Intelligence*, vol. 13, no. 9, pp. 891-906, Sep. 1991.

[55] Simoncelli, E.P., Freeman, W.T., Adelson, E.H., and Heeger, D.J., "Shiftable Multiscale Tranforms," *IEEE Transactions on Information Theory*, vol. 38, no. 2, pp. 587-607, Mar. 1992.

[56] Lee, T. S., "Image Representation Using 2D Gabor Wavelets," *IEEE Transactions on Pattern Analysis and Machine Intelligence*, vol. 18, no. 10, pp. 959-971, Oct. 1996.

[57] Donoho, D. L., "Wedgelets: Nearly Minimax Estimation of Edges," *The Annals of Statistics*, vol. 27, no. 3, pp.859-897, Jun. 1999.

[58] Donoho, D. L., and Huo, X., "Beamlets and Multiscale Image Analysis," in T. Barth, T. Chan and R. Haimes (eds.). *Multiscale and Multiresolution Methods* (Springer Lecture Notes in Computer Science Engineering, vol. 20), pp. 149-196, Springer, Berlin, 2002.

[59] Do, M. N., and Vetterli, M., "The Contourlet Transform: An Efficient Directional Multiresolution Image Representation," *IEEE Transactions on Image Processing*, vol. 14, no. 12, pp. 2091-2106, Dec. 2005.

[60] Labate, D., Lim, W.-Q., Kutyniok, G., and Weiss, G., "Sparse multidimensional representation using shearlets," in *SPIE Wavelets XI*, San Diego, CA, vol. 5914, 2005, pp. 254-262.

[61] Demanet, L., and Ying, L., "Wave Atoms and Sparsity of Oscillatory Patters," *Applied and Computational Harmonic Analysis*, vol. 23, no. 3, pp. 368-387, Nov. 2007.

[62] Willett, R. M., and Nowak, R. D., "Platelets: A Multiscale Approach for Recovering Edges and Surfaces in Photon-Limited Medical Imaging," *IEEE Transactions on Medical Imaging*, vol. 22, no. 3, pp. 332-350, Mar. 2003.

[63] Lu, Y. M., and Do, M. N., "Multidimensional Directional Filter Banks and Surfacelets," *IEEE Transactions on Image Processing*, vol. 16, no. 4, pp. 918-931, Apr. 2007.

[64] Everitt, B. S., and Skrondal, A. (2010) *The Cambridge dictionary of statistics*. Fourth Edition, Cambridge University Press, New York.

[65] Lazo, A. V., and Rathie, P., "On the Entropy of Continuous Probability Distributions," *IEEE Transactions on Information Theory*, vol. 24, no. 1, pp. 120-122, Jan. 1978.

[66] Park, S. Y. and Bera, A. K., "Maximum Entropy Autoregressive Conditional

Heteroskedasticity Model," *Journal of Econometrics*, vol. 150, no. 2, pp. 219-230, Jun. 2009.

[67] Ahmed, N. A., and Gokhale, D.V., "Entropy Expressions and Their Estimators for Multivariate Distributions," *IEEE Transactions on Information Theory*, vol. 35, no. 3, pp. 688-692, May 1989.

[68] Cover, T. M., and Thomas, J. A. (2006) *Elements of information theory.* Second Edition, Wiley & Sons, Inc., New Jersey.

[69] Beaulieu, M., Foucher, S., and Gagnon, L., "Multi-Spectral Image Resolution Refinement Using Stationary Wavelet Transform," in 2003 *IEEE International Geoscience and Remote Sensing Symposium*, vol. 6, Jul. 2003, pp. 4032-4034.

[70] Peng, X., Wei, B., and Chen, Q., "An efficient image registration method based on mutual information model" in 2010 Seventh *International Conference on Fuzzy Systems and Knowledge Discovery*, Yantai, Shandong, Aug. 2010, pp. 2168-2172.

APPENDIX A

The test images used in this thesis are shown below:

Toy

Image 1 (left focused)

Image 2 (middle focused)

Image 3 (right focused)

Room

High light exposure

Low light exposure

Synthetic aperture RADAR (SAR) 1

(Sensor: daedalus scanner)

Mode 1

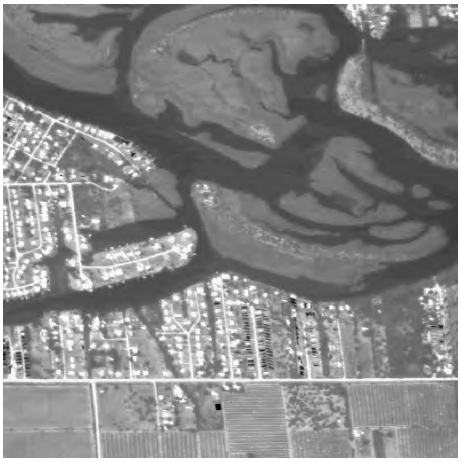

Mode 2

Tree

(Sensor: Hyp. 30- 30 channel DRA hyperspectral scanner)

Mode 1

Mode 2

Navigation

Image 1

Visual-image from a Philips LTC500 CCD camera (f/1.2 50dB s/n at 0.4 Lux) sensitive from visual to near IR (400-900 nm)

Image 2

Infrared-image from a AMB Radiance HS IR camera (Raytheon), sensitive for 3-5 microm

Image 3

Infrared-image from an AIM 256 microLW camera (AEG), sensitive for 8-10 microm

MRI

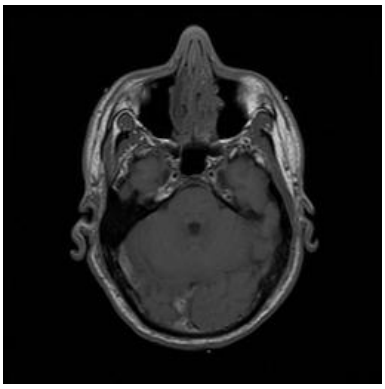

T1 mode

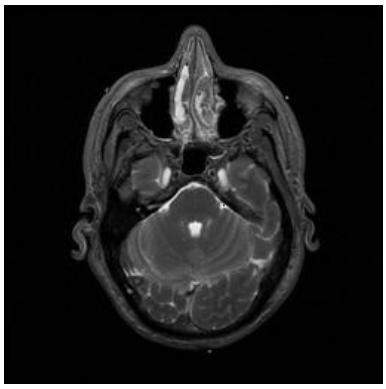

T2 mode

Synthetic aperture RADAR (SAR) 2

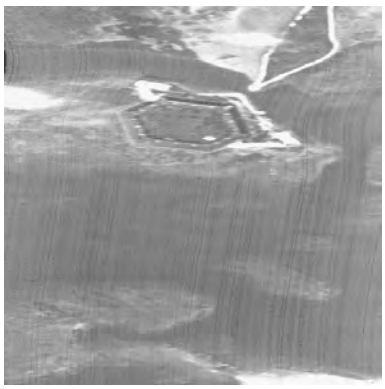

Mode 1

Mode 2

Doll

Middle focused

Left focused

SAR3

Mode 1

Mode 2